7.12 Mantle Geochemical Geodynamics

PJ Tackley, Institut für Geophysik, ETH Zürich, Switzerland

7.12.1 Observations and the Origin of Heterogeneity

7.12.1.1 Introduction

Geochemical constraints on mantle heterogeneity are thoroughly reviewed in several papers (e.g., Caro, 2011; Graham, 2002; Hilton and Porcelli, 2003; Hofmann, 2003; White, 2010), but as they are so important for understanding this chapter, it is appropriate to briefly summarize here the basic observations and 'traditional' interpretations. New interpretations are discussed in **Section 7.12.5**. It is noted that with modern analysis techniques, particularly MC-ICPMS machines, the number of isotopes that geochemists are measuring has increased, and while many isotope systems are consistent in their behavior, additional complexity in interpretation is introduced by isotope systems that are affected by additional processes.

This review starts with models of the bulk silicate Earth (BSE) composition and then constraints on the variations of composition, which fall into three main categories: (i) mass balance arguments based on the inferred composition of the mid-ocean ridge basalt (MORB) source and continental crust, (ii) noble gas constraints, and (iii) end-member components identified by analysis of the trace-element isotopic compositions of ocean island basalts (OIBs) and MORBs. This section also reviews geophysical constraints on chemical heterogeneity and mantle structure and the major types of mantle conceptual model that have been proposed to explain geochemical and/or geophysical observations.

7.12.1.2 Bulk Earth and BSE models

The bulk composition of the whole Earth (i.e., core + mantle + crust) is estimated using a variety of constraints as reviewed in Palme and O'Neill (2003), particularly the composition of the Sun, meteorites, and upper mantle-derived rocks. The relative abundance of refractory elements is typically thought to be chondritic (i.e., solar), while nonrefractory to volatile elements show increasing degrees of depletion. The composition of the silicate part, that is, Bulk Silicate Earth (BSE), is further influenced by core extraction, which enriched the mantle in nonsiderophile elements but depleted it in siderophile elements. Knowledge of the trace-element content of the BSE is important in making 'mass balance' arguments summarized

later, as is the knowledge of the composition of the continental crust (e.g., Rudnick, 1995; Rudnick and Fountain, 1995; Taylor and McLennan, 1995). A commonly used compositional BSE model is that of McDonough and Sun (1995), while a more depleted model was proposed by Lyubetskaya and Korenaga (2007a). It is also possible that the Earth is not chondritic, as argued, for example, by Drake and Righter (2002) and Campbell and O'Neill (2012). The reader is referred to the previously cited literature for further detailed discussions.

7.12.1.3 Fractionation of Major and Trace Elements

When solid and liquid coexist in equilibrium with each other in a multicomponent material such as mantle silicates, the composition of the solid and liquid components is different in both major and trace elements. The two main situations for solid–liquid equilibration are partial melting (caused by, e.g., a decrease of pressure in an upwelling or by infiltration of volatiles) and the crystallization of a magma ocean.

A crude way of viewing major-element fractionation is that different minerals have different melting temperatures – for example, in the shallow mantle, garnet and clinopyroxene melt at a lower temperature than olivine. Thus, partial melting followed by melt segregation and eruption causes both the crust that forms from the resulting melt and the residual solid to have a different composition from the original rock. In a cooling magma ocean, this results in the solid crystals that form having a different composition from the remaining liquid, which might allow them to settle to the top or bottom due to related density differences. Indeed, density differences that result from differences in major-element composition may well play an important role in mantle dynamics, as discussed in later sections.

Trace-element partitioning between solid and liquid is expressed in terms of partition coefficients d, which describe the equilibrium concentration of the element in the solid divided by the concentration in the liquid:

$$d = \frac{C_{\text{solid}}}{C_{\text{liquid}}} \quad [1]$$

where C_{solid} and C_{liquid} are the concentrations of the element in the solid and liquid, respectively. A partition coefficient $\ll 1$ means that the element preferentially enters the melt and is known as an incompatible element. Conversely, a partition coefficient $\gg 1$ indicates that the element is compatible and stays in the solid. The partition coefficient depends on the element (because different elements have different sizes and electronic properties), which results in trace elements being fractionated during melting, that is, the ratio of their concentrations changes. Partition coefficients may also depend on pressure (depth), oxygen fugacity, and the minerals present. Different isotopes of the same element have partition coefficients that are almost the same and can be treated as identical for the situations discussed in this chapter. For more information, see Righter and Drake (2003), Wood and Blundy (2003), and **Chapter 2.04**.

This fractionation of trace elements plays a key role in the evolution of isotope ratios of interest in mantle geochemistry. In a simple radioactive decay system in which a parent isotope radioactively decays to a daughter that is a different element, the parent to daughter ratio (P/D) will change as a result of melting and crustal formation, whereas the ratio of the daughter to a stable isotope of the same element (D/D_S) will not change. This change in (P/D) affects the future rate of change of (D/D_S). By analyzing the (D/D_S) ratio in two or more samples that have experienced fractionation in a single event, it is possible to derive the elapsed time since the fractionation event, and this is the principle of radiogenic dating. The specific example of Pb–Pb dating is more complicated because it combines two decay systems, but this also makes it more robust (for details, see, e.g., Stacey, 1992).

The concentration of trace elements in the melt depends not only on the partition coefficient but also on the melt fraction. For example, a highly incompatible element essentially enters the melt, which means that its concentration in the melt is inversely proportional to melt fraction. In the more general case, it is straightforward to derive an equation for the equilibrium concentration of a trace element in the melt (Shaw, 1970):

$$C_{\text{liquid}} = \frac{C_0}{F + d(1-F)} \quad [2]$$

where F is the melt fraction and C_0 is the concentration in the total (bulk) system. Thus, the enrichment of a magmatic product in trace elements relative to its source can be used to estimate the melt fraction.

7.12.1.4 Trace-Element Budgets of the Crust and Mantle

The trace-element composition of the continental crust and the inferred composition of the MORB source are often compared to the composition of the BSE discussed in **Section 7.12.1.2**. This comparison indicates that the continental crust is strongly enriched in incompatible trace elements – by a factor of ~50–100 in the most incompatible elements, whereas the MORB source is depleted. Furthermore, the patterns of enrichment and depletion (i.e., as a function of elements) appear to be complementary. The enriched continental crust and the depleted MORB source region have thus long been thought to be complementary in their trace-element signature, implying that the MORB source region is the residue from melting that produced the continental crust (e.g., Hofmann, 1988). Mass balance calculations have been used to estimate the fraction of the mantle that must have been depleted to make the continental crust (e.g., Allegre et al., 1983a; Davies, 1981; Hofmann, 1988; Jacobsen and Wasserburg, 1979; O'Nions et al., 1979) with the estimated depleted reservoir size ranging greatly between 30% and 97% of the mantle (50–80% of the mantle according to Hofmann (2003)) and the rest of the mantle being primitive, that is, roughly chondritic. A curious feature of this calculation is that the degree of melting required to produce continental crust is small, for example, ~1% (Hofmann, 2003) – about an order of magnitude lower than the 8–10% melting thought to produce present-day MORB. This indicates that incompatible trace elements must be scavenged from a large volume and concentrated into a small volume in order to produce the concentrations observed in continental crust, as discussed in **Section 7.12.1.5.2**.

7.12.1.4.1 Reservoir of 'missing' elements

The previous mass balance calculation implies the existence of a primordial reservoir of primitive (i.e., BSE) composition containing the trace elements that are 'missing' from the continental crust plus depleted (MORB source) mantle. This inferred reservoir of volume 20–50% of the mantle is often argued to be important in explaining the mantle's heat budget, as it would contain a large amount of heat-producing elements, and the concentration of heat-producing elements in the MORB source appears to be too low to explain the mantle's heat budget. The reservoir is argued to be 'hidden,' in the sense that it produces no observed geochemical signature, except perhaps that of high $^{3}He/^{4}He$. As an alternative to this relatively large reservoir, it has been proposed that the 'missing' trace elements are contained in a small, early enriched reservoir (EER) (e.g., Boyet and Carlson, 2006; Coltice and Ricard, 1999; Tolstikhin and Hofmann, 2005; Tolstikhin et al., 2006). Another possibility is that the bulk Earth composition is more depleted than previous estimates (Lyubetskaya and Korenaga, 2007a), which would not require any hidden reservoir (Lyubetskaya and Korenaga, 2007b).

7.12.1.5 Origin of Heterogeneities

Chemical variations inside the mantle could arise either from primordial differentiation of the Earth, through subsequent magmatism, or through possible chemical reactions with the core; these are discussed in this section. Quantitative models of either process require knowledge of the bulk composition of the mantle, which was discussed in **Section 7.12.1.2**.

7.12.1.5.1 Primordial differentiation (fractionation of magma ocean, core formation, and early atmosphere)

The extent to which the mantle might have started off layered due to fractional crystallization of a magma ocean has been hotly debated over the years. Key issues are whether a deep magma ocean existed, and if so whether its cooling would result in a fractionation due to crystal settling, or whether it would instead solidify into a chemically homogeneous mantle. This depends on various factors such as the type of transient atmosphere present, grain size, viscosities, and convection mode (Abe, 1997; Elkins-Tanton et al., 2003; Solomatov and Stevenson, 1993a,b). The existence of a deep magma ocean has previously been argued against because the geochemical signature of the mantle is inconsistent with wholesale fractionation (e.g., Ringwood, 1990a), but if magma ocean convection is vigorous enough that crystals do not settle (Solomatov et al., 1993; Solomatov and Stevenson, 1993b; Tonks and Melosh, 1990), then this difficulty vanishes. Furthermore, models of the Earth's formation predict collisions with planetesimals the size of the Moon or even Mars (the latter of which offers the most popular explanation for the formation of the Moon), which would inevitably result in large-scale melting and a deep terrestrial magma ocean (e.g., Benz and Cameron, 1990; Melosh, 1990). Another possibly important aspect of magma ocean evolution is its interaction with the primordial atmosphere, through which it might have absorbed volatile elements (e.g., Ballentine, 2002; Dasgupta, 2013; Elkins-Tanton, 2008; Zahnle et al., 2010), although Ballentine et al. (2005) suggested that this was not important for primitive volatile (particularly He/Ne) acquisition.

While there is therefore much uncertainty about magma ocean evolution, a synthesis by Solomatov (2000) offers a scenario that is consistent with both geochemical and dynamic constraints. In this case, following a giant impact, the lower mantle solidifies rapidly (i.e., <1000 years) and is undifferentiated, leaving a shallow magma ocean in which fractionation and much slower cooling occur. This is consistent with the earlier work of Abe (1997), who also found that following a giant impact, lower mantle differentiation is uncertain, whereas upper mantle differentiation is likely, and a shallow magma ocean could remain for 100–200 My.

Another chemically important process is the separation of the metal core from the remaining silicate. Metal–silicate separation is likely to have occurred in (at least) two environments (Karato and Murthy, 1997; Stevenson, 1990): small metal droplets (arising either from dispersed metal particles in undifferentiated solid chondritic material or from emulsification of the cores of differentiated impacting bodies) falling through a magma ocean, where separation would occur rapidly (Hoink et al., 2006; Rubie et al., 2003; Solomatov, 2000; Tonks and Melosh, 1990; Ulvrova et al., 2011), and large metal diapirs (arising either from pools of liquid metal at the base of a shallow magma ocean or from the cores of impacting differentiated bodies) sinking through solid silicate or primitive material. The details of these strongly influence the partitioning of trace elements between the mantle and the core as well as the extent to which the core and mantle are chemically equilibrated in general. Specifically, chemical equilibration is efficient in a magma ocean but has generally been thought to be less effective for large sinking diapirs, leading to the view that metal–silicate equilibration last happened at temperatures and pressures relevant to the base of the magma ocean (Murthy and Karato, 1997). However, Samuel and Tackley (2008) showed that sinking iron diapirs of radius 1–100 m can chemically equilibrate, so this conclusion is called into question. Such mechanisms are relevant to questions such as whether the core contains potassium, carbon, or noble gases, as well as whether reactions between the mantle and the core take place.

In summary, at present, the consensus from geochemical constraints combined with dynamic considerations is that primordial chemical stratification in the deep mantle is unlikely, whereas primordial upper mantle chemical stratification is likely. Partitioning of elements between the mantle and the core is sensitive to poorly known processes that occurred during core–mantle separation.

7.12.1.5.2 Formation of continental and oceanic crust

It is clear that much differentiation has taken place due to melting subsequent to Earth's formation. The most obvious manifestations of this are (i) the formation of the continental crust, which is strongly enriched (by a factor of up to 50–100) in incompatible trace elements compared to BSE models and can survive over billions of years, and (ii) the formation of the oceanic crust, which is less enriched and gets subducted back into the mantle after 100–200 My, possibly to get mixed again (see later discussion). A thorough review of crustal formation and its geochemical consequences was given in Hofmann

(2003); here, the main points relevant to the discussion in this chapter are summarized.

7.12.1.5.2.1 Continental crust

As discussed in the preceding text, from a trace-element perspective, the (enriched) continental crust is typically thought to be complementary to the depleted mantle, with an implied degree of melting of ~1%. This is very low and indicates that the continental crust is produced by more complex processes than simple partial melting (by ~1%) and eruption – indeed, melting experiments carried out on peridotite produce magmas that do not resemble (i.e., are less 'evolved' than) the continental crust in their major-element composition (Hirose and Kushiro, 1993; Rudnick, 1995). The continental crust has two layers, a lower crust with an approximately basaltic composition and an upper crust with a roughly granodioritic composition. A two-step process is commonly envisaged (Hawkesworth and Kemp, 2006). First, a new juvenile continental crust with a basaltic composition is produced mostly by water-induced melting of the mantle above subducting slabs at convergent margins; Stern and Scholl (2010) estimated 1.5 $km^3 year^{-1}$ from oceanic arcs and 1.0 $km^3 year^{-1}$ from continental arcs out of a total of 3.2 $km^3 year^{-1}$. This water-induced melting is caused by dehydration of subducted crust and movement of the resulting fluid through the mantle wedge (together with incompatible trace elements), followed by metasomatism and melting. A secondary source of new continental crust is intraplate volcanism (i.e., flood basalts on continents or accretion of oceanic plateaus). The lower continental crust is thought to have a similar composition to the juvenile continental crust (Hawkesworth and Kemp, 2006). Second, the upper continental crust forms by partial melting and resulting differentiation of this juvenile crust. The degree of partial melting is about 14% (Hawkesworth and Kemp, 2006), which results in a large volume of residue that is not observed in continents; this residue is dense so is thought to delaminate and founder into the mantle, where it might contribute to OIB sources. Delamination of lower crustal residual material is thus an important process, although it may only be possible over a certain range of temperature and pressure conditions (Jull and Kelemen, 2001). Indeed, Tatsumi et al. (2013) found that the residue is denser than pyrolite all the way to the core–mantle boundary (CMB) and may therefore contribute to any dense piles that exist there. Processes generating continental crust may have been different in the Archean and Hadean (e.g., Condie and Kröner, 2013; Foley et al., 2003; Rudnick, 1995; Taylor and McLennan, 1995). Johnson et al. (2014) calculated that the thickness of very early crust was limited to about 45 km by phase transitions to denser minerals; below this depth, the relatively dense crust drips back into the mantle.

The growth history of continents is highly uncertain and reflects a balance between processes of production of new continental material and the loss of old continental material from subduction, at collision zones or by foundering of lower crustal material. Several continental growth curves have proposed, largely on the basis of geochemical arguments; for a comparison of growth curves and review, see Harrison (2009) and Taylor and McLennan (1995), and for a recent model constrained by isotopes in zircons, see Dhuime et al. (2012). Continents may have grown in several pulses such as at 2.7, 1.9, and 1.2 Ga ago (Hawkesworth and Kemp, 2006). At the present day, creation and destruction of continental crust are roughly balanced (Stern and Scholl, 2010). Very little ancient continental crust is preserved; however, recent zircon data imply that continental crust already existed 4.4–4.5 Gy before present and was metamorphosed under aqueous conditions at pressures corresponding to >20 km depth and moderate temperatures (Harrison, 2009; Harrison et al., 2005).

Also important and compositionally distinct is the continental mantle lithosphere. A useful review of its composition, formation, and destruction of this can be found in Lee et al. (2011). Formation mechanisms and the compositions of the continental lithosphere and crust have changed with time due to higher mantle temperatures in the Archean (Herzberg and Rudnick, 2012).

7.12.1.5.2.2 Oceanic crust

While continental crust formation is generally considered to be the dominant influence on the trace-element abundances in the mantle (the present-day oceanic crust is much less enriched and smaller in volume), a large fraction of the mantle has passed through the melting ('processing') zone beneath mid-ocean ridges, and thus, the production and recycling of oceanic crust have had a major influence on mantle heterogeneity. The rate at which this happens is somewhat uncertain and is discussed in detail in the next section. Regardless of the exact rate of processing, subducted MORB is clearly a volumetrically significant component in the mantle that is responsible for much of the observed isotopic heterogeneity (e.g., Stracke, 2012) so should not be ignored in calculating mantle geochemical evolution.

7.12.1.5.3 Processing rate of mid-ocean ridge melting and residence time

The volume of material that has been processed by MOR melting is quite uncertain, because of differing estimates of the present-day rate of processing and uncertainty about how this changed in the past over billions of years. One measure of the processing rate is the 'residence time,' which for random sampling of the mantle is equal to the length of time taken for the mass of the mantle to pass through the processing zone. At present rates of seafloor spreading, estimates of this processing time or residence time have varied widely, from 2.9 to 10 Ga. Example estimates are 4 Gy (O'Connell and Hager, EOS 61, 373, 1980, as referenced in Davies (1981)), 10 Gy (Gurnis and Davies, 1986b), 5.7 Gy (Kellogg and Wasserburg, 1990), 9.5 Gy (Phipps Morgan, 1998), 3–6 Gy (Davies, 2002), 4.5 Gy (Xie and Tackley, 2004b), and 2.9 Gy (Coltice, 2005; Huang and Davies, 2007c). It is worth analyzing why there is such a large variation in these estimates. The processing rate, expressed as the volume of mantle processed per year, is given by

$$P = Ad\rho \qquad [3]$$

where A is the area of oceanic seafloor produced per year, d is the depth of onset of melting beneath spreading centers, and ρ is the density of the processed material. Observations of the age distribution of ocean floor (e.g., summarized in Phipps Morgan (1998)) indicate that $A = 2.7\ km^2 year^{-1}$ for seafloor

produced in the last 1 Ma, or $A = 2.9$ km^2 year^{-1} based on an average over the last 100 Ma, the latter being similar to the 3.0 km^2 year^{-1} estimated by Stacey (1992). Other authors have preferred to use 'back of the envelope' estimates, for example, Davies (2002) assumed a ridge length of 40 000 km and spreading velocity of 5–10 cm year^{-1} (giving $A = 2$–4 km^2 year^{-1}) and Coltice (2005) assumed a ridge length of 60 000 km and plate velocity of 5 cm year^{-1} ($A = 6$ km^2 year^{-1}). Regarding the onset depth of melting d, Phipps Morgan (1998) assumed that the oceanic crustal thickness of 6.5 km was produced with 10% melt ($d = 65\rho_{crust}/\rho_{mantle}$ km), whereas Davies (2002) assumed that $d = 100$ km, and Coltice (2005) assumed that $d = 150$ km. Using the observationally constrained $A = 2.9$ km year^{-1} together with, for example, $d = 80$ km and peridotite density $= 3000$ kg m^{-3} leads to $P = 6.96 \times 10^{14}$ kg year^{-1}, which gives a residence time of 5.74 Gy to process the mantle mass of 4×10^{24} kg. Thus, estimates of processing (residence) time as low as 3 Gy should be regarded as extreme lower limits. Estimates of the present-day processing time based on geochemical fluxes (Albarède, 2005b) range from 4 to 9 Gy, bracketing the geophysical value discussed earlier; this estimate is further discussed in **Section 7.12.2.5**.

It is likely that the rate of seafloor spreading and hence crustal production was considerably higher in the past when the mantle was hotter, which would greatly reduce the processing/residence time in the past (Gurnis and Davies, 1986b). In addition, the depth of melting would have been larger due to the hotter mantle, as considered by Davies (2002) and Tajika and Matsui (1992, 1993), further increasing the processing rate. The appropriate increase of seafloor spreading in the past is not known: in simple, internally heated convection in secular equilibrium, the surface velocity scales as (radiogenic heat production). Davies (1980) and Phipps Morgan (1998) gave detailed arguments why this also applies to plate tectonics. It is, however, likely that the early Earth did not have plate tectonics as it exists today because the thicker oceanic crust and younger oceanic plates (when they reach subduction zones) would make plates difficult to subduct (Davies, 1990, 1992; Vlaar, 1985) and perhaps because the mechanical oceanic lithosphere was thicker because water depletion, which causes an increase in viscosity, occurred deeper (Korenaga, 2003). Thus, the most likely increase in crustal production rate lies between constant and H^2, where H = radiogenic heat production rate.

To give some quantitative examples of the influence of faster processing in the past, (i) Xie and Tackley (2004b) calculated the volume of oceanic crust produced over the age of the Earth to be ~10% of the mantle mass if the present-day production rate is applied to the whole Earth's history, 54% if the H^2 law of Davies (1980) is applied, or 82% if the increase in depth of melting due to higher mantle temperatures is additionally taken into account. In the latter two cases, this clearly implies that the same material melts two or more times, as it is not possible to produce this amount of MORB from the residue of continental crust production. (ii) Davies (2002) calculated that the H^2 law leads to four times the amount of processing over geologic time, which he expressed as being equivalent to 18 Gy of constant-rate processing. This means that 98.6% of the mantle is processed if the present-day residence/processing time is 4.2 Gy.

Outgassing of ^{40}Ar is also closely related to the processing/residence time. As mentioned earlier, the ~50% outgassing constraint can be matched by a residence time of 9.5 Gy and a processing rate scaling with H^2 (Phipps Morgan, 1998). With a much smaller processing time varying from 1.98 to 4.23 Gy through the calculation, Huang and Davies (2007a) obtained 81% argon outgassing, suggesting that such processing times are too small.

These issues are further discussed from the perspective of modeling in **Section 7.12.2.5**.

7.12.1.5.4 Reactions with the core

Some researchers have studied the possibility of an iron-rich layer forming above the CMB caused by reactions with the core. There is some geochemical evidence (based on the Os–Pt system) for mass exchange between the mantle and the core (Brandon et al., 1998, 2003; Humayun et al., 2004; Walker et al., 1995), but this is controversial (Brandon and Walker, 2005; Schersten et al., 2004).

Experiments indicate that iron reacts with silicate perovskite to form iron oxide and silica (Knittle and Jeanloz, 1989, 1991). Experiments with liquid iron and solid silicate show that the silicate becomes depleted in Fe and O (Goarant et al., 1992). Liquid iron also reacts with Al_2O_3 at CMB pressures (Dubrovinsky et al., 2001) but not with silica (Dubrovinsky et al., 2003). Using thermodynamic calculations, Song and Ahrens (1994) determined that the observed reactions are thermodynamically possible. Thus, core–mantle reactions are expected from an experimental standpoint, although it is possible that the presence of water inhibits them (Boehler et al., 1995; Poirier et al., 1998).

It appears difficult to generate significant mantle heterogeneity this way, because the thickness of the reaction zone is relatively small. Poirier (1993) and Poirier and Le Mouel (1992) found that liquid Fe can penetrate 1–100 m into the mantle along grain boundaries if it reacts with the silicate. Knittle and Jeanloz (1991) proposed that the Fe ascents by a capillary action driven by surface tension. However, recently, based on laboratory experiments, Otsuka and Karato (2012) identified a morphological instability by which Fe-rich liquids could penetrate into (Mg, Fe)O, due to the two not being in chemical equilibrium. They estimated that via this mechanism, Fe could penetrate ~50 km into the mantle in a billion years, which is much faster than the previous estimates. A dynamic mechanism could be a suction mechanism in areas of downwelling (where the CMB is depressed), which may entrain Fe of order ~1 km into the mantle with fractions of up to 10%, depending on parameters such as the effective bulk viscosity (Kanda and Stevenson, 2006; Stevenson, 1988). Petford et al. (2005) also proposed a dynamically assisted Fe transfer mechanism assuming that the D″ region behaves as a poro-viscoelastic granular material with dilatant properties, but the required strain rates are rather high (10^{-12} s^{-1}). Thus, it appears that Fe might be able to infiltrate up to ~1–10s km at significant volume fractions, but this needs further study.

If Fe infiltrates the mantle in some regions in a thin layer and reacts to form dense products, the question is then whether the continual flux of new mantle material through this reaction zone is sufficient, over geologic time, to affect a volumetrically significant amount of mantle material. Knittle

and Jeanloz (1991) suggested that the material would not be raised far into the mantle because of its increased density and could accumulate into a approximately few 100 km thick D″ layer, but this needs to be tested using detailed modeling. Numerical models of this performed to date have parameterized core reactions as an effective chemical diffusivity, which may not correctly capture the process. The most advanced model is that of Kellogg (1997), who parameterized the infiltration of Fe using a chemical diffusivity 100–1000 times smaller than the thermal diffusivity and found that large density contrasts ($B=10$) result in a thin (<100 km) layer that slows further growth, whereas lower density contrasts ($B=1$) result in an undulating layer several 100s km thick that piles up under upwellings, as is observed in earlier calculations (Hansen and Yuen, 1988). If a metal-bearing layer does build up, it could have a thermal conductivity an order of magnitude higher than that of silicates (Manga and Jeanloz, 1996), which could further influence mantle convection.

It has been proposed that silicate melt (partial melt fractions up to 30%) exists in some areas at the CMB as an explanation of seismically observed ultra-low velocity zones (ULVZs) (Lay et al., 2004; Williams and Garnero, 1996), as further discussed in **Section 7.12.3.1.5**. Such areas of partial melt could have interesting geochemical consequences, as discussed in Labrosse et al. (2007) and in **Section 7.12.5.2.5**. In the present context, they might facilitate reactions between the mantle and the core due to the larger flux of mantle material that comes into contact with the core and also because chemical diffusion is faster in liquids (see also **Chapter 7.11**).

7.12.1.6 MORB and OIB Trace-Element Signatures

7.12.1.6.1 Noble gases

The most common noble gases considered in mantle geochemistry are the isotopes of He and Ar, with Ne and Xe also sometimes considered.

7.12.1.6.1.1 ^{3}He/^{4}He ratios

The two isotopes of helium are ^{3}He, which is primordial, and ^{4}He, which in rocks is almost all produced by the radioactive decay of U and Th (the primordial abundance of ^{4}He is small compared to that of U and Th because He is volatile). Histograms of the ratio of ^{3}He/^{4}He for MORBs and OIB show clear differences. MORBs have a relatively constant ^{3}He/^{4}He ratio with a mean value of 1.16×10^{-5}, which is a factor of 8.4 higher than the atmospheric value (Allegre et al., 1995; Graham, 2002; Kurz et al., 1983). The range of ^{3}He/^{4}He ratios between 7 and 9 is thus taken as representative of the depleted upper mantle. OIB ^{3}He/^{4}He ratios are, in contrast, extremely heterogeneous, extending to both higher and lower values than MORB, with the highest ratios measured (at Baffin Island) about 50 times the atmospheric value (Stuart et al., 2003).

There are several possible explanations for the high ^{3}He/^{4}He material. The 'traditional' interpretation is that this component comes from an undegassed, 'primitive' source, because noble gases are highly incompatible and volatile and are thus expected to enter any melt and be heavily outgassed prior to or during eruption (Allegre et al., 1983b; Farley et al., 1992; Porcelli and Wasserburg, 1995; note that outgassing requires CO_2 bubbling, which occurs at depths <60 km). This component has traditionally been identified as the lower mantle, consistent with the need to keep it intact for billions of years, with other arguments for the lower mantle being primitive, and with the idea of plumes sampling the lower mantle and spreading centers sampling the upper mantle. However, the actual volume and location of this component are not constrained. If the 'primitive' interpretation is correct, one might expect the absolute concentration of He in OIB to be higher than that in MORB, but this is not observed, perhaps because magma chamber processes cause the loss of He (Farley and Neroda, 1998).

The leading alternative explanation for high ^{3}He/^{4}He is that it is associated with recycled depleted oceanic lithosphere (Albarède, 1998; Anderson, 1998; Coltice and Ricard, 1999, 2002; Ferrachat and Ricard, 2001). This is based on the fact that high ^{3}He/^{4}He simply requires high ^{3}He/(U+Th) because decay of U and Th produces ^{4}He, therefore, an alternative to high [^{3}He] is low [U+Th], which is found in material that has been depleted in incompatible trace elements due to melting. The evolution of He ratios is illustrated in **Figure 1**. Note that ^{3}He/^{4}He decreases with time in all 'reservoirs' due to the radiogenic ingrowth of ^{4}He. If the ratio ^{3}He/(U+Th) is changed in different components due to fractionation (during which ^{3}He/^{4}He remains the same), then with time, it will evolve ^{3}He/^{4}He that is higher or lower than the original material. If He is less incompatible than U and Th (e.g., Graham et al., 1990), and as found in some laboratory experiments (Parman et al., 2005) although not others (Heber et al., 2007), then ^{3}He/(U+Th) is higher in the depleted residue, and after some time, its ^{3}He/^{4}He will be higher than that of the original material. However, Anderson (1998), Coltice and Ricard (1999, 2002), and Ferrachat and Ricard (2001) showed that

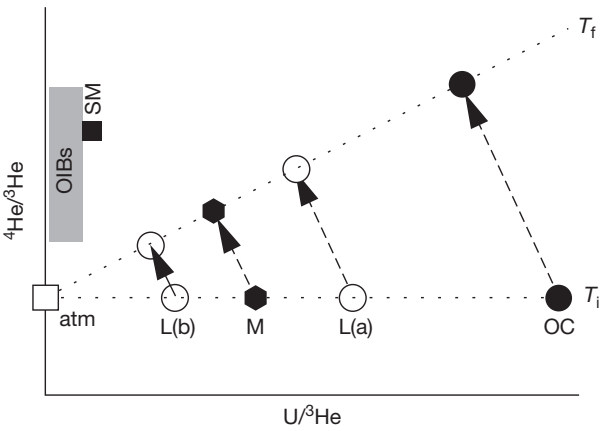

Figure 1 Schematic diagram showing the helium isotope evolution of different mantle components, from Coltice and Ricard (2002). M, mantle; L, lithosphere; atm, atmosphere; OC, oceanic crust. When M melts, it produces oceanic crust and lithosphere (a) or (b) depending on the relative partition coefficients of U and He, and some He is lost to the atmosphere. Between melting events, U decays and produces ^{4}He, so U/^{3}He decreases and ^{4}He/^{3}He increases. The shallow mantle (SM) is a mixture of recycled lithosphere and oceanic crust, so recycled lithosphere will always have lower ^{4}He/^{3}He (high ^{3}He/^{4}He) than the average, regardless of the relative partition coefficients. With successive melting events, the mantle average ratios move to the right due to He outgassing.

it is not necessary for He to be less incompatible if the residuum is stored for substantial time periods while the rest of the mantle becomes increasingly outgassed. To understand this, note that in the crust, $^{3}He/(U+Th)$ is extremely low due to degassing of He and concentration of U and Th, so the crust will have much lower $^{3}He/^{4}He$ regardless of the exact relative He and U partitioning. If the mantle is almost all differentiated, such that to first order it is made of a mixture of subducted crust and depleted residue, then the average mantle $^{3}He/^{4}He$ will inevitably be in between the ratios in residue and subducted crust, making residue $^{3}He/^{4}He$ appear to be high.

Another proposed explanation of the 'primordial' helium component is that it comes from the core. However, the only measurements of noble gas partitioning between silicate melt and iron melt under pressures up to 100 kilobars indicate that the partition coefficients are much less than unity and that they decrease systematically with increasing pressure (Matsuda et al., 1993). These results suggest that the Earth's core contains only negligible amounts of noble gases if core separation took place under equilibrium conditions at high pressure, although the uncertainties are too great to rule out the core as a potential mantle ^{3}He source (Porcelli and Halliday, 2001).

Finally, it has been proposed that a large amount of ^{3}He has been delivered to the Earth's surface by cosmic dust and then recycled to the mantle (Allegre et al., 1993; Anderson, 1993). Several arguments have been made against this proposal (Farley and Neroda, 1998); in particular, the dust flux is several orders of magnitude too low to account for the ^{3}He flux out of the mantle, and ^{3}He is expected to be degassed from the dust particles during subduction.

7.12.1.6.1.2 Heat–helium imbalance

The present-day flux of ^{4}He out of the mid-ocean ridge system has been estimated by measuring the concentration of ^{4}He in ocean water. O'Nions and Oxburgh (1983) pointed out that this ^{4}He flux is only a small fraction of what would be expected from the concentration of ^{238}U, ^{235}U, and ^{232}Th in MORB and even lower than U and Th in BSE, which has led to the term 'heat–helium imbalance.' The 'traditional' explanation of this is that the radiogenic sources are trapped in the lower mantle, from which heat can escape by conduction across a thermal boundary layer (TBL), but ^{4}He cannot. It has been suggested that the concentration of ^{4}He might be misleading because this is influenced by short-timescale processes such as variations in eruption rate, whereas the concentration of U and Th is a long-timescale process. Possible solutions to this are discussed in **Sections 7.12.4.1.1** and **7.12.5.1**.

7.12.1.6.1.3 Argon outgassing

Argon has three stable isotopes, the two of most interest being 'primitive' ^{36}Ar and 'radiogenic' ^{40}Ar. There is virtually no primordial ^{40}Ar in the Earth (Ozima and Kudo, 1972), it being entirely produced by the decay of ^{40}K. As Ar does not escape from the atmosphere (unlike He) due to its large atomic mass, the amount of ^{40}Ar in Earth's atmosphere represents the total amount of argon degassed from the Earth's interior over the age of the Earth. This atmospheric ^{40}Ar budget, when combined with an estimate of the total ^{40}K content of the Earth, implies that approximately half of all ^{40}Ar produced within the Earth since its formation is retained within the solid Earth (Allegre et al., 1996; O'Nions and Tolstikhin, 1996), which gives a constraint on the fraction of the mantle that has been processed through mid-ocean ridge or other melting environments. There is some uncertainty in this figure due to uncertainty in the amount of ^{40}K in the mantle and a fairly small uncertainty in how much of the ^{40}Ar in continental crust has actually outgassed. The uncertainty in total amount of K arises because in the planetary formation process, K is moderately volatile, so the total amount of K is usually calculated from the total amount of (refractory) U assuming some a particular K/U ratio, estimates of which range from a widely accepted value of 12 700 (Jochum et al., 1983) to as low as 2800 (Stacey, 1992). The continental crust contains ~1/3–1/2 of the K budget (Rudnick and Fountain, 1995) and for the earlier mass balance calculation is usually assumed to be completely outgassed in the resulting ^{40}Ar, which may not be the case (see, e.g., discussion in Phipps Morgan, 1998). The linkage between K assimilation by the continental crust and ^{40}Ar crust and mantle outgassing can be used to constrain the relative amounts of K in the crust and Ar in the atmosphere (Coltice et al., 2000a). In any case, this '50% outgassing' constraint is commonly misinterpreted to mean that 50% of the mantle is undegassed – in fact, because Earth's ^{40}Ar was continuously produced over geologic time from a negligible initial concentration, the mantle could have almost entirely degassed early in its history and still match the Ar constraint. In other words, early or accretionary degassing events do not influence ^{40}Ar outgassing. Quantitatively, for a constant convective vigor, van Keken and Ballentine (1999) showed that outgassing 50% radiogenic ^{40}Ar implies outgassing 72% of primordial, nonradiogenic species. If the convective vigor were higher in the past, then the latter fraction can be much higher. Phipps Morgan (1998) showed that the outgassing constraint is perfectly compatible with whole-mantle convection, even if the processing rate was much higher in the past: for example, assuming that the present-day processing time is 9.6 Gy and was faster according to $(\text{heating rate})^2$ in the past, one obtains 93% outgassing of primitive ^{36}Ar but only 58% outgassing of radiogenic ^{40}Ar, or 98% primitive outgassed while retaining 31% of radiogenic Ar. A better expression of this constraint is "50% of the mantle has been undegassed *since the ^{40}Ar was produced in it*" (Phipps Morgan, 1998).

7.12.1.6.1.4 The argon paradox

A more problematic constraint arises from the concentration of Ar in the MORB source region, which is much lower than what would be expected if the ^{40}Ar remaining in the mantle were evenly distributed (Turner, 1989). This has traditionally been interpreted to mean that the additional, 'missing' ^{40}Ar must be 'hidden' in the lower mantle, which should have about 50 times the ^{40}Ar concentration of the upper mantle (Allegre et al., 1996). It has been argued that this difficulty could be resolved if the amount of ^{40}K in the mantle were lower than commonly estimated (Albarède, 1998; Davies, 1999; Lyubetskaya and Korenaga, 2007b). Another reconciliation is that this, as well as the heat–helium imbalance and the apparent need for a deep ^{3}He reservoir, could be reconciled if the estimate of ^{40}Ar in the shallow mantle, which comes from measured short-term ^{3}He fluxes into the oceans, were too low by a factor of 3.5 (Ballentine et al., 2002). It is important to note that the possibility of K in

the core does not help with this paradox, because it is the imbalance between mantle Ar and K that is the problem.

7.12.1.6.1.5 Neon, xenon, and krypton

Far less attention has been paid to isotopes of these elements, largely because of atmospheric contamination problems (Ballentine, 2002; Ballentine and Barford, 2000; Farley and Neroda, 1998), but some recent work has important implications for mantle processes. Neon has three isotopes (atomic weights 20, 21, and 22), of which ^{21}Ne is radiogenic and ^{20}Ne and ^{22}Ne are primordial. Measurements of ^{20}Ne/^{22}Ne in magmatic CO_2 well gases (Ballentine et al., 2005) provide the first unambiguous value for the convecting mantle noble gas abundance and isotopic composition and indicate that the upper mantle has a ^{20}Ne/^{22}Ne similar to that of solar wind-irradiated meteorites (~12.5, so-called Neon-B), which is significantly lower than ^{20}Ne/^{22}Ne of the solar nebula (13.6–13.8). This Neon-B value is reproduced in samples from Iceland and Hawaii (Trieloff et al., 2000) and Réunion (Hopp and Trieloff, 2005). Some studies (e.g., Dixon et al., 2000; Honda et al., 1999; Moreira et al., 2001) have argued for a solar component based on extrapolating plots of ^{20}Ne/^{22}Ne versus ^{21}Ne/^{22}Ne, but their measured ^{20}Ne/^{22}Ne values are not higher than the Neon-B value. However, some samples from Iceland (Harrison et al., 1999) and the Kola Peninsula (Yokochi and Marty, 2004) appear to have ^{20}Ne/^{22}Ne > 12.5, which if verified would represent a minor component.

These measurements imply that the convecting mantle is dominated by neon gained by solar wind irradiation of accreting material (Neon-B) but that another 'solar' component might exist, sometimes sampled by plumes, associated with early accreted material with a solar nebula composition. The latter might be in the deep mantle or core (Ballentine et al., 2005). Alteration by recycled material appears to have played a minimal role. While measured Xe and Kr ratios generally appear air-like (Ballentine, 2002), evidence for 'solar' Xe has also been detected in CO_2 well gases by Caffee et al. (1999). A recent analysis suggests that the mantle content of 'heavy' noble gases (i.e., Xe, Kr, and Ar) is dominated by ocean water subduction (Holland and Ballentine, 2006), consistent with the finding of Sarda et al. (1999) that a significant amount of mantle Ar is recycled. Subduction of oceanic lithosphere plays a strong role in generating heterogeneity in many isotopes, as discussed in the succeeding text.

7.12.1.6.2 The end-member 'zoo'

Analysis of the varying trace-element isotopic compositions of OIB and MORB, particularly those of Sr, Nd, Hf, and Pb, suggests that they are the result of mixing between several 'end-members,' which are typically referred to as DMM, HIMU, EM1, and EM2 (Carlson, 1994; Hofmann, 2003; White, 1985, 2010; Zindler and Hart, 1986). Additionally, considering He data leads to a further component, commonly referred to as FOZO. The common interpretations of these will be discussed later. Another approach to understanding heterogeneity and its origins has been to identify the key directions (rather than end-members) in isotopic space using a principal component analysis or independent component analysis, which suggest that the observed variation is the result of only a few processes: according to Stracke (2012), 94.3% of the isotopic variation in oceanic basalts can be fit by two principal components corresponding to the DMM–PREMA trend and Pitcairn-like enriched mantle (EM), and adding Samoa-like EM and HIMU brings the fit to 99.2%; the independent component analysis of Iwamori et al. (2010) finds that 99.4% of the variance can be explained by only 3 independent components, which may be caused by oceanic melting followed by crustal recycling and segregation, variations in the amount of water, and continental crust.

7.12.1.6.2.1 Depleted MORB mantle

This end-member represents the most depleted MORB. Most MORBs are not as depleted as DMM, but plot on the DMM–FOZO trend.

7.12.1.6.2.2 High μ

μ is the ratio ^{238}U/^{204}Pb. As U and Th decay into ^{207}Pb and ^{206}Pb with time, high μ leads to a high ratio of radiogenic to primordial lead, that is, ^{206}Pb/^{204}Pb – a 'radiogenic' signature. This component is typically interpreted to be recycled oceanic crust (Allegre and Turcotte, 1986; Chase, 1981; Hofmann, 1997; Hofmann and White, 1982). However, as U and Pb are approximately equally compatible (or U is slightly more incompatible) when making oceanic crust, some additional mechanisms must be invoked to fractionate U and Pb to make the HIMU signature. The invoked mechanisms are hydrothermal removal of Pb from the subducted slab into subduction-related magmas (Hofmann, 1988) and enrichment of the oceanic crust in continental U carried by eroded sediments.

7.12.1.6.2.3 Enriched Mantle 1 and 2

These signatures are observed in OIBs, but their origin is still under discussion. Leading explanations are Carlson (1994) and Hofmann (2003): EM1 may originate from either recycling of delaminated subcontinental lithosphere or recycling of subducted ancient pelagic sediment (e.g., Rapp et al., 2008), while EM2 may be recycled oceanic crust with a small amount of sediment, melt-impregnated oceanic lithosphere, or sediment contamination of plume-derived magmas as they pass through the crust.

7.12.1.6.2.4 Focus zone

This corresponds to the high ^{3}He/^{4}He component and in other isotopes has a composition on or close to the DMM–HIMU trend. Samples from many OIB associations appear to form linear trends that radiate from focus zone (FOZO) to various enriched compositions (Hart et al., 1992; Hilton et al., 1999). FOZO is also referred to as PREMA (prevalent mantle) (Stracke, 2012). Components that are very similar to FOZO are C (Hanan and Graham, 1996), PHEM (primitive helium mantle) (Farley et al., 1992), PREMA (Zindler and Hart, 1986), and HRDM (^{3}He recharged depleted mantle) (Stuart et al., 2003). A detailed discussion of the similarities and differences between these (as well as between FOZO and HIMU) is given by Stracke et al. (2005) and Stracke (2012), who argued that FOZO/PREMA is a ubiquitous component that is most likely related to subducted MORB/eclogite, something that is also concluded in the independent component analysis of isotopes in OIBs and MORBs by Iwamori and Albarede (2008).

7.12.1.6.2.5 Isotopic 'Ages'

As discussed earlier, isotope ratios evolve along separate paths in different materials due to fractionation of radiogenic parent and daughter elements during melting and subsequent radiogenic ingrowth of daughter isotopes. The resulting slopes on isotope diagrams indicate an age of fractionation and are widely used to date geologic processes. Even though the mantle has undergone continuous differentiation rather than a single differentiation event, plots of $^{207}Pb/^{204}Pb$–$^{206}Pb/^{204}Pb$ from MORB and OIB samples display a coherent line, or 'pseudoisochron,' from which an 'effective age' can be calculated. The Pb system has the advantage that Pb isotopes do not fractionate from each other on melting, which is a disadvantage with, for example, the Sm–Nd system. Pb–Pb plots display a trend from DMM to the highly radiogenic HIMU end-member. The Pb–Pb pseudo-isochron ages for various MORB and OIB groups correspond to effective ages of 1.5–2 Gy (Hofmann, 1997), although the exact meaning of these ages is not straightforwardly interpretable (Albarède, 2001; Hofmann, 1997). A recent mathematical analysis reveals that for ongoing differentiation, the Pb–Pb 'pseudo-isochron' age is generally much larger than the average age of crustal differentiation (Rudge, 2006).

7.12.1.6.2.6 Lead paradoxes

Another constraint is that all oceanic basalts and most MORB plot to the high $^{206}Pb/^{204}Pb$ side of the geochron, implying that the mantle has experienced a net increase in μ and implying that there is a hidden reservoir of unradiogenic (low μ) material. This problem is still unresolved and is discussed in more detail in Hofmann (2003) and Murphy et al. (2003). A second lead paradox, often called the kappa conundrum, is related to the discrepancy between measured $^{208}Pb/^{206}Pb$ ratios and the ratio of their parents, $\kappa = {}^{232}Th/^{238}U$. A layered-mantle 'steady-state' solution to this was proposed by Galer and O'Nions (1986), with a more recent layered solution proposed by Turcotte et al. (2001). Other recent work has focused on reconciling it with whole-mantle convection; a reasonable resolution is starting to recycle uranium into the mantle ~2.5 billion years ago (Elliott et al., 1999; Kramers and Tolstikhin, 1997).

7.12.1.6.2.7 Other isotopes

Several other isotopes give clues about long-term storage of oceanic crust and the origin of isotopic heterogeneity; some examples are given here. Cabral et al. (2013) used sulfur isotopes in plume lavas to infer subducted crust older than 2.45 billion years. Chauvel et al. (2008) used Hf–Nd array to infer that the source of OIBs must include subducted oceanic sediments as well as subducted MORB. Cottrell and Kelley (2013) examined the oxidation state of MORB, finding fine-scale variations in which the EM is more reduced than depleted mantle, which may be related to the action of carbon producing enriched, reduced magmas.

7.12.1.6.3 Nd isotopes and early differentiation and mixing processes

The Sm–Nd system has two decays that are of geochemical usefulness: ^{147}Sm decays to ^{143}Nd with a half-life of 103 Ga, and ^{146}Sm decays to ^{142}Nd with a half-life of 106 Ma. The latter system, in particular measurements of ^{142}Nd anomalies in Archean rocks, has in recent years given us great new insights into processes happening in the first few 100 Ma, as reviewed in Caro (2011).

Firstly, the presence of ^{142}Nd anomalies in some cratonic rocks indicates an early formation (4.39–4.42 Ga) of primordial crust. Several lines of evidence suggest that this was related to crystallization of a global magma ocean, nonfractional in the lower mantle but fractional in the upper mantle (see **Section 7.12.1.5.1**). This Hadean reservoir remixed on a timescale of >1 Ga (Debaille et al., 2013), leading to homogeneous ^{142}Nd ratios in the modern mantle.

Secondly, the ^{142}Nd composition of the measurable Earth is different from that of chondrites, for which two explanations have been proposed:

(i) The early formation of an EER that has never remixed (Boyet and Carlson, 2006; Carlson and Boyet, 2008) and is probably located at the base of the mantle. This could also hold other 'missing' trace elements discussed earlier. A problem with this is that it would be expected to be sampled in some mantle plumes, but there is no clear evidence for this.

(ii) A nonchondritic Earth. A nonchondritic Earth might result from impact erosion of early crust that was enriched in incompatible elements (O'Neill and Palme, 2008); the isotopic similarity of the Earth and Moon suggests that this would have occurred before the Moon-forming impact (Caro, 2011). Campbell and O'Neill (2012) pointed out that a nonchondritic Earth also helps resolve other geochemical paradoxes, including those related to He and Ar (**Section 7.12.1.6.1**).

More constraints are needed to distinguish which of the previously mentioned possibilities is correct. While Rizo et al. (2012) found geochemical evidence for a Hadean enriched reservoir in 3.7 Ga old rocks, this could be caused by proto-crust rather than EER. Evidence for a very old primitive reservoir with high $^{3}He/^{4}He$ and a Pb isotopic age of about 4.5 Ga was found in relatively recent rocks by Jackson et al. (2010), but these also do not distinguish the two possibilities: from ratios of Nd and other isotopes, the reservoir could be either the residual reservoir from EER formation or the original nonchondritic Earth.

7.12.1.7 Length Scales: Geochemical and Seismological

Of primary interest for understanding mantle mixing processes and the preservation of chemical end-members is the length-scale distribution of chemical heterogeneity in the mantle, so this section reviews constraints from geochemical and seismological observations. In general, it is observed that heterogeneity exists at all scales, but quantitative constraints on the spectrum are minimal.

7.12.1.7.1 Geochemical scales

Chemical heterogeneity is observed at all scales (Carlson, 1987, 1994; Meibom and Anderson, 2004), even within the relatively uniform MORB source. For example, at the smallest

scale (i.e., melt inclusions in olivine phenocrysts), Pb isotope ratios in OIB span a large fraction of the global range (Hauri, 2002; Saal et al., 1998; Sobolev, 1996; Sobolev et al., 2000; Sobolev and Shimizu, 1993), while Nd ratios in the Ronda peridotite massif in Spain exceed the global OIB Nd ratio variation (Reisberg and Zindler, 1986). According to Sobolev et al. (2000), extreme heterogeneity of trace-element patterns in olivine phenocrysts at Hawaii indicates that the isotopic signature is maintained up to crustal magma chambers, limiting the scale of heterogeneities in the source region to a few kilometers or less. At the centimeter to meter scale, mantle rocks outcropping in peridotite massifs have been observed to contain centimeter to decimeter thick isotopically enriched pyroxenite veins embedded within a mostly depleted peridotite matrix (Pearson et al., 1993; Polve and Allegre, 1980; Reisberg and Zindler, 1986; Suen and Frey, 1987). Such variations have inspired the proposal of a 'marble cake' or 'plum pudding' style of chemical variation in the mantle, in which small volumes of enriched material reside within a matrix of depleted MORB mantle (DMM) (Allegre and Turcotte, 1986), a concept that has been the topic of much recent investigation as discussed in later sections. At the longest scale, there is also abundant evidence for compositional heterogeneity at scales of >1000 km in the form of the Dupal anomaly (Castillo, 1988; Dupre and Allegre, 1983; Hart, 1984; Klein et al., 1988; Schilling, 1973), a $\sim 10^8\,km^2$ region centered in the Indian Ocean that stretches in an almost continuous belt around the Southern Hemisphere between the equator and 60° S and is characterized by its anomalous Sr and Pb ratios.

Limited information exists about the spectrum of geochemical heterogeneity from sampling variations in isotope ratios along mid-ocean ridges. An early compilation of $^{87}Sr/^{86}Sr$ data from MORB and OIB (Gurnis, 1986b) seemed consistent with a flat or 'white' spectrum, but the wealth of data that have been gathered since then reveal more complex patterns. The spectrum of $^{3}He/^{4}He$ for 5800 km of the Southeast Indian Ridge displays periodicities of 150 and 400 km (Graham et al., 2001), which was interpreted to be indicative of upper mantle convection. Using new high-resolution MC-ICPMS data, Agranier et al. (2005) plotted the spectra of various isotope ratios along the Mid-Atlantic Ridge, finding two distinct signals. The first is a 6–10° length scale signal visible in Pb, Sr, and He ratios and the principal component 1, which is associated with the Iceland hot spot, while the second is a power-law spectrum with a slope of -1 visible in Nd, Hf ratios and principle component 2, which is perhaps indicative of dynamics stretching processes discussed later. Graham et al. (2006) found a bimodal distribution of hafnium isotope ratios along the Southeast Indian Ridge, which appears to indicate compositional striations with an average thickness of ~40 km in the upper mantle.

7.12.1.7.2 Seismological scales

The long-wavelength spectrum of heterogeneity is revealed by global seismic tomographic models, but much of the heterogeneity at this wavelength is thermal. There have, however, been attempts to separate thermal and chemical components to the seismic velocity variations (e.g., Forte and Mitrovica, 2001; Ishii and Tromp, 1999; Mosca et al., 2012; Romanowicz, 2001; Simmons et al., 2010; Trampert et al., 2004). Particularly notable are those studies that use normal mode splitting data because these are sensitive to density variations, providing an additional constraint. In particular, at the longest wavelengths of 1000s km, Ishii and Tromp (1999), Trampert et al. (2004), and Mosca et al. (2012) found that a substantial fraction of the shear wave heterogeneity in the deepest mantle is due to compositional variations and that the two low-velocity 'megaplumes' seen in global tomographic models seem to have dense material at their bases. Short-wavelength heterogeneity is constrained by scattering: short-period precursors to PKP reveal the presence of small ~8 km, weak (1% rms.) velocity perturbations throughout the mantle (Hedlin et al., 1997). There are strong regional differences in scattering strength (Hedlin and Shearer, 2000), with strong scattering beneath South and Central America, eastern Europe, and Indonesia, and some correlation with large-scale anomalies revealed by seismic tomography including the African superplume and Tethys Trench. Other types of seismic observation find structure with a gradient in velocity that is too large to be explained by diffusive thermal structures, including a dipping low-velocity layer in the mid lower mantle (Kaneshima and Helffrich, 1999) and sharp sides to the deep mantle 'superplumes' beneath Africa and the Pacific (Ni et al., 2002). Kaneshima and Helffrich (2009) found scatters of size ~10 km in the lower mantle at depths 1100–1800 km beneath the Pacific subduction zones, consistent with folded MORB. In summary, while there is ample seismic evidence for chemical heterogeneity in the mantle, it is not sufficient at this point to constrain the spectrum over all wavelengths, and in particular not to the sub-kilometer wavelengths to which subducted MORB is expected to be stretched.

The spectrum of heterogeneity expected from stirring theory is discussed in **Section 7.12.2.7**.

7.12.1.8 Geophysical Constraints in Favor of Whole-Mantle Convection

A number of types of geophysical evidence argue that mantle convection is not completely layered at the 660 km discontinuity, which is in conflict with the earliest models based on mass balance of Ar and other trace elements discussed earlier.

Firstly, seismological observations have long favored penetration of slabs into the lower mantle. While arguments initially revolved around interpreting travel times (Creager and Jordan, 1984, 1986), subsequent three-dimensional regional or global seismic tomographic models (Fukao, 1992; Fukao et al., 1992; Grand, 1994; Masters et al., 2000; Van der Hilst et al., 1997) clearly show slabs penetrating immediately in some areas or penetrating after a period of stagnation in other areas, although it has also been argued that thermal coupling in a two-layered convection could produce similar features (e.g., Cizkova et al., 1999). Significant flow stratification should lead to a strong decorrelation in global tomographic models across 660 km depth, which is not observed (Jordan et al., 1993; Puster and Jordan, 1994, 1997; Puster et al., 1995). Subsequent tomographic models have also revealed some upwelling plumes that appear to be continuous across the whole depth of the mantle (Montelli et al., 2004), although there is an active debate on this topic. Recent regional tomography appears to show plumes extending to at least the top of the lower mantle beneath (Wolfe et al., 2011) and Iceland (Shen et al., 1998), and both tomography and

660 km boundary topography indicate a plume below Yellowstone (Schmandt et al., 2012; Smith et al., 2009).

Several types of geodynamic evidence also favor penetration of flow into the lower mantle. Firstly, if the 660 km discontinuity were a total barrier to convection, then there would be a strong TBL at the base of the upper mantle, and all of the heat coming from the lower mantle would be carried by strong upwellings in the upper mantle. As demonstrated by Davies (1988), such pervasive strong hot upwellings would violate constraints based on the topography and geoid of the ocean floors, which instead appear to be passively spreading. Identifiable hot-spot swells assumed to be caused by upwelling plumes only account for 6–10% of the global heat flow (Davies, 1988; Sleep, 1990). Secondly, modeling the global geoid and dynamic topography using driving forces derived from seismic tomography indicates a better fit to observations with whole-mantle flow than with layered flow (Hager et al., 1985; Hager and Richards, 1989; Ricard et al., 1988, 1989), although some successful fits are possible with layered models (Wen and Anderson, 1997). A third line of evidence comes from correlating global tomographic models with the spatial locations of subduction zones in the past 140–180 Ma (Kyvalova et al., 1995; Richards and Engebretson, 1992; Scrivner and Anderson, 1992): Past subduction appears to match well with lower mantle tomography, implying that the subducted slabs are in the lower mantle. Extending this approach, 3-D mantle structure models have been constructed by combining historical plate reconstructions with a global flow solver, and the results show a reasonable match to fast structures observed in global tomographic models (Bunge et al., 1998; Deparis et al., 1995; Megnin et al., 1997; van der Meer et al., 2009). Finally, numerical convection models indicate that the endothermic phase transition at 660 km depth is too weak to completely layer the flow at present-day convective vigor – only intermittent regional layering is plausible (Bunge et al., 1997; Christensen and Yuen, 1985; Machetel and Weber, 1991; Peltier and Solheim, 1992; Tackley et al., 1994), although this does not rule out chemical layering per se, as chemical layering with a large enough density contrasts is additive to the phase change buoyancy effect (Christensen and Yuen, 1984).

While complete layering at 660 km depth seems ruled out, there is evidence in favor of chemical layering in the lowest approximately few hundred km of the mantle, perhaps localized in certain regions. Firstly, the D″ region has long been found to be seismically highly heterogeneous (e.g., Lay and Garnero, 2004), which might require compositional variations to explain. Second, long-wavelength seismic tomographic models robustly find two large regions of low seismic velocity underneath Africa and the Pacific. While these might plausibly be smeared-out groups of narrow plumes (Schubert et al., 2004), seismic evidence indicates that these are not purely thermal in origin, including (i) the lack of correlation and anomalous scaling between *P*-wave and *S*-wave velocities in the deepest part of the mantle (Bolton and Masters, 2001; Ishii and Tromp, 2004; Kennett et al., 1998; Masters et al., 2000; Saltzer et al., 2004; Simmons et al., 2010), (ii) negative correlation between bulk sound velocity and shear wave velocity (Antolik et al., 2003; Kennett and Gorbatov, 2004; Su and Dziewonski, 1997), (iii) a positive density anomaly, according to some models that use normal mode splitting data (Ishii and Tromp, 1999; Mosca et al., 2012; Trampert et al., 2004), and (iv) sharp sides, which are difficult to maintain with a diffusive thermal field (Luo et al., 2001; Wen, 2001, 2002). Some thermochemical convection models discussed later produce structures that are consistent with these seismological observations.

It has also been argued that geophysical evidence favors a ~1300 km deep, highly undulating layer in the deep mantle (Kellogg et al., 1999; van der Hilst and Karason, 1999). The boundary of this should, however, produce strong observable signatures (heterogeneity and scattering) that have not presently been found (Castle and van der Hilst, 2003a, b; Tackley, 2002; Vidale et al., 2001). At the present time, the evidence favors a deeper layer that is probably not global (see also **Chapter 7.11**).

7.12.1.9 Overview of Geochemical Mantle Models

Before discussing the geophysical findings regarding thermochemical convection, it is useful to give an overview of the major models that have been proposed to explain geochemical observations and reconcile geochemical and geophysical observations. Some of these are discussed in more detail in the final section. Rather than discuss a large number of proposed models, some of which have similarities, it is useful to discuss the two main characteristics that differ among models and that tend to be the aspects that models focus on. **Figure 2** schematically represents the main models.

7.12.1.9.1 Vertical layering

7.12.1.9.1.1 Layered at 660 km

The traditional layered model is chemically and dynamically stratified at the 660 km discontinuity (e.g., slabs do not penetrate), with the upper mantle being a depleted, degassed region that is the complement of the continental crust, and the lower mantle being primitive – the repository for 50% of the BSE's argon, for the high $^{3}He/^{4}He$ component, and for other trace elements that are missing from the (MORB source + continental crust) according to mass balance calculations (Allegre et al., 1996). Variations on this model include intermittent breakdown of layering (Stein and Hofmann, 1994), the idea that this layering broke down in recent history (Allegre, 1997), and the model of Anderson (1995), in which the upper mantle is divided into an enriched shallow layer (the source of OIBs) and a depleted transition zone (the source of MORB). This model is contradicted by a number of geophysical observations, as discussed in **Section 7.12.1.8**.

7.12.1.9.1.2 Deep, highly undulating layer (hidden anomalous layer)

This model, proposed by Kellogg et al. (1999), is conceptually similar to the traditional layered model except that the layer boundary is moved downward to ~1300 km above the CMB, undulating by ~1000 km. Recycled components reside on top of the layer. The layer is 'hidden' because the seismic wave velocity anomalies caused by the different composition and higher temperature cancel out. While this proposal has been thought-provoking and has stimulated increasing progress toward findings a unified model, it should produce a seismic signature that is not found, as discussed in **Section 7.12.1.8**.

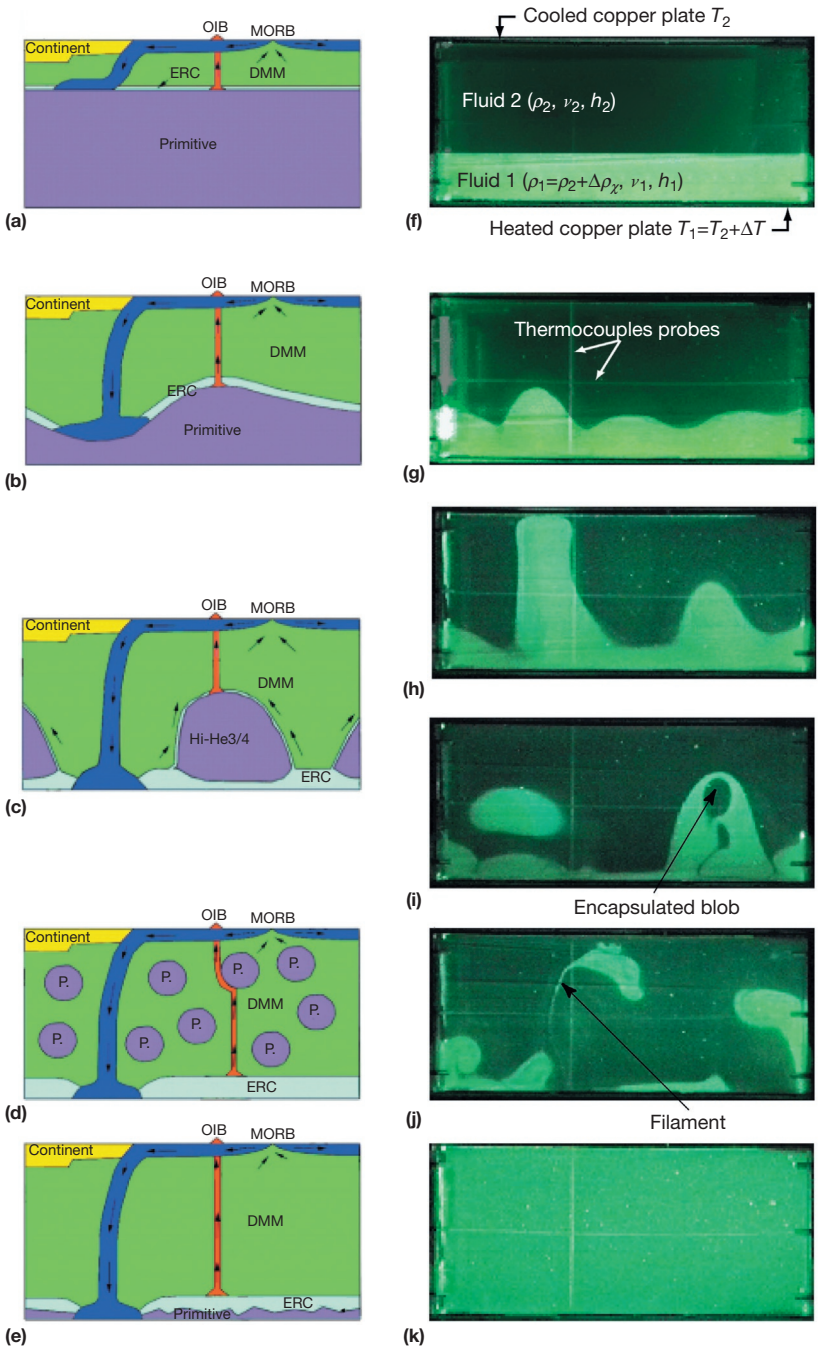

Figure 2 Various mantle models proposed to explain geochemical observations compared to results from a laboratory experiment at different times in its evolution, taken from Le Bars and Davaille (2004b). Cartoons in the left column are from Tackley (2000). (a) Layered at the 660 km discontinuity, (b) deep, high-topography hidden layer (Kellogg et al., 1999), (c) 'piles' (Tackley, 1998) or 'domes' (Davaille, 1999a), (d) primitive blobs (Becker et al., 1999; Davies, 1984; du Vignaux and Fleitout, 2001; Manga, 1996), (e) whole-mantle convection with thin dense layer at the base. (f)-(k) show the results of a laboratory experiment, which goes through different phases that display similar structure to the cartoons in the left column. Time increases from top (f) to bottom (k).

7.12.1.9.1.3 Thin layer (D″ region)

A approximately few hundred km thick layer above the CMB, perhaps highly undulating and/or localized into certain areas, and which could potentially contain primitive material, recycled material, or some mixture of the two, is a possibility. It has long been proposed that such a layer could contain recycled oceanic crust that provides the HIMU signature (Hofmann and White, 1982). Such oceanic crust contains a higher concentration of incompatible trace elements than primitive material so could also account for the 'missing' trace elements (about 1/3 of the total inventory of heat-producing elements according to Coltice and Ricard (1999)).

Whether such a layer could exist depends on the density contrast of subducted MORB at these high pressures and temperatures, as discussed in Section 7.12.3.3.2. It has been argued that this enriched layer may have formed shortly after the Earth's accretion process (Boyet and Carlson, 2005; Tolstikhin and Hofmann, 2005; Tolstikhin et al., 2006). Another proposal is that the layer preferentially contains oceanic crust containing oceanic plateaus, with normal oceanic crust not reaching this depth (Albarède and van der Hilst, 2002). Seismological observations support the existence of an intermittent layer that may extend several hundred km above the CMB, as discussed in Section 7.12.1.8.

7.12.1.9.2 Distributed heterogeneity

Instead of, or as well as, radial stratification, lateral compositional heterogeneity is thought to exist. An early justification for this was that mantle rocks outcropping in peridotite massifs have been observed to contain centimeter to decimeter thick isotopically enriched pyroxenite veins embedded within a mostly depleted peridotite matrix (Pearson et al., 1993; Polve and Allegre, 1980; Reisberg and Zindler, 1986; Suen and Frey, 1987). Such variations have inspired the proposal of a 'marble cake' or 'plum pudding' style of chemical variation in the mantle, in which small volumes of enriched material reside within a matrix of DMM (Allegre and Turcotte, 1986), a concept that has been the topic of much recent investigation as discussed in later sections, with several variations and refinements proposed. At the larger scale, it has been proposed that very large (~100 km scale) blobs may exist (Becker et al., 1999). Seismic scattering supports distributed heterogeneity, as discussed in Section 7.12.1.7. Dynamically, key issues are how rapidly distributed heterogeneity gets mixed (Section 7.12.2), which will be influenced by any composition dependence of viscosity (Section 7.12.2.3.5).

7.12.1.10 Mantle–Exosphere (Biosphere) Interactions: Water and Carbonate Cycling

Cycling of volatiles (particularly water and carbonate) between the interior and fluid envelope of a terrestrial planet could play a major role in the evolution of the fluid envelope and hence the long-term habitability of the surface environment. The mantle influences the fluid envelope by volatile outgassing associated with volcanism and by volatile recycling back into the interior. Indeed, a long-term cycle associated with carbonate recycling and reoutgassing may provide a critical feedback mechanism that maintains surface temperature in a habitable range (Kasting et al., 1993b; Sleep and Zahnle, 2001; Walker et al., 1981). Even on a plate tectonics timescale, changes in global subduction and spreading rates could influence climate (Lee et al., 2013). Volatile recycling also affects the redox state of the mantle, which, through outgassing, influences the redox state of the atmosphere (Delano, 2001; Kasting et al., 1993a; Lecuyer and Ricard, 1999; Trail et al., 2011; Zahnle et al., 2010), and may have been responsible for the rapid rise in atmospheric oxygen ~2 Gy ago (Kump et al., 2001). Crucial to recycling is the existence of plate tectonics, through which carbonate, water, and other volatiles are subducted into the mantle (e.g., Ruepke et al., 2004). Thus, the existence of plate tectonics on Earth may be important for long-term habitability.

Multiple feedbacks exist in the fluid envelope–mantle–core system. Both water and carbonate affect the physical properties of the mantle. Water strongly affects the viscosity of silicates (Hirth and Kohlstedt, 1996; although this has been disputed (Fei et al., 2013)), so water exchange between the mantle and exterior may have had important influences on the evolution of the coupled system. Furthermore, water greatly reduces the strength of the lithosphere through its effect on faults and the yield strength and is thus commonly thought to be necessary for plate tectonics to exist. Thus, the convective regime and heat flow out of the mantle are strongly affected by the fluid envelope through the influence of water on mantle viscosity and plate tectonics. Water also influences silicate melting, substantially reducing the solidus (see also Chapter 7.07).

Carbon is also important inside the mantle because it influences the physical properties, in particular having a major effect on melting and making water more mobile. In contrast to water, the amount of carbon in the Earth's interior is far greater than the amount in the exosphere. Detailed reviews of the origin and distribution of Earth's carbon and its influence on magma ocean and long-term processes can be found in Dasgupta (2013) and Dasgupta and Hirschmann (2010). Carbon's influence on silicate melting is greater than that of water, reducing the solidus by 100s K. Carbon can be present either as carbonated minerals or as diamond or graphite; indeed, Walter et al. (2011) found diamonds inferred to have formed in the lower mantle in subducted MORB. Carbonated melt could form in trace volumes and extract trace elements from great depth. Rohrbach and Schmidt (2011) found that carbonate-induced melting may occur in subducted lithosphere in the transition zone and lower mantle and freeze to form diamond. Later, diamonds could cause deep-seated melting at ~660 and ~250 km depth. Dasgupta et al. (2013) found that the depth of onset of melting under ridges is ~180 km for dry carbonated peridotite and 220–300 km for hydrated carbonated peridotite, although Stagno et al. (2013) obtained a shallower depth of 150 km due to a higher oxygen fugacity.

Modeling studies on the subduction of water and the influence of water on mantle thermal and geochemical evolution are discussed in Section 7.12.5.3. The influence of carbonate has so far been ignored in mantle modeling studies.

7.12.2 Mantle Stirring and Mixing of Passive Heterogeneities

7.12.2.1 Stirring, Stretching, Mixing, and Dispersal

It is important to distinguish between different concepts that are all sometimes loosely referred to as 'mixing.' Strictly speaking, 'mixing' involves homogenization of the chemical differences by a combination of stirring and chemical diffusion. Stirring involves stretching, which is the process by which an initial 'blob' of chemically distinct material is elongated into a thin tendril or lamella by strain caused by the convective flow. This greatly increases the surface area of the heterogeneity and decreases its width, facilitating chemical diffusion. Chemical diffusion of most elements is extremely slow, acting over length scales of centimeters to meters over geologic time; thus, it is necessary to stretch heterogeneities to this scale before they can be mixed. As will be discussed later, however,

observed MORB or OIB compositions probably involve averaging over a volume that is larger than this, so stretching to diffusion scales may not be necessary to eliminate the signature of an individual heterogeneity during melting. Furthermore, the presence of partial melt greatly increases the rate of chemical diffusion.

'Dispersal' refers to the dispersal of initially proximal heterogeneities evenly around the mantle. While this occurs partly by similar processes to stretching (i.e., the increasing separation of two initially very close points), effective dispersal involves material transport across convective 'cells.' It is possible in some flows for rapid stretching to occur within a cell, but for intercell transfer to be slow. Conversely, as will be discussed later, high-viscosity blobs undergo very slow stretching but may get rapidly dispersed around the domain.

Many of the concepts introduced in this section are illuminatingly illustrated in the review of van Keken et al. (2003). See also **Chapter 7.02**.

7.12.2.2 Stretching Theory: Laminar and Turbulent Regimes

7.12.2.2.1 Finite deformation tensor

The mathematical description of finite deformation was presented by McKenzie (1979) following Malvern (1969). We are interested in the deformation tensor relating the vector $\mathbf{y}'(t)$, which joins two particles in a fluid element at positions $x_1'(t)$ and $x_2'(t)$, to $\mathbf{y}$, the vector joining the same two particles at $t=0$:

$$\mathbf{y}'(t) = \mathbf{F}(t)\mathbf{y} \qquad [4]$$

The $\mathbf{F}$ matrix is initially the unit matrix and evolves according to

$$D_t F_{ij} = L_{ik} F_{kj} \qquad [5]$$

where D_t is the Lagrangian time derivative and $\mathbf{L}$ is the velocity gradient tensor:

$$L_{ij} \equiv \frac{\partial v_i}{\partial x_j} \qquad [6]$$

that can also be written in the material frame (Farnetani et al., 2002), which is a combination of the strain rate tensor (symmetrical part of $\mathbf{L}$) and the vorticity tensor (antisymmetric part of $\mathbf{L}$).

As the $\mathbf{F}$ tensor has nine components in three dimensions, or four components in two dimensions, it is desirable to extract a simpler quantity to describe the stretching. In two dimensions, a convenient scalar measure is the logarithm of the aspect ratio of the strain ellipse (McKenzie, 1979), that is,

$$f(t) = \log_{10}(a/b) \qquad [7]$$

where a and b are the major and minor axes of the ellipse, respectively, and a/b can be found from the second invariant of the $\mathbf{F}$ tensor, that is,

$$a/b = \gamma + \left(\gamma^2 - 1\right)^{1/2};\ \gamma = \frac{1}{2} F_{ij} F_{ij} \qquad [8]$$

Some authors prefer to measure the change in the semimajor or semiminor axis of the strain ellipse, which is the square root (or one over the square root) of (a/b). In two dimensions, Kellogg and Turcotte (1990) showed how a complete description of the total deformation of a heterogeneity can be obtained by tracking only two quantities for each tracer, the aspect ratio $(a/b \equiv e)$ and orientation θ of the strain ellipse. In three dimensions, the strain ellipse becomes an ellipsoid; a simplified method of tracking it is given in Subramanian et al. (2009).

7.12.2.2.2 Asymptotic stretching rate

Two types of shear flow, simple shear and pure shear, result in two different asymptotic stretching behaviors termed laminar and turbulent, respectively (see **Figure 3**). The theory is described by Olson et al. (1984a,b) based on previous theory by Batchelor (1952, 1959) and Corrsin (1961) and is briefly summarized here (see also Ricard, **Chapter 7.02**).

Laminar mixing (**Figure 3(a)**) occurs in a simple shear flow and involves a linear increase in the cumulative strain ε with time t:

$$\varepsilon = \dot{\varepsilon} t \qquad [9]$$

where $\dot{\varepsilon}$ is the average strain rate experienced by the heterogeneity. A linear decrease with time occurs for the component of the wave number vector that is perpendicular to the velocity:

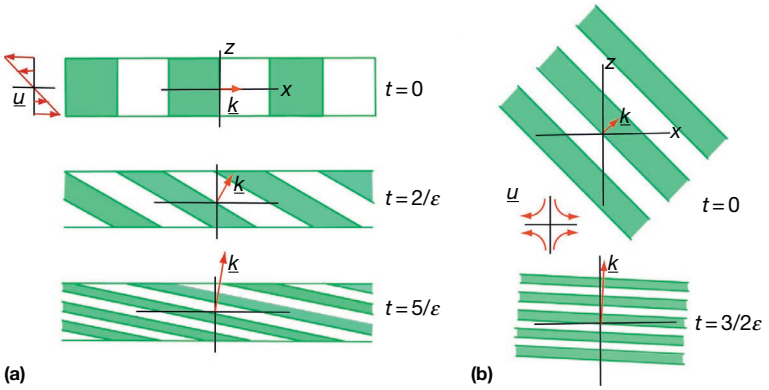

Figure 3 Diagrams illustrating the evolution of a single Fourier component of a passive anomaly for (a) uniform laminar shear flow and (b) stagnation point flow, based on Figures 4 and 5 of Olson et al. (1984b). The velocity field $\mathbf{u}$ is sketched for each case. In a uniform shear flow (a), the Fourier component is rotated into the direction of shear, while its wavelength decreases, such that the wave number magnitude $|\mathbf{k}|$ grows at a rate $\dot{\varepsilon}$, the Lagrangian strain rate. Near a stagnation point (b), the Fourier components also become rotated, this time into the direction of compression, but the wave number magnitude grows at a rate that is proportional to time, that is, $\dot{\varepsilon}t$.

$$k_x(t) = k_x(0);\ k_z(t) = k_z(0) + k(0)\dot{\varepsilon}t \qquad [10]$$

for a shear flow described as $\mathbf{u} = -\dot{\varepsilon}z\widehat{\mathbf{x}}$. This effectively describes a cascade of heterogeneity to shorter wavelengths, with 'blobs' being stretched into thin strips aligned with the direction of flow velocity. In the absence of diffusion, the Fourier amplitude of the heterogeneity does not change, it simply moves to higher k. For the case with diffusion, see the succeeding text.

Turbulent mixing is associated with pure shear (also known as normal strains (Olson et al., 1984a,b)), which occurs at stagnation points in convective flows (**Figure 3(b)**). In this case, the velocity is proportional to the distance from the stagnation point ($\mathbf{u} = -\dot{\varepsilon}z\widehat{\mathbf{x}} - \dot{\varepsilon}z\widehat{\mathbf{z}}$), so the cumulative strain increases exponentially with time:

$$\varepsilon = \exp(\dot{\varepsilon}t) \qquad [11]$$

with wave numbers evolving exponentially in both directions:

$$k_z(t) = k_z(0)\exp(\dot{\varepsilon}t);\ k_x(t) = k_x(0)\exp(-\dot{\varepsilon}t) \qquad [12]$$

As turbulent mixing is far more rapid than laminar mixing, it is important to establish which regime is most appropriate to characterize flows associated with mantle convection, so this has been a major focus of research. This issue has been investigated theoretically, for kinematically driven flows and for convectively driven flows. The general findings are that (i) the type of mixing can be quite sensitive to the exact flow, although greater time dependence results in a greater tendency toward turbulent mixing, and (ii) different 'blobs' may undergo substantially different rates of stretching in the same flow depending on their location in that flow. This is discussed in the next section.

Some semantic issues are worth noting: Firstly, the very high Prandtl number flow that the mantle undergoes should actually be termed laminar due to the unimportance of inertial terms; nevertheless, it can lead to the turbulent stretching regime. Secondly, turbulent mixing is often referred to as chaotic mixing, and laminar mixing is often referred to as regular mixing (see also **Chapter 7.02**).

7.12.2.2.3 Measures of stretching

Most measures of stretching are based on the elongation of an infinitesimal strain ellipse, that is, the ratio of the major axis to its original value (a/a_0), calculated using the equations in **Section 7.12.2.2.1** and tracked using infinitesimal tracer particles distributed throughout the domain. In two dimensions, the width of the strain ellipse is the inverse of this value. Values of (a/a_0) exhibit a considerable spread, so it is important to consider the range in values as well as the average. When the time-averaged stretching rate increases exponentially with time, the appropriate average to take is the median (Christensen, 1989a) or the geometric mean, which is related to the mean in logarithmic space. In this approach, the strain ellipse is always considered to be infinitesimal in size even if it reaches 10^{10} or larger, so these measures are not appropriate for estimating the separation of two initially closely spaced points, a quantity that cannot become larger than the size of the domain.

Other than the median or geometric mean stretching, it is useful to consider quantities that convey information about the distribution of strains. The statistical distribution of stretching can be plotted in various ways; for example, Kellogg and Turcotte (1990) plotted the probability distribution of strain (a/a_0 vs. number of tracers), the cumulative distribution (a/a_0 vs. fraction of particles exceeding (a/a_0)), and the time dependence of strain evolution (time vs. a/a_0 with different lines for the percentage of tracers exceeding a/a_0). An example of the latter quantity is the size reduction exceeded by 90% of tracers plotted by Christensen (1989a).

Often, the goal is to determine what fraction of heterogeneities has 'mixed,' in the sense of being stretched to less than the diffusive or sampling length scale. Kellogg and Turcotte (1990) plotted as a function of time the fraction of tracers that have been completely homogenized. Gurnis and Davies (1986b) were interested in heterogeneities that remained relatively intact, so they plotted as a function of time the fraction that has strain <5.

7.12.2.2.3.1 Lyapunov exponents

The Lyapunov exponent is the exponential coefficient for the rate at which two initially close heterogeneities are separated. This can be written as

$$\lambda\left(P, \vec{\gamma}\right) = \lim_{\substack{t\to\infty \\ \gamma\to 0}} \left[\frac{1}{t}\ln\left(\frac{\gamma(t)}{\gamma}\right)\right] \qquad [13]$$

where γ is the length of separation vector $\vec{\gamma}$ located at position P and $\gamma(t)$ is its length after a time t. This is zero for laminar stretching and positive or negative for exponential stretching. The value depends on the direction of $\vec{\gamma}$ relative to the velocity gradient tensor, so λ has maximum and minimum values. Kellogg and Turcotte (1990) used the maximum Lyapunov exponent and the minimum Lyapunov exponent to quantify the stretching (Wolf, 1986), and these are straightforwardly related to $\overline{\alpha}_e$, the average strain rate measured from the numerical experiments, by

$$\lambda_{\max} = \frac{\overline{\alpha}_e}{\ln 2} \qquad [14]$$

where

$$\overline{\alpha}_e = \frac{1}{\tau}\ln\left(\frac{a}{a_0}\right) \text{ or } a = a_0\ \exp(\overline{\alpha}_e\tau) \qquad [15]$$

In numerical applications, it is often more convenient to calculate the Lyapunov exponent using finite rather than infinitesimal time difference t, or finite separation γ, for example, by considering the motion of nearby tracers. Lyapunov exponents calculated using these finite quantities are referred to as finite-time or finite size Lyapunov exponents, respectively, and have been used in the mantle dynamics literature (Farnetani et al., 2002; Farnetani and Samuel, 2003; Ferrachat and Ricard, 1998, 2001).

In general, for finite quantities, we can write using the previous equations that

$$\frac{\gamma(t)}{\gamma(0)} = \frac{|\mathbf{F}(t)\mathbf{y}|}{|\mathbf{y}|} = \left(\frac{\mathbf{y}^{\mathrm{T}}\mathbf{F}^{\mathrm{T}}(t)\mathbf{F}(t)\mathbf{y}}{\mathbf{y}^{\mathrm{T}}\mathbf{y}}\right)^{1/2} \qquad [16]$$

The maximum and minimum eigenvalues of the right Cauchy–Green strain tensor $\mathbf{F}^{\mathrm{T}}\mathbf{F}$ can then be used to calculate the maximum and minimum finite-time Lyapunov exponents (e.g., Farnetani and Samuel, 2003):

$$\lambda_{max} = \frac{1}{t} \ln \sigma_{max};\ \lambda_{min} = \frac{1}{t} \ln \sigma_{min} \qquad [17]$$

In 2-D incompressible flow, $\lambda_{min} - \lambda_{max}$.

The hyperbolic persistence time method is a method to analyze stable or unstable material trajectories (unstable meaning that nearby particle trajectories separate from it) and was introduced to the mantle community by Farnetani and Samuel (2003). Readers are referred to this paper for more details.

7.12.2.3 Stretching: Numerical Results

7.12.2.3.1 General discussion

A convective flow includes both stagnation points (e.g., at the corners of a 'cell'), which will be associated with pure shear and exponential stretching, and laminar regions (away from corners), which will be associated with simple shear and linear stretching. It is therefore likely that a heterogeneity will experience linear stretching most of the time, with the occasional episode of exponential stretching. Which regime dominates the long-term behavior depends on the details of the flow. If the flow is steady state and two-dimensional, then most of the heterogeneities never pass close to a stagnation point, so the average stretching rate follows a linear stretching law (McKenzie, 1979; Olson et al., 1984b). If the flow is highly unsteady, then the stagnation points move around and new ones are generated, allowing essentially all heterogeneities to pass close to stagnation point at some point and giving on average an exponential stretching rate. The overall behavior is, however, highly sensitive to the details of the time dependence, and this has been studied by a variety of models ranging from purely kinematic flows to purely convective flows (e.g., Christensen, 1989a). As all heterogeneities are not stretched at the same rate, it has proven important to study the range of stretching rates as well as the average. Most of the research has been done in two dimensions, so three-dimensional studies are discussed in a later section.

7.12.2.3.2 Steady-state 2-D flows

Steady-state 2-D Bénard convection cells follow the laminar stretching law, whether kinematic (Olson et al., 1984b) or convective (McKenzie, 1979). The fit to theory is reasonable for both nondiffusive and diffusive heterogeneities (Olson et al., 1984b). It is instructive to understand the resulting stretching regime as a baseline for interpreting more complex flows. Heterogeneities are stretched into spirals of lamellae that are locally oriented subparallel to the streamlines, because different streamlines are rotating at a different rate. For example, near the top of the domain, the lamellae are locally subhorizontal. In a completely heated-from-below steady-state Bénard convection cell, the interior of the cell (far from the boundaries) undergoes almost rigid-body rotation with an associated low stretching rate, but near the boundaries, where heterogeneities pass close to stagnation points in the corners, the cumulative strain can increase substantially (e.g., the aspect ratio of the strain ellipse (a/b) by a factor of 1000) over one rotation (McKenzie, 1979). It is interesting to note that strain does not increase monotonically, but rather as large oscillations with a superimposed linear trend (McKenzie, 1979). The parts of these oscillations where the strain decreases have been termed 'unmixing.' The addition of internal heating makes the situation more complex as there is no uniformly rotating area in the middle, but again, the cumulative strain (a/b) undergoes considerable oscillation and near the edge of the 'cell' can reach a factor of 100 over one rotation (McKenzie, 1979). The highest strain rates (hence velocity gradients) occur near the downwelling. For finite-sized bodies (initially cylinders), Hoffman and McKenzie (1985) found that for pure basal heating, the amount of stretching was rapid for a blob initially situated near the edge of the flow, but with internal heating, the blob became deformed but not greatly stretched in one revolution.

Steady corner flows relevant to mid-ocean ridges and subduction zones have also been studied (McKenzie, 1979). The most severe strain ($a/b \sim 30$) was experienced in the corner above a subducting slab, with the principal axis of the strain ellipse aligned subparallel to the streamline. Again, strain does not necessarily increase monotonically with time.

7.12.2.3.3 Time-dependent 2-D flows

Various types of 2-D flow have been studied, including purely kinematic flows, purely convective flows, and convective flows with kinematic upper boundary conditions. This has led to the identification of three main stirring regimes (Christensen, 1989a): a regime in which all particles are undergoing exponential stirring, a 'slow' regime similar to the laminar regime, and a hybrid regime in which some particles/regions are undergoing turbulent stretching while some are undergoing slow laminar stretching. Fully time-dependent convection with no kinematic constraints has always been found to give turbulent mixing, whereas controlling the flow with a kinematic upper boundary condition or fully kinematic description may lead to the 'slow' or hybrid regimes, though some kinematic flows lead to the turbulent mixing regime (e.g., Kellogg and Turcotte, 1990). More discussion of the factors that lead to these regimes now follows.

7.12.2.3.3.1 Slow stirring regime

In this regime, most heterogeneities are stretched into long streaks, but clumps exist where the streaks get folded, leading to the simultaneous existence of tendrils with average stretching rate and blobs with very slow stretching (Gurnis, 1986c) that can survive for up to tens of transit times. This regime has been observed in kinematically prescribed flows consisting of two counterrotating cells with a boundary that moves smoothly and periodically with time (Christensen, 1989a; Gurnis, 1986c; Gurnis and Davies, 1986b). While visually the system may look reasonably well mixed, the average stretching rate is slow compared to the other regimes and lies somewhere between exponential and linear with time (Christensen, 1989a; Gurnis, 1986c). Gurnis and Davies (1986b) also obtained a regime visually similar to this with a combination of convection and kinematic plates, but the asymptotic stretching rate was not analyzed.

7.12.2.3.3.2 Exponential stirring regime

In this regime, all heterogeneities experience exponential stretching, although at different rates. There are no unmixed islands or persistent large blobs. All fully time-dependent purely convective (i.e., with no kinematic control) 2-D flows in the mantle convection literature that have been suitably analyzed

are in this regime, including those in Christensen (1989a) and Hoffman and McKenzie (1985). So are kinematic flows in which there is an oscillation between a single-cell and a three-cell structure, like those of Kellogg and Turcotte (1990) and simplified versions in Christensen (1989a). A characteristic that this kinematic flow shares with time-dependent convection is the creation of new cell boundaries, which can occur due to plume formation, sublithosphere convection or delamination, or new subduction zone formation. In some cases, it can also be obtained by two-cell kinematic flow with the boundary motion containing more than one frequency component (Christensen, 1989a).

It is important to note that the effective stretching rate that goes into the exponential stretching law (sometimes called the Lagrangian strain rate (Coltice, 2005)) is much lower than the mean strain rate of the flow – ~10–30 lower according to Christensen (1989a). In two-dimensional convective flows with internal heating up to $Ra = 10^{10}$ and with basal heating up to $Ra = 10^{9}$, Coltice (2005) found that the Lagrangian strain rate scales in proportion to the convective velocity, that is, $Ra^{1/2}$ and $Ra^{2/3}$, respectively, even though the higher Ra flows are more time-dependent, implying that the stretching rate is simply proportional to the rate at which material is moving, provided the flow is time-dependent. This finding also applied to cases with a 100- or 1000-fold viscosity jump at mid depth.

7.12.2.3.3.3 Hybrid stirring regime

In this regime, most of the flow is exponentially stirred but there exist unmixed regions or 'islands' in the flow; the histogram of strain distributions can exhibit a bimodal distribution with one peak at very low strains (Christensen, 1989a). In the experiments of Christensen (1989a), this was found in relatively few cases – in two of the kinematic flows with more than one driving frequency. Nevertheless, it is a mode that is commonly observed in mixing experiments performed outside the solid Earth science community (see Metcalfe et al., 1995 and references therein). The wide range of stretching rates observed in this mode and the 'slow stirring' mode earlier indicate the importance of considering the range rather than only the median or mean.

The statistical range of heterogeneity stretching in the turbulent mixing regime was studied by Kellogg and Turcotte (1990) using a chaotic kinematic flow with time dependence driven by the Lorenz equations. Specifically, the flow had two cells, and the boundary between moved smoothly but chaotically such that sometimes, there was only one cell. Into this, they injected a large number of particles with different starting positions, in order to obtain robust statistics regarding their stretching. Naturally, exponential (turbulent) stretching was obtained, but the amount of strain experienced by different tracers varied very widely, such that after, for example, five overturns, the semimajor axis of the strain ellipse divided by its initial radius (a/a_0) averaged 10^4 but varied between ~10^1 and ~10^7 (first to ninety-ninth percentile) or ~10^2–~10^6 (tenth to ninetieth percentile). In other words, the (logarithmic) variation in cumulative strain is as large as the average cumulative strain. It is thus not meaningful to talk about precise quantities such as 'mixing time' based on average stretching; everything must be qualified in terms of probability distributions. The effective strain rate for this stretching was found to be 13% of the maximum strain rate that occurred at the stagnation point in the corner of the cell.

7.12.2.3.4 3-D flows

It may be expected that mixing in three dimensions is quantitatively different from that in two dimensions, but so far, studies have been few and appear contradictory about the sign of the change. Two key concepts are relevant:

(i) *Toroidal motion*. 3-D flows can have toroidal motion – the component of motion associated with rotation about a vertical axis and strike-slip motion – whereas 2-D flows (in a vertical plane) cannot. In steady-state 2-D flows, the streamlines (particle paths) are always closed, but in 3-D, the presence of toroidal motion can cause chaotic, space-filling particle paths, even if the flow is stationary in time (Ottino, 1989). One way of viewing this, as discussed by Ferrachat and Ricard (1998), is that toroidal motion increases by one the number of degrees of freedom of the Hamiltonian, for which one degree of freedom gives regular mixing and two degrees of freedom give chaotic flow. For steady-state flows driven by an upper boundary condition mimicking a spreading center with a transform offset, this effect was demonstrated by Ferrachat and Ricard (1998). Areas of rapid, turbulent mixing, as well as islands of laminar mixing, were identified based on Poincaré sections and maps of finite-time Lyapunov exponents. Quantitatively, a 3-D flow with zero toroidal component was found to give similar Lyapunov exponent to 2-D flow, while the addition of a toroidal component increased the exponents by a factor of ~2. A large lower mantle viscosity tends to confine toroidal motion to the upper mantle (Ferrachat and Ricard, 1998; Gable et al., 1991).

(ii) *Plumes versus sheets*. Because 3-D upwellings (and downwellings if slabs are not included) can be columnar plumes rather than infinite sheets, they have a smaller effect on disrupting the flow pattern and causing intercell mixing. This was apparent in time-dependent, constant-viscosity convection at Rayleigh numbers up to 8×10^5 calculated by Schmalzl et al. (1996): after several overturns, tracers had dispersed efficiently within individual cells (as indicated by histograms of tracer vertical positions), but dispersal between cells was much slower in 3-D than in equivalent calculations in 2-D. However, a subsequent suite of calculations comparing 2-D and 3-D (poloidal only) flows up to much higher Rayleigh numbers found that 2-D and 3-D flows have approximately the same Lagrangian strain rate (Coltice and Schmalzl, 2006). It could be that Rayleigh number is a key factor that was unrealistically low in the earlier studies.

Similar numerical mixing experiments in 2-D and 3-D were performed by Davies (2002) and Huang and Davies (2007a), respectively. In these, passive heterogeneities introduced by subduction were tracked with a focus on sampling statistics. They found essentially no difference between 2-D and 3-D for the diagnostics studied. In summary, these results plus those of Coltice and Schmalzl (2006) imply that overall mixing efficiency in 3-D is likely to be similar to that in 2-D with the same parameters. Toroidal motion may influence this and needs to be studied more in the future.

7.12.2.3.4.1 Particle trajectories

It is worth considering the particle trajectories in 3-D flows. In steady-state 3-D convection with zero toroidal component, intercell transfer is zero because individual flow lines lie on a two-dimensional distorted (but closed) toroidal surface (Schmalzl et al., 1995). Individual streamlines are generally not closed in a small number of orbits around the torus, but rather, the surface is progressively filled by the trace of a single streamline. Extreme shear strains can occur but mixing is in 2-D. This is illustrated in **Figure 4**. With the addition of time dependence, boundary layer instabilities perturb these 'toroidal' structures, allowing for cross cell mixing (Schmalzl et al., 1996). Here, it is important to note that the 'toroidal paths' followed by particles in a steady-state flow are completely different to the 'toroidal motion' caused by surface rotation and strike-slip motion – indeed, toroidal motion breaks up the tori found with purely poloidal motion (Ferrachat and Ricard, 1998). The only relevant laboratory experiments were the steady-state experiments of Richter et al. (1982) in which for convective rolls, blobs were smeared out into spiral sheets or corkscrews in a superimposed lateral motion, with more complicated topologies for spoke pattern convection, but still within individual cells and not cross cell.

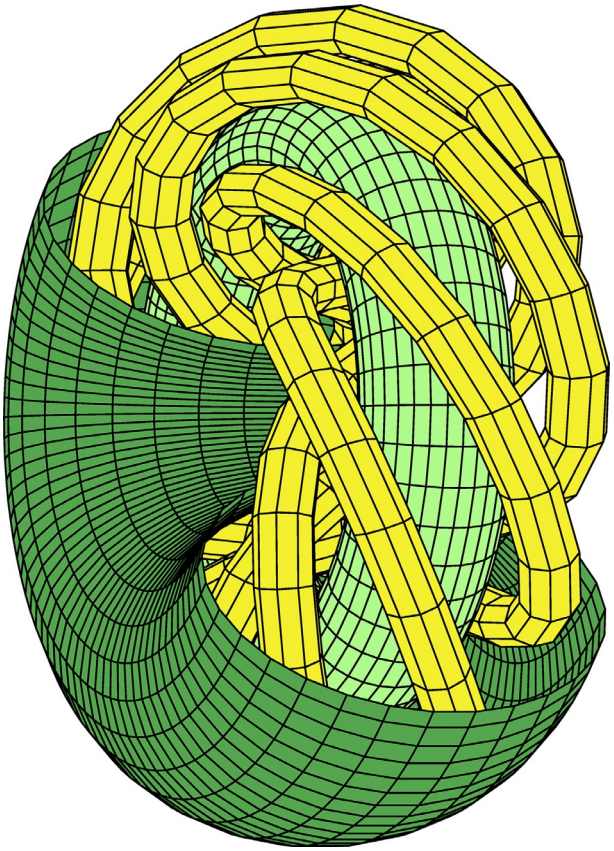

Figure 4 The topology of the pathlines for 3-D flow that is purely poloidal, extracted from a figure from Ferrachat and Ricard (1998). Individual tracer paths are restricted to tubes or tori, which they spiral round. Adding increasing amounts of toroidal motion breaks up the tubes and then the tori.

7.12.2.3.4.2 Spherical 3-D steady-state flows

The analysis of mixing in steady-state 3-D flows was extended to spherical geometry by van Keken and Zhong (1999), using a flow intended to be similar to the flow in the present-day mantle, that is, generated by buoyancy from a slab model combined with an approximate plate rheology. As with the simple flow of Ferrachat and Ricard (1998), only limited regions exhibited laminar mixing, with most other regions containing corkscrew-like particle tracks and probably chaotic mixing: The areas with highest stretching rates are those with high toroidal motion. Long-range dispersal was also studied, as discussed in a later section.

7.12.2.3.5 Effect of viscosity variations

7.12.2.3.5.1 Depth-dependent viscosity

For some time, it was thought that if the lower mantle has a substantially higher viscosity, then motion would be so sluggish that chemically distinct material could be retained for long periods of time (e.g., Davies, 1983). Numerical studies have, however, found that the effect of higher lower mantle viscosity on stirring and residence times is relatively small and that it cannot provide an explanation for long-lived heterogeneities per se. These numerical studies, which all study passive tracers, are discussed in this section.

Somewhat confusingly, the earliest study to address this issue (Gurnis and Davies, 1986a) did appear to show very slow stirring in a 100 times higher-viscosity lower mantle, even though the heterogeneities were passive, that is, had no density anomaly to keep them in the lower mantle. The circulation in these cases was however extremely sluggish and was arguably driven mainly by a prescribed platelike boundary condition rather than convection. (Although the authors were careful to make the prescribed surface velocities consistent with convection for constant-viscosity cases, this was not the case for depth-dependent viscosity cases (Christensen, 1989a, 1990).)

With a much higher convective vigor more relevant to the Earth and free-slip upper boundary, a lower mantle viscosity up to a factor of 100 higher than the upper mantle viscosity does not prevent large-scale mixing of the mantle (van Keken and Ballentine, 1998). The latter's calculations tracked helium degassing and ingrowth by radioactive decay, and it was found that the horizontally averaged %degassed and $^{3}He/^{4}He$ ratio were approximately constant with radius even for high-viscosity lower mantle cases, indicating good vertical mixing, although lateral heterogeneity was observed. Curiously, higher lower mantle viscosity seemed to cause higher outgassing rates – this was because the viscosity of the upper mantle was decreased in order to maintain the same surface heat flux in all cases, which led to higher velocities in the shallow mantle, hence more rapid outgassing. Subsequent models (van Keken and Ballentine, 1999) demonstrated that temperature-dependent viscosity and an endothermic phase change at 660 km depth also do not result in chemical stratification, even when the mantle starts out layered in trace-element content, although again, there was a significant amount of lateral heterogeneity (i.e., $^{3}He/^{4}He$ varied from 0 to a maximum value of 36–72).

Regarding stretching rate, a 100-fold viscosity jump was found by Coltice (2005) to make no difference to the average Lagrangian strain rate for internally heated convection, but for

basally heated convection, it decreased strain rate by a factor of ~4, probably because plumes from the lower boundary are affected by the viscosity jump, but instabilities from the upper boundary are not. In these calculations, the upper mantle viscosity and Rayleigh number were held constant.

Processing (residence) time was found to be insensitive to a viscosity jump, regardless of heating mode (Coltice, 2005). Consistent with random sampling and the He ratio results of van Keken and Ballentine (1998), Hunt and Kellogg (2001) found that a 100-fold viscosity jump at 660 km depth did not cause any age stratification. Seemingly inconsistent with Coltice (2005), Hunt and Kellogg (2001) found that the mean particle age increased by a factor of ~2, but this could be because they removed particles not only when they were sampled by melting but also when they became widely dispersed from other particles that were introduced at the same time, which means that the mean age cannot be interpreted as a simple residence time. The viscosity jump does, however, make a substantial difference to the ability of tracers to migrate laterally from their starting positions, because the flow is more steady, and this is something that should be studied further.

A nonconvective, steady-state flow, driven by top boundary forcing and assumed idealized density anomalies due to downwelling slabs, was studied by Ferrachat and Ricard (2001), who found that a 100-fold viscosity jump at mid depth increased the lower mantle mixing time (using a modified version of Olson et al. (1984a) definition based on even dispersion across boxes) by a factor of ~5 and that the finite-time Lyapunov exponents increased by a factor ~2–3. It is not clear how much such an idealized flow applies to the real Earth, however.

7.12.2.3.5.2 Composition-dependent viscosity

If a blob of compositionally distinct material has a higher viscosity than its surroundings, then the rate at which it gets stretched is considerably reduced. Simple theory predicts that in pure shear, the deformation rate is proportional to $1/(\lambda+1)$, where λ is the viscosity contrast (Manga, 1996; Spence et al., 1988). In a steady-state 2-D convective flow, Manga (1996) found that the deformation rate of extremely large (diameter ~1000 km) blobs was dramatically reduced with only a factor of ~10 viscosity increase, whereas if the viscosity of the blob is lower than its surroundings, then it rapidly gets stretched into tendrils. Manga (1996) also found that these large high-viscosity blobs tend to aggregate, raising the possibility that they could combine into even larger blobs.

For time-dependent convection (with a prescribed time-dependent top velocity condition), du Vignaux and Fleitout (2001) showed that stretching rate is more highly dependent on viscosity ratio than in simple shear and that the stretching is exponential with time, consistent with the turbulent mixing regime. Specifically, they found that

$$e_m \equiv \frac{d \ln (a^*/a_0)}{dt} = \frac{C}{(1+\lambda)^2} \qquad [18]$$

where e_m is the mixing efficiency, a^* is the mean distance between two points initially at separation a_0, and C is a constant. The quantity a^* is commonly used in mixing studies as a measure of stretching (Ottino, 1989) and is related to, but not the same as, the semimajor axis of the strain ellipse a (du Vignaux and Fleitout, 2001). This equation is valid for viscosity contrast λ of approximately an order of magnitude or more. This scaling can be explained using an analytic theory of a blob experiencing repeated pure shear events in random directions (du Vignaux and Fleitout, 2001). While one might intuitively expect repeated shear in random directions to average out, or at least add like a random walk, the fact that when the major axis of the ellipse is at an angle like 45° to the pure shear direction, the stretching increases regardless of its orientation means that the overall effect is one of exponentially increasing strain.

Thus, differing viscosity of components can have a dramatic effect on the rate at which they get stretched and hence mixed. It is quite likely that chemically different components have different viscosities. Subducted basaltic crust in the upper mantle has a large proportion of garnet, which has a relatively high viscosity (Karato et al., 1995). The presence of water can reduce viscosity by up to approximately two orders of magnitude (Hirth and Kohlstedt, 1996), which will increase the viscosity of depleted residue and possibly decrease the viscosity of primitive material, which is rich in volatiles. In the lower mantle, magnesiowüstite likely has a lower viscosity than perovskite (Yamazaki and Karato, 2001), so assemblages that have different proportions of these minerals will have differing viscosity. Grain size also has a major influence on viscosity such that 'old' heterogeneities could have a higher viscosity (Solomatov and Reese, 2008).

7.12.2.3.5.3 Non-Newtonian viscosity

Mineral physics results suggest that a substantial part of the upper mantle is undergoing non-Newtonian dislocation creep (Karato and Wu, 1993), yet very few studies have addressed the influence of non-Newtonian power-law rheology on mixing. In a series of papers, Ten et al. (1996, 1997, 1998) compared the mixing properties of highly time-dependent Newtonian and non-Newtonian flows of similar vigor, in 2-D models that also had temperature- and pressure-dependent viscosity. Their basic finding is that mixing is less efficient in non-Newtonian flows, with unmixed 'islands' persisting for long time periods, in both plumes (Ten et al., 1996) and global convection (Ten et al., 1997, 1998). The local patterns of mixing were quite different between the different rheologies, with a greater richness in the scales of spatial heterogeneities in the non-Newtonian case (Ten et al., 1997). Non-Newtonian rheology causes chemical heterogeneity to persist for longer, implying that original chemical heterogeneities can remain unmixed for a long period and may be concentrated at certain depths (Ten et al., 1998). These results suggest that Newtonian models underestimate the mixing time in the upper mantle, something that warrants further study.

7.12.2.4 Dispersal

7.12.2.4.1 Measures of dispersal

7.12.2.4.1.1 Based on sampling cells

One class of measure for measuring the dispersal of initially close particles through the domain is based on dividing the domain into sampling cells and using statistical measures based on the number of particles in each cell. Initially, all the tracers will be in one cell, but when they are completely dispersed, the distribution of number of particles per cell will be indistinguishable from a random distribution.

Measures that have been used include the fraction of sampling bins with 0 tracers (Christensen, 1989a), or the fraction of sampling bins with greater than five times the average number of tracers (Christensen, 1989a) (both measures decrease with time), or the fraction of cells with >1 tracer, which increases with time (Schmalzl et al., 1996). Schmalzl et al. (1996) plotted statistics for each of several initial blocks and derived a 'rate of mixing' from the slope.

The statistics of the number of particles/cell can also be used to directly calculate a 'mixing time' (Olson et al., 1984a), which is the decay time for the reduction of the variance, as described in **Section 7.12.2.6.1**.

7.12.2.4.1.2 Based on separation

Given a distribution of particles, the *two-particle correlation function* $H(r)$ gives the fraction of pairs of particles with separation less than r (Schmalzl and Hansen, 1994). To calculate $H(r)$, all pairs of particles, that is, $N(N-1)/2$ combinations, must be considered. $H(0)$ is zero, and then $H(r)$ increases with r, reaching a maximum at either the size of the domain or the size of the tracer cloud (if smaller than the domain). The initial increase can generally be approximated as $H(r) \sim r^{\alpha}$, where α is the *correlation dimension*, and gives information about the dimensionality of the tracer cloud. In particular, $\alpha = 1$ corresponds to tracers spread into a line, $\alpha = 2$ to well-mixed 2-D convection, and $\alpha = 3$ to well-mixed 3-D convection. In spherical geometry, a random distribution of heterogeneities has a correlation dimension that depends on length scale, rising to a maximum of 2.8 at ~4000 km, falling monotonically to ~2 at ~7500 km, and then plunging to 0 by 10 000 km (Stegman et al., 2002).

The *root-mean square dispersion index* was introduced by Hoffman and McKenzie (1985) to quantify long-wavelength dispersion. It is defined as the square root of the second moment of the autocorrelation of the density distribution, the general form of which is

$$R_2 = \frac{\left(\iint r^2 \mathrm{d}V_1 \mathrm{d}V_2\right)^{1/2}}{\left(\iint \mathrm{d}V_1 \mathrm{d}V_2\right)^{1/2}} \qquad [19]$$

where r is the separation of two volume elements $\mathrm{d}V_1$ and $\mathrm{d}V_2$ of the same body. To study the one-dimensional horizontal dispersion of a body represented by N tracers in a 2-D domain, this is simplified to

$$R_2 H = \frac{1}{N}\left(\sum_{i=1}^{N}\sum_{j=1}^{N} x_{ij}^2\right)^{1/2} \qquad [20]$$

where x_{ij} is the horizontal separation of two particles i and j and this measure reaches an asymptotic value (for perfectly random mixing) of

$$R_2 H(\infty) = \left[1/6\left(N^2 - 1\right)\right]^{1/2} \qquad [21]$$

7.12.2.4.1.3 Other

Other quantities that have been used are the time spectrum of a tracer's vertical position, which gives the 'overturn time' of the convection (Schmalzl et al., 1996), and Poincaré sections (Ferrachat and Ricard, 1998; Schmalzl et al., 1995), that is, 2-D slices of a 3-D volume showing where the particle paths intersect it. These are useful for identifying whether motion is restricted to closed 2-D surfaces as in Schmalzl et al. (1995) or is chaotic (Ferrachat and Ricard, 1998).

7.12.2.4.2 Numerical results

Many discussions of 'mixing' actually refer to the dispersal of heterogeneities around the domain, rather than the process of stretching and diffusion previously discussed. This dispersal is often studied by placing an array of tracers in one part of the domain and studying how rapidly they spread out and become evenly distributed. A common observation in laboratory and numerical experiments (e.g., Richter et al., 1982; Schmalzl and Hansen, 1994) is that dispersal (and mixing) occurs rapidly inside a convective cell but much more slowly between one cell and another; that is, long-range lateral dispersal can be a relatively slow process. Another way of expressing this is that 'mixing' properties depend on spatial scale. The rate of cross cell dispersal depends on how time-dependent the flow is, for example, how time-dependent upwellings and downwellings at the cell boundaries are and whether and how often the cell pattern reorganizes. In the limit of steady-state flow, intercell dispersion is zero in 2-D flows and in 3-D flows with only poloidal motion, but nonzero if toroidal motion is present, as will be discussed later.

7.12.2.4.2.1 Intracell dispersal

The dispersal of tracers within a cell scales similarly to stretching. In the experiments of Christensen (1989a), using a variety of kinematic and convective flows as discussed earlier, stretching-related diagnostics and dispersion-related diagnostics were compared and found to obey similar behaviors, including the delineation of three regimes of mixing.

7.12.2.4.2.2 Intercell dispersal

For time-dependent 2-D flows, several numerical studies have studied the rate of lateral dispersion as a function of parameters. Convection that is completely internally heated is typically highly time-dependent with no long-lived cells, and Richter et al. (1982) found that at $Ra = 1.4 \times 10^6$, tracers were fairly rapidly (e.g., in 0.1 diffusion times) dispersed across a box of aspect ratio 8 in what visually resembles a diffusion process. Using an analytic time-dependent flow, they argued that rapid long-wavelength dispersal requires that the convective pattern change on a timescale comparable to the overturn time. Basally heated convection tends to have a steadier cellular pattern. Hoffman and McKenzie (1985) presented a series of calculations, also in an 8×1 box at $Ra = 1.4 \times 10^6$, with either 100% internal heating or 50% basal and 50% internal, and found that the flows with basal heating produced slower lateral dispersal, although it was still quite rapid. Completely heated-from-below flows were investigated by Schmalzl and Hansen (1994), who found that at range $Ra = 10^6$–10^8, heterogeneities within one cell are destroyed rapidly, while two adjacent cells can remain unmixed for substantially longer, although at $Ra = 3 \times 10^6$, particles were well dispersed by nondimensional time 0.02. They found the particle correlation function $H(r)$ and corresponding correlation dimension to be effective

measures of long-wavelength dispersion, with a value of 2 corresponding to a perfectly dispersed field. Higher Rayleigh number flows are more time-dependent such that the increase in the rate of laterally dispersion with *Ra* is higher than the increase in velocity with *Ra* (Schmalzl and Hansen, 1994).

7.12.2.4.2.3 3-D spherical results

Results regarding intercell dispersal in Cartesian 3-D flows were mentioned in **Section 7.12.2.3.4**. Long-range dispersal in steady-state 3-D spherical flows was studied by van Keken and Zhong (1999), using a flow intended to be similar to the flow in the present-day mantle, generated by buoyancy from a slab model combined with an approximate plate rheology. They found that particles could be efficiently transported far from their source: after 4 billion years of motion in this steady-state flow, pairs of particles initially 10 km apart were dispersed around the mantle with an almost flat probability distribution (i.e., number vs. separation). This suggests that dispersal in the actual mantle is relatively efficient. Stegman et al. (2002) extended such 3-D spherical modeling in order to determine whether dispersal is reduced by higher lower mantle viscosity (see **Figure 5**). Using the correlation dimension to measure dispersion, they found that in a model with 100 times higher lower mantle viscosity and driven by a slab model and present-day plate motions, the correlation dimension reached after a few billion years is only of order 1, which is normally indicative of stretching into a line. A representative structure can be seen in **Figure 5**. They also found that in a model with 100 times higher lower mantle viscosity and driven by a slab model and present-day plate motions, the upper mantle became mixed about 60% faster than the lower mantle, which mixing is determined by the correlation dimension. They conclude that this is insufficient differential mixing to explain the difference between the relatively high heterogeneity of OIBs and relatively low heterogeneity of MORBs, although it could be argued that the latter is related to the small-scale structures in the melting region, whereas the correlation dimension is quantifying variations at ~1000 km length scales.

7.12.2.4.3 Eddy diffusivity?

In the atmospheric community, long-wavelength lateral dispersal is commonly treated using an 'eddy diffusivity,' although it has been found to be dependent on the initial length scale (separation) being considered: larger separations lead to larger estimates of effective eddy diffusivity (Richardson, 1926; Richter et al., 1982). It is interesting to know whether this concept could be applied to the mantle. Olson et al. (1984b) studied whether an effective diffusion could be used to parameterize mixing within a convecting cell (an 'eddy') and concluded that it could not, because the effective diffusion coefficient would need to be larger for larger heterogeneity size. However, the two studies that have attempted to fit lateral dispersal across convective cells with an effective 'eddy' viscosity do appear to have had reasonable success.

For internally heated convection at $Ra = 1.4 \times 10^6$, Richter et al. (1982) used the distance-neighbor approach of Richardson (1926) to estimate an eddy diffusivity for the large-scale dispersal of heterogeneities at a scale length several times that of the depth and estimated a value of 30 times the thermal diffusivity, that is, ~0.003 $m^2 s^{-1}$, independent of initial separation. In similar experiments but with varying heating modes, Hoffman and McKenzie (1985) estimated a value of 25 times the thermal diffusivity for internally heated convection and 20 times the thermal diffusivity for 50% internal heated convection, by fitting the time evolution of the horizontal rms dispersion index with a diffusion curve, that is,

$$R_2 H = \sqrt{kt} \qquad [22]$$

The slight difference from the almost identical experiment of Richter et al. (1982) is probably due to difference in estimation technique and is not meaningful. They found that their

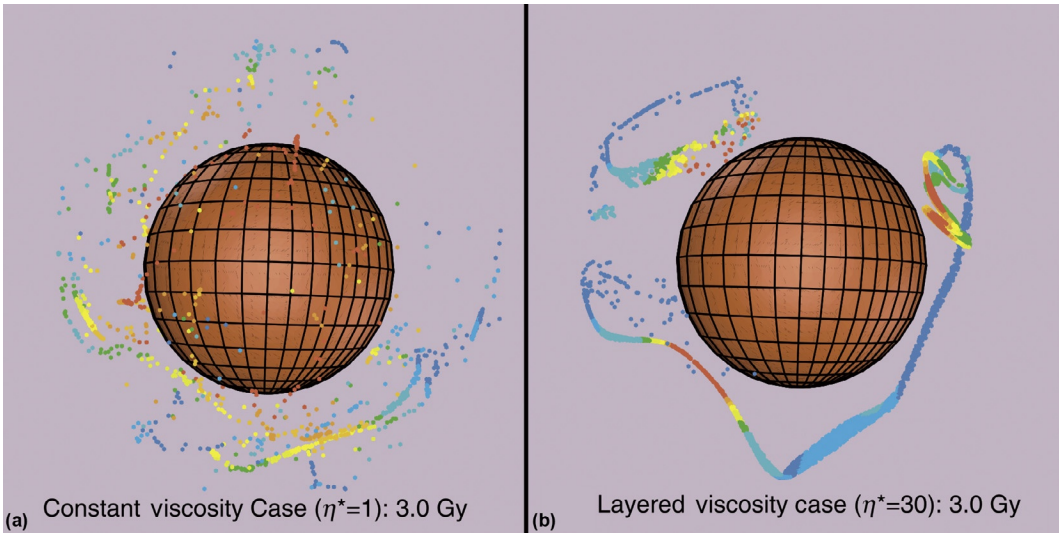

Figure 5 Dispersal of an initial 125 km radius cluster of tracers around the mantle after 3 Gy, from Stegman et al. (2002). Mantle flow is driven entirely by plate-like boundary conditions. The two panels show the effect of a 30* viscosity increase at the 660 km discontinuity. In the lower mantle, the heterogeneity is stretched into a ribbonlike structure, but this is more rapidly destroyed in the upper mantle or in an isoviscous mantle, where toroidal flow is more prominent.

numerical experiment agrees with this square root of time curve, so that eddy diffusivity is a good approximation for large scales of over 3 times the layer depth, and they got 20 times the thermal diffusion coefficient rather than 30 times. Based on these two studies, an eddy viscosity seems to offer a reasonable parameterization of lateral dispersal over distances greater than ~3 times the layer depth in a simple 2-D convective system, but the application to more complex situations and as a function of convective parameters remains to be determined.

7.12.2.5 Residence Time

The concept of residence time plays a central role in geochemical theory (e.g., Albarède, 1998) and also in numerical calculations of stirring and mixing processes. Residence time is defined as the length of time a heterogeneity (tracer) stays in the specified reservoir or other container. In geochemical box modeling, it may be applied to how long (on average) an isotope stays in a reservoir such as the continental crust and lower mantle. In numerical modeling of mantle evolution, it usually means the average length of time before a tracer is sampled by melting, from either the beginning of the calculation or, if tracers are being continually introduced at subduction zones, the average length of time before they are next sampled (melted). For whole-mantle convection in statistical equilibrium, this is equal to the processing time, that is, the time taken for one mantle mass to pass through the mid-ocean ridge processing zone, as discussed in **Section 7.12.1.5.3** where it was argued that this is around 6 Gy at the present processing rate but could have been much faster (i.e., lower) in the past.

From a chemical perspective, the mantle residence time for lithophile elements was calculated by Albarède (2005b) by dividing the amount of the element in a mean mantle model (i.e., BSE–continental crust) by the current rate at which the element is extracted into the oceanic crust. Residence times in the range 4–9 Gy were obtained, which bracket the geophysically constrained value of ~6 Gy discussed in **Section 7.12.1.5.3**. Again, it is likely that processing was substantially faster in the past.

In geochemical box modeling, it is commonly assumed that a reservoir is randomly sampled, that is, the probability of melting each atom or tracer in the reservoir is the same regardless of how long they have been in the reservoir, in which case the overall process is analogous to radioactive decay. Thus, if a reservoir starts off with N_0 atoms or tracers of a particular isotope, the rate of sampling is given by

$$\frac{dN}{dt} = \frac{N}{\tau} \quad [23]$$

where τ is the residence time. Hence, the number left after time t is given by

$$N = N_0 \exp(-t/\tau) \quad [24]$$

This residence time can be directly related to the mean age, where the age of a piece of mantle is defined as the time since it was last involved in a partial melting event or formation of the Earth. In equilibrium, of course, the mean age is equal to the processing time, but in the Earth, it is less than this because no piece of mantle can be older than the Earth and because the processing rate was likely faster (residence time was lower) in the past. For a constant processing rate, the mean age a is given by Huang and Davies (2007c):

$$a(t) = \tau(1 - \exp(t/\tau)) \quad [25]$$

For small times, this expression reduces to t and for long times, it asymptotes to τ, as expected. If the processing time is equal to 4.5 Gy, the mean age is thus ~2.8 Gy. If the processing rate were higher in the past according to (heating rate)^2, this reduces to 1.8 Gy, and if an increase in the depth of onset of melting is additionally taken into account, it reduces to 1.65 Gy (Xie and Tackley, 2004b).

The random sampling assumption is valid if tracers are effectively dispersed throughout the domain in question by time-dependent flows. This seems likely because (as discussed in **Section 7.12.2.3.3**) fully time-dependent free convection (i.e., without kinematic constraints) experiments have always displayed chaotic mixing, which effectively disperses tracers. This contrasts to steady-state 2-D flows, in which tracers are instead restricted to individual streamlines, only streamlines that intersect the sampling area are sampled with the result that amount of sampling increases linearly with time until all tracers on the those streamlines have been sampled (Coltice, 2005). Testing of this for mantle convection-like flows, as well as the influence of dense heterogeneities and viscosity variations, is now discussed.

The earliest study to check residence times was Gurnis and Davies (1986b), who investigated a low-Ra flow driven by internally heated convection at $Ra = 10^5$ and 'organized by' a kinematic platelike surface velocity condition. Tracers were introduced at the simulated moving trench, and it was found that the length of time tracers spend in the box before being sampled was easily predicted by the applied volumetric sampling rate and the rate of introduction of new tracers, consistent with the random sampling assumption. For more vigorous plate-organized flows in 2-D and 3-D, random sampling was verified by Davies (2002) and Huang and Davies (2007a,c), respectively. For free convection, Coltice (2005) confirmed that random sampling applies when the mixing is chaotic.

7.12.2.5.1 Effect of chemical density differences

While early models (Gurnis, 1986a) suggested that chemical density variations have little effect on sampling statistics, with a more Earth-like convective vigor, a significant effect is found (Christensen and Hofmann, 1994; Davies, 2002). Davies (2002) used roughly the correct convective vigor for Earth with chemical buoyancy ratios of up to 0.8 and found a significant difference for mid-ocean ridge sampling and for plume sampling. Mean residence times for MORB melting remained consistent with random sampling, with the mean age of tracers only slightly increased (from a scaled 2.42 to 2.52 Ga). However, some dense basaltic tracers settled into piles at the base, and their mean age increased by 32% from 2.57 to 3.38 Ga, with this higher age potentially being sampled by plume volcanism. If tracers are truly randomly sampled, then the distribution of ages should have a particular probability distribution that depends on the source function. Davies (2002) showed that tracers settling the base of the domain have a probability density function that is dramatically different from those in the

MORB sampling region, which implies that random sampling does not apply to all tracers even though the average residence time may not change much. Using a similar setup except in 3-D, Huang and Davies (2007a,b) verified that these conclusions also apply in 3-D. An appropriate description is probably that a different residence time applies to material that settles above the CMB; Christensen and Hofmann (1994) calculated such a quantity for calculations in which somewhat more basalt settling was obtained. They obtained residence times in the dense basal layer of between 0.36 and 1.62 Ga depending on parameters. For the whole system, they did not calculate the 'mean age' but rather the lead–lead pseudoisochron age; changing the buoyancy ratio from 1.0 to 2.25 while keeping other parameters constant changed the Pb–Pb age from 1.37 to 2.66 Ga. Thus, if density contrasts cause a layer to form, it is important to study residence times in the layer, and not just the average of the whole system.

7.12.2.5.2 Effect of viscosity variations and convective vigor

The effect of viscosity stratification and heating mode on residence time was determined by Coltice (2005). When the Ra is high enough for the flow to effectively disperse the tracers, the residence time scales with the theoretical prediction based on fraction of the mantle sampled per unit time, independent of viscosity contrast. This is consistent with earlier works that studied the effect of viscosity stratification on the depth distribution of mean age (Hunt and Kellogg, 2001; van Keken and Ballentine, 1998) – the effect is minimal. The 3-D spherical models of Huang and Davies (2007a,c) provided further evidence that viscosity stratification, temperature-dependent viscosity, convective vigor (Ra), and dimensionality do not have an effect on sampling statistics: the sampling is effectively random meaning that residence time depends only on the rate at which material is processed by partial melting.

7.12.2.6 Mixing Time

7.12.2.6.1 Background

Several definitions of 'mixing time' have been used, which, together with sensitivity of stirring rate to the exact type of assumed flow, has led to a wide variety of estimates for mixing time in the mantle. Some estimates have been based on stretching, while others have been based on dispersal. As discussed previously, 'mixing' (dispersal) across several convective cells can be far slower than 'mixing' in a single convective cell. In any case, a key quantity is the length scale of interest, which could be the diffusion length scale or sampling length scale.

The strictest definition of mixing time is the time required for the heterogeneities to become stretched thin enough to be homogenized by diffusion, which requires stretching down to submeter length scales for silicate rocks. It is questionable, however, whether such small-scale variations can be observed in geochemical observations (see later discussion), so an important concept is that of sampling volume (or, in 2-D, sampling area; Richter and Ribe, 1979), which can be reexpressed as a sampling length scale by taking the cubed (or square) root (Olson et al., 1984a,b). This sampling volume describes the region over which heterogeneities are homogenized by the sampling process, such as partial melting and extraction and mixing of magmas with each other and with the rock through which they are passing. While this has often been assumed to be approximately tens of kilometers, some of the geochemical observations discussed in Section 7.12.1.7 indicate that shorter-length-scale heterogeneity can be preserved in the resulting rocks. When calculating compositional heterogeneity in models, heterogeneity should be integrated (averaged) over the sample volume. In summary, the mixing time is the time required for heterogeneity to get stretched to the sampling size or the diffusion length scale, whichever is larger.

It has been usual to scale estimates of mixing time to either upper mantle convection or whole-mantle convection, which generally results in rather small estimated timescales for upper mantle mixing. These are probably irrelevant to the present-day mantle, as it is now clear that the upper mantle is not convecting independently as a simple heated-from-below Rayleigh–Bénard system, but instead, the convective regime is dominated by whole-mantle flow and the plates impose a long-wavelength organization to the upper mantle. It is possible that small-scale convection below the plates exists in the upper mantle (see Chapter 7.08), but this would be less vigorous than assumed in the 'upper mantle' mixing estimates and its effect on mixing has not yet been evaluated.

Some important statistical measures of heterogeneity are now introduced, following Olson et al. (1984a). The two-point correlation function is given by

$$R(\mathbf{r}, t) = \langle \theta(\mathbf{x}')\theta(\mathbf{x}' + \mathbf{r}) \rangle \quad [26]$$

where $\theta(\mathbf{x})$ is the compositional field, $\mathbf{x}$ is the position vector, $\mathbf{r}$ is the separation vector, and the angle brackets denote the volume average. Its Fourier transform, the energy spectral density (Olson et al., 1984a) in n spatial dimensions, is given by

$$E(\mathbf{k}, t) = \left(\frac{1}{\pi}\right)^n \int_0^\infty R(\mathbf{r}, t)\exp(-i\mathbf{k}\cdot\mathbf{r})\mathrm{d}\mathbf{r} \quad [27]$$

and the related variance of composition σ^2 is given by

$$\sigma^2 = R(0, t) = \int_0^\infty E(\mathbf{k}, \mathbf{t})\mathrm{d}\mathbf{k} \quad [28]$$

If heterogeneity is not created or destroyed but only changes wavelength, the variance remains constant with time (see Ricard, Chapter 7.02). However, if there is a sampling wavelength below which heterogeneity can no longer be detected, then it is appropriate to use the corresponding wave numbers as the upper limit for the integration, leading to the sampling variance

$$\overline{\sigma}^2 = \int_0^{k_s} E(\mathbf{k}, \mathbf{t})\mathrm{d}\mathbf{k} \quad [29]$$

which will decrease with time due the cascade of heterogeneity to shorter wavelengths if heterogeneity is not replenished at long wavelengths. This has led to one definition of the mixing time (Olson et al., 1984a):

$$\tau_{\mathrm{mix}} = \int_0^\infty \frac{\overline{\sigma}^2(t)}{\overline{\sigma}^2(t_0)}\mathrm{d}t \quad [30]$$

the physical meaning of which is the time needed to reduce the sample variance of the composition significantly. A modification of this should be made when calculating $\overline{\sigma}^2 = C_2(\kappa h_0/B^2)Ra^{1/3}$ numerically using a finite number of

sampling cells containing a finite number of tracer particles, as described by Ferrachat and Ricard (2001). In this situation, it does not tend asymptotically to zero, so the integral does not converge. Instead, the statistical limit is

$$\lim_{t\to\infty}\frac{\overline{\sigma}^2(t)}{\overline{\sigma}^2(t_0)}=\frac{s-1}{n} \quad [31]$$

where s is the number of sampling cells and n is the number of particles. Thus, Ferrachat and Ricard (2001) introduced a definition for mixing time that includes this and does converge:

$$\tau_{\text{mix}}=\int_0^\infty\left(\frac{\overline{\sigma}^2(t)}{\overline{\sigma}^2(t_0)}-\frac{s-1}{n}[1-\exp(-t/\tau_{\text{mix}})]\right)\mathrm{d}t \quad [32]$$

The mixing time is expected to depend on sampling length scale, as discussed earlier. To test this, the number of sample cells s can be varied, as was done by Ferrachat and Ricard (2001) and Olson et al. (1984a). Ferrachat and Ricard (2001) found that the mixing time increases regularly with 1/length scale, with a moderate increase in mixing time for decreasing cell size – approximately a factor of 4–5 for factor 32 decrease in length scale.

7.12.2.6.2 Laminar flows

A heterogeneity is stretched until it either is homogenized by diffusion or has a width of less than the sampling length scale. The balance between diffusion and sampling length scale in controlling the mixing time was analyzed by Olson et al. (1984b) for idealized flows and then compared to numerical results of a steady-state Rayleigh–Bénard convection cell in which the stretching rate is laminar with time. Substituting the spectral expansion of a heterogeneity into the previous equation led to the mixing time for nondiffusive laminar stirring being proportional to initial length scale/sampling length scale, that is,

$$\tau_{mix}\approx\frac{\pi}{\dot{\varepsilon}k_0\Delta z}=\frac{\lambda_0}{2\dot{\varepsilon}\Delta z} \quad [33]$$

where λ_0 is the initial wavelength of heterogeneity (if a localized heterogeneity, twice its size) and Δz is the sampling length scale. If, however, diffusion is rapid enough to homogenize the heterogeneity before it reaches the sampling length scale, a different expression is obtained:

$$\tau_{\text{mix}}\approx\left(\frac{\lambda_0^2}{4\kappa\dot{\varepsilon}^2}\right)^{1/3} \quad [34]$$

where κ is the diffusivity. There is a smooth transition between these types of behavior.

Olson et al. (1984b) tested these equations using a single Bénard convection cell and found that the results fitted reasonably well, for both nondiffusive and diffusive heterogeneities. Scaled to the Earth with an assumed $F=C/B^2$, an initial anomaly wavelength equal to the depth, and a sampling length scale of 5 km, this leads to mixing time of 2.3 Gy for upper mantle convection or 10 Gy for whole-mantle convection.

In the convective + kinematic internally heated ($Ra=10^5$) flows of Gurnis and Davies (1986b), long-lived clumps (folded strips of crust) that persisted over tens of transit times were observed, even though most tracers were well dispersed. Based on qualitative measures, the authors estimated the survival time of the clumps to be 2.4, or 1.4 Gy if faster processing in the past is taken into account.

7.12.2.6.3 Turbulent regime

For turbulent mixing, the equivalent result for nondiffusive flow is logarithmic and thus more rapid (Olson et al., 1984b):

$$\tau_{\text{mix}}\approx\frac{1}{\dot{\varepsilon}}\ln\left(\frac{2\lambda_0}{\Delta z}\right) \quad [35]$$

It is important to note that effective strain rate that goes into this equation can be more than an order of magnitude smaller than the average (e.g., root-mean-square) strain rate of the flow and depends on the details of the flow. For the convective flows investigated by Christensen (1989a) at Rayleigh numbers in the range 10^5–10^6, the effective strain rate was a factor of 10–30 less than the mean strain rate of the flow. The effective strain rate scales in proportion to convective velocity over a wide range of Rayleigh number for both basally heated and internally heated flows (Coltice, 2005).

As for mixing time, Christensen (1989a) assumed that the mantle is well mixed when >90% of the heterogeneities had been reduced to <1/50th of their original size and scaled his numerical results to the Earth using the transit time. This led to an estimate of 200–300 Ma for upper mantle convection or 1500–2000 My for whole-mantle convection with a reasonable viscosity increase with depth. There are two points to note: This mixing criterion involves stretching oceanic crust down to 100 m thickness, which is larger than what other estimates have assumed: if instead the mixing is taken to meter scale, this timescale estimate is approximately doubled to 3–4 Gy for whole-mantle convection. Secondly, there is a wide distribution in stretching rates, so that even when the 'mixed' criterion is met, there are still heterogeneities that are substantially larger and could influence isotopic signatures.

Hoffman and McKenzie (1985) also estimated mixing time from the scaling relationships that they found for small-scale stretching and large-scale dispersion. They estimated that 'any reasonable body' experiencing upper mantle convection will be thinned to 10^{-3} layer depths (700 m) in 400 My and 10^{-6} layer depths (0.7 m) in 700 My; for whole-mantle convection, these timescales are 1.0 Gy (for 3 km) and 1.5 Gy (for 3 m). However, lateral dispersion takes much longer: for half the circumference of the Earth and whole-mantle convection, the timescale is 4.6 Gy, similar to the age of the Earth.

The mixing time for subducted oceanic crust in a kinematic chaotic flow was calculated by Kellogg and Turcotte (1990). They assumed that a heterogeneity must be stretched thin enough for diffusive homogenization to take place based on the model of Kellogg and Turcotte (1986), which gives an equation for mixing time of

$$t_{\text{h}}=\frac{12h}{\pi u_{\text{sm}}\overline{\alpha}_{\text{e}}}\ln\left[4b_0\left(\frac{\pi u_{\text{sm}}\overline{\alpha}_{\text{e}}}{12Dh}\right)^{1/2}\right] \quad [36]$$

where D is the chemical diffusivity (assumed to be 10^{-19} m^2s^{-1} based on Hofmann and Hart (1978) and Sneeringer et al. (1984)), h is the depth of the convecting layer, b_0 is the initial heterogeneity size (assumed to be 6 km), u_{sm} is the average surface velocity (assumed to be 10 cm year^{-1}), and $\overline{\alpha}_{\text{e}}$ is the

effective strain rate from the numerical experiments. With these assumptions, t_h was calculated to be 240 and 960 million years for upper mantle convection and whole-mantle convection, respectively, which is the time for 50% of the heterogeneities to be homogenized by diffusion and corresponds to nine overturns. The diffusive homogenization length scale for this is <1 cm for both cases, and the amount of thinning is six to seven orders of magnitude. Due to idealizations in their model, however, these times must be interpreted as lower limits. One idealization is that this is not a real convective flow and it is not clear how representative the effective strain rate will be of the real mantle. For example, in the real mantle, the viscosity increases with depth, which will reduce the strain rate in the deep mantle and increase the 'overturn time,' a concept which itself is not well defined for flow in the actual mantle. An obvious quantitative issue is that the assumed average surface velocity of 10 cm year^{-1} is approximately three times larger than Earth's actual mean poloidal surface velocity, the poloidal component of which is around 3.5 cm year^{-1} (Lithgow-Bertelloni et al., 1993). If the times are recalculated with this value, they change to 660 and 2630 million years, respectively, the latter of which may well be consistent with geochemical evidence for survival of geochemical heterogeneity over 2 billion-year timescales.

In the actual mantle, heterogeneity is continuously introduced at the same time as 'old' heterogeneity is destroyed by stirring and diffusion, so Kellogg and Turcotte (1990) also considered the fraction of the mantle that is completely homogenized by the present day when oceanic crust is continuously introduced into the mantle over geologic time. For this, it is first necessary to assume an equation for crustal production versus time, and they assume that oceanic crustal production in the past scales with radiogenic heat production in the mantle with a $1/e$ decay time of 2.5 Gy (Turcotte and Schubert, 1982), that the present rate of production is 2.8 km^{2}year^{-1}, and that the processing depth under mid-ocean ridges is 60 km, assumptions that lead to half of the mantle being processed in 800 My for layered convection or 2200 My for whole-mantle convection. Combining this melting model with their mixing model, they derive an expression for $F(d)$, the fraction of particles narrower than d. Hence, setting d to the diffusion length scale of 10^{-7}, they obtain a curve for the fraction of particles that have been completely homogenized, in terms of the mixing time. For their estimated whole-mantle mixing time of 960 My, 67% of the mantle is perfectly mixed, but for the adjusted mixing time of 2.6 Gy as discussed earlier, this fraction is 28%, that is, over 70% of the present-day mantle is still in the form of strips of varying thickness. Thus, they predict substantial chemical heterogeneity even with the relatively rapid mixing in their experiments.

Kellogg and Stewart (1991) estimated the effective strain rate and mixing time for a chaotic flow using the same method, but this time, the flow is the nonlinear interaction of a single convection roll with a single spatial subharmonic, and the obtained mixing times are about a factor of 2 smaller.

7.12.2.6.4 Summary of different 'mixing time' estimates

Table 1 summarizes the various estimates of mixing time for whole-mantle convection, as discussed earlier. As far as the author is aware, these are all the published estimates given in dimensional time units, although it might be possible to obtain additional estimates by scaling nondimensional results from other studies. Estimates vary by an order of magnitude, from 1 to 10 Gy, because of different assumptions about the length scale to which heterogeneities should be stretched, the type of flow, and the flow velocity. Gurnis and Davies (1986b) were concerned with the survival of large clumps, so their estimate is not directly comparable to the other estimates. The estimate of Olson et al. (1984b) is large because they assumed laminar flow, whereas it is now established that time-dependent convective flows tend to give turbulent mixing, as occurred in the last three estimates. The estimate of Kellogg and Turcotte (1990) should be at least tripled because their assumed velocity was too large, as discussed in the preceding text. The estimate of Christensen (1989a) refers to stretching oceanic crust to ~100 m thickness and should be at least doubled for comparison with the Kellogg and Turcotte (1990) estimate. The estimate of Hoffman and McKenzie (1985) was made before it was established that the lower mantle is probably a factor of ~30 more viscous than the upper mantle (they assumed a factor of 3) so should be at least doubled when this is taken into account. When such scaling is done, estimates are in better agreement, in the 3–4 Gy range for stretching crust to the submeter length scale. If an equivalent table were constructed for upper mantle convection estimates, then the times would be much shorter, but as argued earlier, geophysical constraints indicate that the dominant mode of convection in the present Earth is whole mantle and the effect of possible 'small-scale' convection beneath the oceanic plates has not yet been evaluated.

7.12.2.7 Spectrum of Chemical Heterogeneity

As was discussed in Section 7.12.1.7, our knowledge of the spectrum of chemical heterogeneity in the mantle is far from perfect, but some useful information does exist. Geochemical

Table 1 Summary of mixing time estimates

Study	*τ_{mix} (Ga)*	*Length scale (inner)*	*Notes*	*Rescaled τ_{mix} (Gy)*
Gurnis and Davies (1986b)	2.4	Visible clumps	Survival time	
Olson et al. (1984b)	10	Diffusion	Laminar stretching	
Christensen (1989a)	1.5–2.0	1/50 (~100 m)	90% reduced to this size	3–4
Hoffman and McKenzie (1985)	1.0	3 km	only 3* viscosity increase with depth	>3
	1.5	3 m		
Kellogg and Turcotte (1990)	0.96	Diffusive	50% homogenized	~3

observations show the existence of heterogeneity at all length scales, from the scale of melt inclusions to thousands of kilometers, and quantitative information regarding the spectrum is becoming available. As also discussed earlier, seismological information points to the existence of scatterers throughout the lower mantle, with the amount of scattering varying from place to place. The longest wavelengths are constrained by seismic tomography but separating thermal from compositional contributions has major uncertainties. This section reviews the dynamic theory about the expected length scales of heterogeneity.

Mantle heterogeneity is introduced at long wavelengths by subduction (and possibly, primordial layering). If subducted material segregates into a layer, then this acts to increase its wavelength, but if it remains in the convective flow, then it is progressively stretched until it reaches small enough length scales to be homogenized by diffusion. Thus, as discussed by Olson et al. (1984a), the spectrum of mantle heterogeneity undergoing stirring is expected to display three regions with increasing wave numbers (decreasing wavelength): a 'source' region corresponding to the spectral characteristics of the source, a 'cascade' region in which the heterogeneities are being stretched to shorter wavelengths, and a 'dissipation' region, in which chemical diffusion acts to eliminate heterogeneity at the shortest scales. It is useful to consider the spectrum that is obtained in statistical equilibrium, in which heterogeneity is introduced at a constant rate and the total spectrum does not change with time. This depends on the stretching regime in the cascade region: For laminar stirring, the wave number k of an individual heterogeneity increases linearly with time, which leads to a flat ('white') spectrum for all heterogeneities in statistical equilibrium (Olson et al., 1984a). In contrast, for turbulent stirring, the wave vector of an individual heterogeneity increases exponentially with time, that is, the rate of increase is proportional to its present value, which leads to a statistical equilibrium spectrum that scales as $1/k$. This at first seems inconsistent with the $-5/3$ slope obtained by Metcalfe et al. (1995) for a kinematic chaotic stirring of a laboratory fluid, but as this system was not in statistical equilibrium, the slope reflects a transient regime.

Geochemical observations, as discussed in **Section 7.12.1.7**, can be compared to these theoretical slopes. The early analysis of Gurnis (1986b) using $^{87}Sr/^{86}Sr$ data from MORB and OIB appeared to be consistent with a 'white' laminar mixing spectrum, but the more highly constrained spectrum of isotope ratios along the Mid-Atlantic Ridge obtained by Agranier et al. (2005) instead indicates the turbulent, $1/k$ regime, consistent with expectations from mantle mixing theory discussed earlier.

Such theory also successfully predicts the smaller scales of heterogeneity observed in peridotite massifs in Beni Bousera (Kellogg and Turcotte, 1990). They derive that the probability of finding a strip of material larger than size d is given by $1/d(1-F(d))$, which, when evaluated for scales between 1 and 100 cm, gives a slope close to -1, indicating that the $(1/d)$ term is dominating and $(1-F(d))$ does not change very much over this range. Field samples match this slope reasonably well.

In any case, it is clear that because thermal heterogeneity diffuses rapidly, whereas chemical heterogeneity does not, short wavelength mantle heterogeneity is dominantly chemical in origin, while thermal heterogeneity should be important, and perhaps dominant, at long wavelengths, although recent seismological studies argue for a large chemical component (Deschamps et al., 2007; Mosca et al., 2012; Trampert et al., 2004). These expectations are confirmed in the thermochemical convection calculations of Nakagawa and Tackley (2005b), in which the slope of the chemical heterogeneity at long wavelengths also appears to be consistent with a $1/k$ scaling, although they do not study how this scales at short wavelengths.

7.12.3 Mantle Convection with Active (Buoyant) Chemical Heterogeneity

This section considers thermochemical mantle convection in which the composition affects density. Studies have typically considered what happens with a preexisting dense layer or the development of a layer over time by settling of dense material or reactions with the core. Because the chemical diffusivity in the mantle is orders of magnitude lower than thermal diffusivity, it is typically assumed that the chemical field is nondiffusive, although if the field is being treated as a continuous field, then some numerical diffusion is typically introduced in order to stabilize the advection. The Lewis number gives the ratio of chemical to thermal diffusivity:

$$\mathrm{Le} = \frac{\kappa_T}{\kappa_C} \qquad [37]$$

Its value is quoted as $\sim 10^8$ by Hansen and Yuen (1989), but the chemical diffusivity quoted by Kellogg and Turcotte (1986) would lead to $\mathrm{Le} = 10^{13}$.

Attention has generally focused on two cases: compositional layering at the 660 km interface and a relatively thin composition layer above the CMB corresponding to D″.

7.12.3.1 Stability and Dynamics of Chemical Layering in a Convecting Mantle

7.12.3.1.1 The balance between chemical and thermal buoyancy

If a layer of dense material is present, the parameter that most strongly influences its dynamics and evolution is the ratio of chemical density contrast to thermal density contrast, that is, the buoyancy ratio, here written as B:

$$B = \frac{\Delta\rho_C}{\Delta\rho_T} = \frac{\Delta\rho_C}{\rho_0 \alpha \Delta T} \qquad [38]$$

where $\Delta\rho_C$ is the density contrast due to composition, $\Delta\rho_T$ is that due to temperature, ρ_0 is the density, and ΔT is the temperature contrast. If ΔT represents the total thermal contrast available in the system, then it has been found that the layering displays long-term stability with a fairly flat interface if B is greater than some critical value of order 1 and undergoes either large-topography layering or various shorter-lived behaviors that end in mixing and whole-mantle convection, if $B < 1$ (Davaille, 1999a; Le Bars and Davaille, 2004a; Montague and Kellogg, 2000; Montague et al., 1998; Olson and Kincaid, 1991; Richter and Johnson, 1974; Richter and McKenzie, 1981). The behaviors of short-lived modes were systematically mapped out as a function of B, viscosity contrast, and layer

thickness using laboratory studies (Davaille, 1999a,b; Le Bars and Davaille, 2004a,b) supplemented by mathematical analysis (Le Bars and Davaille, 2002) and are generally consistent with earlier laboratory and numerical studies, which are as follows and illustrated in the domain diagram of Figure 6:

(i) $B > 1$ stable stratification, both layers convecting with slow entrainment
(ii) $B > 1$ but thin, nonconvecting lower layer
(iii) $1 > B > 0.5$: layered but with large topography
(iv) $0.3 < B < 0.5$, layer thickness between 0.2 and 0.7: doming, the number of pulsations increases rapidly with viscosity contrast
(v) $B < 0.2$: rapid overturn and mixing of layers

If the two layers initially have the same temperature, then additional transient behavior occurs as a temperature difference develops across the layers, thereby decreasing the total (i.e., thermal + chemical) density contrast. In this case, layers that should be unstable according to the previously mentioned criteria may initially be stable, as in the calculations of Samuel and Farnetani (2003). B may decrease with time due to the entrainment of each layer into the other layer, as discussed in the succeeding text. Indeed, in laboratory experiments of Le Bars and Davaille (2004b) (Figure 2), the experiment evolved through several different regimes as the density difference between the layers decreased. Another initial condition that causes transient behavior is a linear compositional gradient throughout the domain and constant temperature, as studied by Hansen and Yuen (2000), who found that after some time, the system developed a stable but large-topography layer. After that, the evolution discussed in the remainder of this section applies.

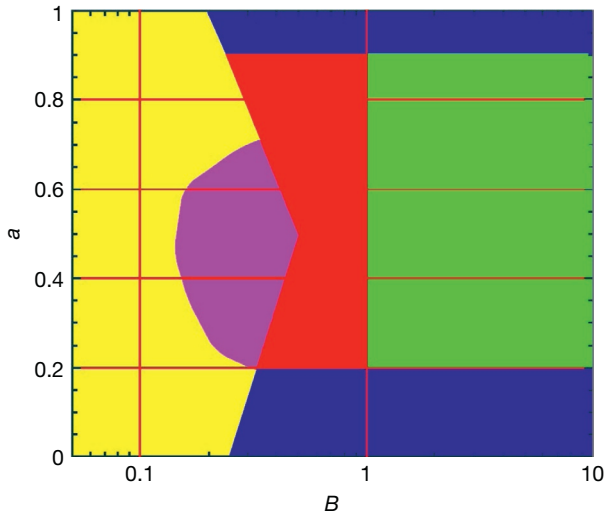

Figure 6 Domain diagram for the behavior of thermochemical convection as a function of buoyancy ratio B and initial depth of dense layer a, as determined by laboratory experiments (Davaille, 1999b; Davaille et al., 2002; Le Bars and Davaille, 2002, 2004a,b). Green, flat layers; red, large-topography layers; pink, transient oscillating domes; blue, thin noninternally convecting layer progressively entrained by thermochemical plumes; yellow, rapid overturn. Adapted from Le Bars M and Davaille A (2004).Whole layer convection in a heterogeneous planetary mantle. *Journal of Geophysical Research* 109: B03403, http://dx.doi.org/03410.01029/02003JB002617.

In the mantle, the relevant physical properties (α, ρ_0) vary with depth, and the previously mentioned criteria are most valid if values of the physical properties close to the chemical boundary area are considered, although some studies have used, for example, reference or 'surface' values and thus require careful interpretation. Scaling to the Earth, the appropriate ΔT is the superadiabatic temperature drop between surface and CMB, which might be 2500 K. For layering at around 660 km depth, $\alpha \sim 2.5 \times 10^{-5}$, so the critical $\Delta\rho_C/\rho_0 \sim 6.25\%$, whereas at the CMB, $\alpha \sim 1.0 \times 10^{-5}$, so $\Delta\rho_C/\rho_0 \sim 2.5\%$. These are rough estimates, as it has been found that other characteristics such as the viscosity contrast between the two layers (a combination of intrinsic viscosity contrast and temperature-dependent contrast), the thickness of the dense layer, and the thermal conductivity of the dense layer also play a role, as will be discussed later.

The detailed dynamics have been investigated variously by laboratory and numerical experiments with some mathematical analyses, with laboratory experiments having the advantage of physical correctness, which is particularly important because entrainment rates are difficult to accurately measure numerically (Tackley and King, 2003; van Keken et al., 1997), whereas numerical experiments have the advantage that the variation of physical properties (viscosity, thermal expansivity, and conductivity) with pressure and temperature can be more realistically ascertained and full information about the various fields is available for analysis. Experiments (both numerical and laboratory) with layering are often initialized in a way that is far from a steady state (e.g., temperature is isothermal instead of higher in the lower layer), which results in a transient behavior. Furthermore, layered experiments are intrinsically transient in that the layering evolves with time, and this may result in the final state retaining a memory of the initial conditions. Further discussion of laboratory experiments can be found in Chapter 7.03.

7.12.3.1.2 Initially stable layering: Pattern and dynamics

7.12.3.1.2.1 Flat, thick, internally convecting layers

For thick, convecting layers, layered convection occurs and a TBL builds up over the interface, with heat transport accomplished by thermal diffusion, substantially reducing the global heat flow and affecting the Earth's thermal evolution (Montague and Kellogg, 2000). For layers of approximately equal thickness and viscosity, as in the laboratory and numerical experiments of Richter and McKenzie (1981), the temperature difference between the layers is $\Delta T/2$ (Richter and McKenzie, 1981), but this varies as the viscosity contrast and thicknesses are changed. The pattern of convection in the upper and lower layers is coupled. When the layers are of similar viscosity, mechanical coupling dominates such that upwellings in one layer match with downwellings in the other layer (Cserepes and Rabinowicz, 1985; Richter and McKenzie, 1981). When there is a large viscosity contrast exceeding a factor of ~100 (Cserepes and Rabinowicz, 1985), however, thermal coupling dominates, in which upwellings in the lower layer underlie upwellings in the upper layer. Intermediate viscosity contrasts, such as 25–30, result in a mixture of thermal and mechanical (viscous) coupling, as show by 3-D calculations (Cserepes et al., 1988; Glatzmaier and Schubert, 1993). In this mixed regime, the flow direction of rolls in the upper layer was observed to become perpendicular to those in

the lower layer by Cserepes et al. (1988). Entrainment occurs at cusps in the interface, as will be discussed later.

If one layer is substantially more viscous, the form of upwellings or downwellings forming at the interface is also different (Davaille, 1999b), with 2-D sheets forming in the more viscous layer but 3-D plumes forming in the less viscous layer, which have different entrainment rates as will be discussed later.

7.12.3.1.2.2 Thin, nonconvecting lower layer

In this case, the lower layer is embedded within the lower TBL of the main convection, and the dense material gets swept by the convection, forming a spoke pattern of ridges on top, with plumes at the junctions of the ridges, and entrainment takes place there, as shown by 3-D numerical experiments (Tackley, 1998) and laboratory experiments (Davaille et al., 2002; Olson and Kincaid, 1991). The numerical experiments show that this dense layer acts like a rigid boundary, reducing the horizontal wavelength of convective planform relative to a free-slip lower boundary (Tackley, 1998), and that if the layer internally convects (Montague and Kellogg, 2000; Montague et al., 1998), as would be the case if its viscosity is low enough (Schott and Yuen, 2004; Solomatov and Moresi, 2002), small-wavelength thermal structure is generated within the layer. These numerical experiments also show that even in 100% internally heated cases, entrainment exists at cusps anticorrelated with where the downwellings are, and larger amounts of internal heating reduce the buoyancy ratio needed for stability. Temperature-dependent viscosity decreases the density contrast needed for stable layering (Schott et al., 2002; Tackley, 1998) and, when the layer is marginally stable, can lead to complicated schlieren structures of entrained material and complicated layer topography (Schott et al., 2002). For reasonable Earth parameters, Tackley (1998) found for an internally heated case that ~1% density contrast was sufficient to maintain a layer over reasonable timescales.

7.12.3.1.2.3 Thick, large-topography lower layer or isolated piles

With a fairly low buoyancy ratio like 0.6 (Montague et al., 1998), the topography on the layer interface is large (Davaille, 1999a; Kellogg et al., 1999), which may result in discontinuous 'piles' or 'hills' if the layer thickness is less than the topography. In 2-D calculations at low Rayleigh number, this results in wide stable 'hills' below the upwelling, which cause strong (approximately several km) negative topography on the CMB (Davies and Gurnis, 1986; Hansen and Yuen, 1989), with temperature-dependent viscosity decreasing the magnitude of this negative topography (Hansen and Yuen, 1989). The topography on a layer interface decreases with increasing Rayleigh number, approximately as $Ra^{-1/3}$ (Davies and Gurnis, 1986; Tackley, 1998), which predicts relatively little topography at the Earth's convective vigor (Montague and Kellogg, 2000). If, however, the increase of viscosity and thermal conductivity and the decrease of thermal expansivity with depth are taken into account, they lead to a low effective *Ra* for the deep mantle, so large interface fluctuations can still occur, as shown in 3-D (Tackley, 1998, 2002). It has been argued that such structures may account for the superplumes observed in seismic tomography, discussed in **Section 7.12.1.8**. An important point shown by van Thienen et al. (2005a) is that any layering around 660 km induced by the postspinel phase transition makes the layer more stable over long time periods, presumably because it reduces the temperature drop across the layer and the convective velocities.

Regarding the three-dimensional structure of a strongly undulating layer, Cartesian calculations (Tackley, 1998, 2002) that were either Boussinesq or compressible with constant, depth-dependent, or depth- and temperature-dependent viscosity, found that the long-term structure of dense piles tends to be ridges/spokes. In spherical geometry Boussinesq calculations (Oldham and Davies, 2004), there is a greater tendency for the piles to be isolated. A viscosity contrast between the layers makes a major difference to the planform: McNamara and Zhong (2004b) showed that temperature-dependent viscosity leads to linear piles that are swept around and spread through the entire lower mantle, whereas composition-dependent viscosity in which the dense material is more viscous leads to isolated round 'superplumes,' particularly with contrasts as large as factor 500. This seems to be consistent with the 'domes' in the laboratory results of Davaille (1999a), except that they also observe domes when the dense layer is less viscous. The reconciliation of these is that such domes are transient features – for long-lived features, domes are only observed when the lower layer is more viscous (McNamara and Zhong, 2004b; see also **Chapter 7.11**).

Comparison of structures obtained from convection models with structures imaged by seismic tomography provides important constraints. Deschamps and Tackley (2008, 2009) performed a systematic suite of thermochemical convection models running for billions of years and compared the results to probabilistic seismic tomography of Trampert et al. (2004). Convection models that matched seismic constraints had a moderate compositional density difference of 90–150 kg m^{-3} (leading to large-topography piles), a large thermal viscosity contrast, and at 660 km depth a viscosity jump by factor 30 and an endothermic phase transition with a Clapeyron slope of -1.5 to -3 MPa K^{-1}.

7.12.3.1.2.4 Long-term fixity of piles?

Based on the observation that present-day hot spots and the reconstructed locations of large igneous provinces (LIPs), both assumed to be caused by plumes from the CMB, often coincide with the edges of the large seismically slow regions above the CMB, particularly under Africa (Burke and Torsvik, 2004; Thorne et al., 2004; Torsvik et al., 2006), it has been proposed that plumes are preferentially generated edges of dense piles that have remained in a similar position for the last ~300 Ma (Burke et al., 2008; Torsvik et al., 2008, 2010). There has even been a proposal that the large-scale structure of the deep mantle has been stable for billions of years (Dziewonski et al., 2010). Important questions are thus (i) whether such long-term stability is dynamically feasible and (ii) why do plumes come from the edges, rather than centers, of the piles? Here, (i) is considered; plumes are discussed in **Section 7.12.3.1.3**. In all laboratory or numerical experiments of thermochemical convection in which the flow is time-dependent, piles of dense material are swept around by the large-scale flow, sometimes being split by new downwelling slabs or merging (e.g., Davaille et al., 2002; Hansen and Yuen, 1989; McNamara et al., 2010; Tan et al., 2011). Thus, stability for billions of years

seems unlikely. However, even in time-dependent, chaotic convection, there are often features that remain in a similar position for some time, and the proposed 300 Ma stability is less than one 'overturn time' of mantle convection. Indeed, in many published numerical or laboratory studies, it is possible to find thermochemical piles that are stable for 100s Ma (e.g., Figure 6 in Tan et al., 2011). Thus, a special explanation for a few 100s Ma fixity of dense piles is probably not required (see also **Chapter 7.11**).

7.12.3.1.2.5 Models driven by plate reconstructions

Several studies have focused on modeling the last ~200 million years of the Earth's evolution by applying plate reconstructions as an upper velocity boundary condition on 3-D spherical thermochemical convection models, following earlier studies for purely thermal convection (e.g., Bunge et al., 1998). McNamara and Zhong (2005) found that thermochemical structures similar to those seismologically observed under Africa and the Pacific were generated. Specifically, the Earth's subduction history tends to focus dense material into a ridge-like pile beneath Africa and a relatively more rounded pile under the Pacific ocean, which they argued is consistent with seismic observations, a point that was further reinforced by performing synthetic seismic tomography of such models (Bull et al., 2009). Bower et al. (2013) performed similar modeling but with the addition of progressive assimilation to guide the thermal structure of the lithosphere and steer the thermal evolution of slabs in the upper mantle and also a different (higher) bulk modulus for the dense material. They obtained deep mantle thermochemical structures that are broadly similar to those of seismic tomography and of McNamara and Zhong (2005), found that spreading slabs can cause steep sides and plumes at the edges of dense piles, and found that having a higher bulk modulus for the dense material was not necessary. While thermochemical structures are typically invoked, there is an active debate as to whether purely thermal convection can generate structures resembling seismic tomography (Davies et al., 2012).

7.12.3.1.2.6 Steep sides

In some places on Earth, sharp near-vertical sides to the large low-velocity provinces are observed seismically (e.g., He and Wen, 2009; Ni et al., 2002, 2005; Wang and Wen, 2007). Two possible causes of these are (i) slabs spreading above the CMB 'bulldozing' the dense material, which is a transient effect, and (ii) the dense material having a higher bulk modulus than the surrounding mantle. Transient steep sides (timescale ~100s Ma) caused by 'bulldozing' were observed in laboratory experiments (Davaille, 1999a) and numerical experiments (Deschamps and Tackley, 2008, 2009) of free convection and numerical experiments with imposed plate motions (Bower et al., 2013; Bull et al., 2009; Lassak et al., 2010; Steinberger and Torsvik, 2012). Long-term stable steep-sided thermochemical piles were investigated by Tan and Gurnis (2005) and Tan and Gurnis (2007), who found that an increase in chemical density contrast with height above the CMB is necessary. This is because the thermal expansivity increases with height above the CMB, making the top of the piles less stable unless the chemical buoyancy contrast also increases. Whether MORB has this property is uncertain, as discussed in **Section 7.12.3.3.3**. Such decreasing MORB density contrast with depth has also been included in some numerical simulations in which a layer accumulates over time by segregation of MORB rather than inserted a priori (Nakagawa and Tackley, 2005a, 2010, 2011, 2013; Xie and Tackley, 2004a,b), and steep-sided thermochemical structures are observed in some of those calculations. The rate at which thermal expansivity changes with depth is very small in the deep mantle (and is exaggerated in by Tan and Gurnis (2005) and Tan and Gurnis (2007) by assuming a linear profile), so the needed difference in compressibility is small.

7.12.3.1.2.7 CMB topography

If piles have a low viscosity, then they do not depress the CMB as earlier models indicated (Hansen and Yuen, 1989), but instead cause relatively flat CMB topography under themselves, with lower CMB topography occurring under slab graveyards (Lassak et al., 2007, 2010).

7.12.3.1.3 Influence of a dense layer on plume dynamics

7.12.3.1.3.1 Temperature

The presence of a dense layer reduces the temperature anomaly of plumes (Farnetani, 1997; Zhong, 2006), which may help to explain why the inferred temperature anomaly of plumes close to the lithosphere is much lower than the estimated temperature drop across the lower TBL for whole-mantle convection.

7.12.3.1.3.2 Stability

Laboratory experiments find that plumes rising from cusps of a dense layer are stable over longer time periods than plumes rising from the lower TBL of whole-mantle convection. In particular, Davaille et al. (2002) found that the dense layer acts as a 'floating anchor,' reducing the lateral migration of plumes, which then have a scaled drift velocity of 1–2 mm year^{-1} – larger than simple scalings predict for thermal plumes. In addition, the dense layer enables them to survive for 100s My. The plume spacing is proportional to the stratified boundary layer thickness. In the laboratory experiments of Jellinek and Manga (2002), the dense, low-viscosity material forms a network of ridges (embayment and divides), and they delineate the trade-off between viscosity contrast and layer topography in the stabilization of plumes. They found that if the dense material has a similar viscosity, the topography required to stabilize plumes is greater than two to three times the TBL thickness (to overcome viscous stresses), but this required topography decreases as the layer viscosity decreases, because the lower layer then acts as a free-slip boundary. Indeed, with >2.5 orders of magnitude viscosity contrast, only minimal topography is needed. With no dense layer present, upwellings are in the form of intermittent thermals.

This laboratory finding that a dense layer stabilizes plumes is seemingly contradicted by numerical experiments (McNamara and Zhong, 2004a). In these numerical experiments, plume stability was quantified as the ratio of horizontal plume velocity to average surface velocity. McNamara and Zhong (2004a) found this to be about the same in layered calculations as it is in isochemical calculations with a rigid lower boundary, regardless of the viscosity contrast of the dense material. They also found that layer topography does not influence fixity, but can lead to longer-lived plume

conduits that follow the topographic peaks around. The reconciliation of these apparently contradictory findings is not clear. One possibility is that the dense layer reduces the convective vigor and that the laboratory experiments did not take this into account. Another is that there is a difference in the dynamics of downwellings (e.g., they might be stronger in the numerical experiments), which push the lower layer and associated hot plumes around. More study is needed to reconcile laboratory and numerical results on this issue.

7.12.3.1.3.3 Plumes from the edges of piles?

Observations suggest that in the Earth, present-day plumes (Thorne et al., 2004) and historical LIPs inferred to be caused by plumes (Burke et al., 2008; Burke and Torsvik, 2004; Torsvik et al., 2006, 2008, 2010) tend to come from the edges of inferred chemically dense piles (i.e., low seismic-velocity provinces), rather than the tops of them. In detail, this appears to be true under Africa, but under the Pacific, plumes also emerge from the tops of the inferred dense pile. In contrast, in most laboratory and numerical experiments of thermochemical convection, plumes typically form from the tops of dense piles or ridges, rather than their edges. Recent numerical experiments indicate that key mechanisms for generating plumes from the edges of piles are slabs and steep sides. Slabs reaching the CMB tend to induce plumes at their edges, even in the absence of chemical layers (e.g., Tan et al., 2002). When chemical piles are present, slabs can 'bulldoze' the dense material to create ridges at their edges, which promotes plume formation. The latter can be seen in thermochemical convection calculations with imposed historical plate motions (Bower et al., 2013; Bull et al., 2009; Lassak et al., 2010; Steinberger and Torsvik, 2012), in which cusps from which plumes can form appear at the edges of the Pacific and African low-velocity provinces. In regional calculations of compositionally stratified slabs reaching the CMB (Tackley, 2011), plumes also tend to form at the edges of regions of dense material, which are also the edges of the slabs. Steep edges can be generated by the 'bulldozer' effect of slabs, potentially helped by the dense material having a higher bulk modulus (Tan and Gurnis, 2005, 2007), although the latter is not sufficient to guarantee edge plumes as the plumes in Tan and Gurnis (2005, 2007), in which there are no cold downwellings, form at the tops of the piles. The most successful models to obtain plumes from the edges of piles without any imposed motions are those of Tan et al. (2011), who performed free convection models of thermochemical convection in 3-D spherical geometry with a moderate viscosity contrast and obtained two to three steep-sided piles with plumes arising mostly from their edges. Another effect that can suppress plumes from the tops of piles is for them to have a compositional gradient rather than a sharp compositional boundary (Tackley, 2011). Layers that build up by segregation of subducted MORB (e.g., Brandenburg et al., 2008; Nakagawa et al., 2010) tend to be topped by such compositional gradients rather than a sharp boundary.

7.12.3.1.3.4 Starting plumes

Despite the effect that a dense layer can have on increasing plume stability as discussed earlier, some studies have found that for starting plumes, the presence of a dense layer can add complexity and modes of time dependence that are not present with purely thermal plumes. Lin and Van Keken (2006a,b) numerically investigated axisymmetric models set up to produce a plume at the axis, various temperature dependences of viscosity, and a dense layer with various thicknesses, buoyancy ratios, and viscosity contrasts. They found that entrainment commonly becomes a transient process for models with variable viscosity. In models where a large fraction of the dense layer was entrained, variable viscosity could lead to secondary instabilities developing after the initial plume head, whereas in models with only a thin filament entrained, variable viscosity could lead to an initial pulse of entrainment. In general, the dense material led to a wider range of plume morphologies than observed with purely thermal plumes. As with results discussed elsewhere, they found that decreasing the viscosity of the layer made it more stable.

Even greater morphological variability and complexity were found in the 3-D models of Farnetani and Samuel (2005), in which thermochemical plume formation was modeled in a compressible mantle with no imposed symmetry, an initially 200 km thick layer with buoyancy ratio $B=0.1$, and T- and depth-dependent viscosity. Plume morphologies were much less regular than 'classical' plumes and included plumes with blob-like or irregular heads, tilted plumes, ~1000 km wide 'megaplumes,' broad plumes without heads, and 'classical' head plus narrow tail plumes, often with several types coexisting. The buoyancy flux of conduits varied widely, and some structures ponded under the 660 km discontinuity. Plume conduits were found to be laterally heterogeneous (i.e., without concentric zonation), but as with previous results (Farnetani et al., 2002), the only material hot enough to melt underneath the lithosphere is from the source region. If the dense material has a different compressibility, this can lead to additional complexity such as plume heads ponding at a certain depth (Samuel and Bercovici, 2006).

Laboratory experiments of thermochemical starting plumes (Kumagai et al., 2008) confirmed the conclusions from the previously mentioned numerical experiments: thermochemical plumes may not have the classical plume structure but can also be fat and patchy, and they may also exhibit more complexity and time dependence than purely thermal plumes.

7.12.3.1.4 Entrainment of surrounding material by mantle plumes

As discussed earlier, plumes clearly entrain material from a dense layer at their base. A long-standing question is how much this composition is diluted by material entrained from the upper layer as they rise. The initial plume head and subsequent conduit have different structure and so are expected to be different in their entrainment characteristics.

Depending on the viscosity contrast, rising hot diapirs, analogous to plume heads, thermally entrain surrounding material as they rise, forming a folded structure (Griffiths, 1986). It was demonstrated that this structure also occurs in plume conduits if they are sheared by the surrounding material (Richards and Griffiths, 1989), to such an extent that "small plumes or narrow plume conduits may consist of only a small fraction of original source material" (Richards and Griffiths, 1989). Hauri et al. (1994) presented analytic solutions for plume conduits, finding that they entrain significant amounts

of ambient mantle due to lateral thermal conduction from the plume. They found a huge range of possible entrainment, depending on the buoyancy flux, with most of the entrained material coming from the lower half of the layer they are passing through.

Although plumes may entrain a significant amount of surrounding material, Farnetani and Richards (1995) found that the entrained material does not contribute significantly to the melt produced by the plume, with >90% of the primary plume magmas being composed of primary plume material. The first-order reason for this is that the entrained material has a much lower temperature than the core of the original plume, and so is much less likely to melt underneath the lithosphere. Reinforcing and extending this finding, Farnetani et al. (2002) analyzed entrainment by a thermal plume with temperature-dependent viscosity contrast 100 and found that the material that melts is from the TBL at the base of the mantle. The material in the plume head was found to be much more extensively stretched and stirred than that in the plume conduit, implying greater homogenization of geochemical anomalies. At that viscosity contrast, the plume head did not entrain surrounding material, although a substantial amount of lower mantle material was advected upward with the plume into the upper mantle. Subsequent models (Farnetani and Hofmann, 2009, 2010) reinforced this conclusion.

The influence of plume entrainment on trace-element signatures is discussed in **Section 7.12.4.4**.

7.12.3.1.5 Ultra-low-velocity zones

A number of geographically localized and vertically thin (~10 s km) zones of very low seismic velocity (5–10% lower than average) directly above the CMB have been detected since the mid-1990s (Garnero and Helmberger, 1995, 1996). Their locations are statistically correlated with hot-spot locations (Williams et al., 1998) and with the edges of large, seismically slow regions (McNamara et al., 2010) that are commonly inferred to be compositionally distinct, as discussed in **Section 7.12.1.5.4**. Two classes of explanation have been proposed: (i) 10–30% partial melt and (ii) some type of iron-enriched solid. Dynamic aspects of these possibilities are reviewed in the succeeding text (see also **Chapter 7.11**).

If ULVZs are caused by 10–30% partial melt (Garnero, 2004; Lay et al., 2004; Revenaugh and Meyer, 1997; Vidale and Hedlin, 1998; Wen and Helmberger, 1998; Williams and Garnero, 1996), a key question is why the melt stays in the solid matrix rather than draining into a pure melt layer above the CMB (if it is denser than the solid) or rising into the colder mantle above and solidifying (if it is buoyant). Dynamic calculations of the deepest mantle including two-phase flow indicated a very narrow parameter range in which melt would remain in the solid to form ULVZ-like features (Hernlund and Tackley, 2007): the melt must be slightly denser than the solid and the permeability curiously very low. These calculations, however, used a simplified treatment of melt migration in which the driving force for melt percolation was purely gravity acting on the density difference between solid and liquid. Hernlund and Jellinek (2010) showed that when dynamic pressure gradients associated with deformation of the solid matrix by surrounding flow are also included, dynamic pressure gradients can dominate gravitational settling and allow the melt to stay in suspension in the solid.

Various solid compositions are also plausible candidates for explaining ULVZ seismic properties and may match better than partial melt. These include iron-rich postperovskite (Caracas and Cohen, 2005; Mao et al., 2006; Stackhouse et al., 2006; Stackhouse and Brodholt, 2008), a mixture of iron-enriched (Mg,Fe)O magnesiowüstite and ambient mantle (Bower et al., 2011; Wicks et al., 2010), and subducted banded iron formations (Dobson and Brodholt, 2005). The origin of iron-enriched material might be the final product of crystallization of a basal magma ocean (BMO) (Labrosse et al., 2007; Nomura et al., 2011; **Section 7.12.5.2.5**) or chemical reactions with the core (**Section 7.12.1.5.4**). It has also been suggested that ULVZs could be caused by accumulated silicate sediments from the core (Buffett et al., 2000).

The dynamic feasibility of the 'dense solid' explanation was demonstrated by McNamara et al. (2010) using calculations of thermochemical convection with two types of dense material, one representing large-scale piles and the other small-scale features with the density seismically inferred for ULVZs. They showed that small volumes of solid ULVZ material can be locally elevated despite its high density and are swept around by the convection to the boundaries of large compositional piles, which periodically break apart and merge together in response to changes in downwelling patterns. When the large piles merge, some ULVZ material is initially located inside the merged pile, in accordance with recent seismological observations (Thorne et al., 2013). The detailed morphology and seismic signature of isolated solid ULVZs was investigated by Bower et al. (2011), who identified a parameter range in which they resemble seismically observed structures (see also **Chapter 7.11**).

7.12.3.2 Long-Term Entrainment of Stable Layers

In a system with stable compositional layering, the system nevertheless evolves with time because the thermal convection in each layer causes entrainment of material from the other layer, in the form of thin schlieren, thereby diminishing the density contrast (Olson, 1984). There are two possible outcomes to this evolution: (i) If the entrainment is asymmetrical (typically due to the lower layer being thinner than the other, e.g., Samuel and Farnetani, 2003), then one layer may eventually disappear due to complete entrainment into the other layer. Indeed, it is likely that in the long term, there is substantial entrainment of any dense material residing above the CMB, which may be balanced by the addition of material by segregation or core reactions, as will be discussed later. (ii) The density contrast decreases to the point where the layering is no longer stable and large-scale overturn and stirring occur. Numerical calculations and laboratory experiments have been useful in elucidating the details of these processes, while mathematical analysis has been useful in developing scaling laws for entrainment.

7.12.3.2.1 Comparison of entrainment laws and estimates

Several authors have obtained expressions for the entrainment rate as a function of parameters such as density contrast, viscosity contrast, and so forth. Studies usually focus on one of

two situations: a thin layer at the base of the mantle or two layers of substantial thickness. While the same laws might apply, the former case obviously has much greater asymmetry and the lower layer might not be convecting.

7.12.3.2.1.1 Laboratory experiments

From studying the entrainment in laboratory experiments with two layers of equal depths, Olson (1984) found that the mixing rate of the two layers, defined as the rate of change of their density divided by the density difference (i.e., the fractional volume flux), scales as

$$\dot{M}/\dot{\varepsilon} \approx 0.046 Ri^{-1} \quad [39]$$

where the Richardson $Ri = \Delta\rho g D/\tau$ with τ being the average viscous stress within each layer. Eliminating Ri leads to

$$\dot{M}/\dot{\varepsilon} \approx 0.046 \frac{\tau}{\Delta\rho g D} \quad [40]$$

For two thick stable layers where the lower layer is more viscous by a factor of $1.0–6.4 \times 10^4$, Davaille (1999b) found that the scaling for entrainment by linear sheets (typically found in the more viscous layer) is different from that for axisymmetric plumes (found in the less viscous layer). For entrainment by linear sheets,

$$Q_{21} = C_1 \frac{\kappa h_0}{B} Ra^{1/5} \quad [41]$$

whereas for columnar plumes,

$$Q_{12} = C_2 \frac{\kappa h_0}{B^2} Ra^{1/3} \quad [42]$$

where Q is flux of material, h_0 is initial thickness of lower layer, κ is thermal diffusivity, and C_1 and C_2 are two experimentally determined constants. The 'plume' law has the same $1/B^2$ form as the one proposed by Sleep (1988) (discussed in the succeeding text). When the lower layer is substantially more viscous than the upper layer, it is difficult for the upper layer to entrain it, requiring an additional factor (Davaille, 1999a):

$$Q = C_1 \frac{\kappa H}{B^2} Ra^{1/3} \frac{1}{1 + \Delta\eta/B} \quad [43]$$

where $\Delta\eta$ is the viscosity contrast. This additional factor applies for $\Delta\eta > 1$, that is, for entrainment of the more viscous layer into the less viscous layer. If the layer being entrained is substantially less viscous than the entraining layer, then Q could also be reduced due to draining of the less viscous material back into the layer it came from, but this was not observed by Davaille (1999a) and Davaille et al. (2002) at $\Delta\eta$ as low as 0.01. This entrainment law was subsequently verified for the case of a thin layer with plume entrainment (Davaille et al., 2002). Depending on parameters, a mantle plume would entrain chemically dense material at a rate of 0.1–15% of its total volume flux. Davaille et al. (2002) presented graphs of layer survival time versus thickness and density contrast, based on thermal expansivity $10^{-5}\,K^{-1}$ and 'temperature heterogeneity' of 500 K. As an example, entrainment of 100 km over 4.5 Gy occurs with a 3.5% density contrast if the layers are of the same viscosity or ~2% density contrast if the dense material is ten times more viscous.

Several other authors have conducted laboratory experiments to study entrainment and long-term evolution. In experiments with an initial layer thickness of 0.2 (600 km) and similar viscosity materials, Gonnermann et al. (2002) found vigorous convection in both layers and entrainment consistent with the scaling laws of Davaille (1999a). They estimated that an initially 300 km thick layer can survive over the Earth's history if it has a 2% density contrast, but if initially thicker, then it can survive if it has a <2% initial density contrast. In some cases, the dynamics changed from stable layering to doming.

The strong influence of viscosity contrast on entrainment of a thin layer was demonstrated by Namiki (2003) using viscosity ratios from 0.1 to 400. It was found that when the lower layer is more viscous, it grows in size due to asymmetrical entrainment of the upper layer. When the lower layer is less viscous, an interfacial layer developed and the volumes of the layers did not change because plumes entrained the interfacial layer, not the lower layer. This interfacial layer is a novel finding not observed in any other mantle-related studies, so it is worth considering what causes it. The layer might develop because of incomplete entrainment of the lower, less viscous layer by the upper layer due to reduced viscous coupling. It might form as a result of double-diffusive convection, which helps to transport material across the boundary (M. Manga, personal communication). If the latter explanation is correct, it would not form in Earth because the chemical diffusion rate is very low. In any case, by considering stresses (as in Olson, 1984), Namiki (2003) derived an entrainment law that is consistent with those discussed earlier:

$$\dot{E}_i \sim \frac{\kappa_i}{B_i^2 \delta_{th_i}} \quad [44]$$

where $\dot{E}_i$ is the entrainment rate of layer i and δ is the TBL thickness, related to the Rayleigh number as $\delta_{th} \sim 5 L_i Ra^{-1/3}$ leading to an overall scaling of

$$\dot{E}_i \sim 0.2 \frac{\kappa_i}{B_i^2 L_i} Ra^{1/3} \quad [45]$$

In this parameterization, the effect of a viscosity difference is to alter the ΔT for each layer, hence B and Ra. The survival time of a 200 km thick layer was calculated as a function of its density difference, assuming the total $\Delta T = 4000$ K, the viscosity of D″ is 10^{19} Pa s, the viscosity of the mantle is 10^{21} or 10^{22} Pa s, and thermal expansivity is $2 \times 10^{-5}\,K^{-1}$. It was estimated that a density difference of at least 300 kg m^{-2} (5.5%) is needed for the layer to survive over geologic time (ignoring the possible presence of an interfacial layer). With a more realistic thermal expansivity of $1 \times 10^{-5}\,K^{-1}$, this would be reduced to 2.75% contrast, comparable with other estimates.

A scaling law that explicitly includes viscosity contrast was proposed by Jellinek and Manga (2002) on the basis of laboratory experiments:

$$q = 0.49 \frac{\kappa}{H} \frac{Ra^{1/3}}{\Delta\eta B} \quad [46]$$

where H is the depth of tank and $\Delta\eta > 1$ is the ratio of upper to lower layer viscosity. This is similar to the expression of Davaille (1999a) given earlier, in the limit of $\Delta\eta \gg B$. It is interesting that in this limit, the dependence on B is $1/B$ rather than $1/B^2$.

7.12.3.2.1.2 Mathematical or numerical approaches

Gradual entrainment of thin chemical layer at the base of the mantle by either 2-D upwelling sheets or axisymmetric plumes was analyzed by Sleep (1988) to determine the fraction of entrained material in the upwelling as a function of chemical density contrast. The analysis did not consider the details of the entrainment process, but rather the carrying capacity of the plume conduit. Thus, a 1-D section across the upwelling was considered, with the entrained material in the form of a thin filament in the center of the upwelling. To determine the thickness of this filament, it was assumed that the thickness adjusts so as to maximize entrainment rate (e.g., if it is too thick, then the upwelling velocity decreases). The models included temperature-dependent viscosity. While a general scaling law for all parameter combinations was not explicitly stated, the general form was found to be

$$F = C/B^2 \qquad [47]$$

where C is a constant and B is the chemical buoyancy ratio. Based on these models, Sleep (1988) estimated that a chemical density contrast of 6% is necessary for a 100 km thick, non-convecting layer to survive over the age of the Earth if the thermal expansivity is $2 \times 10^{-5}\,\mathrm{K}^{-1}$. Subsequent mineral physics data (e.g., Anderson et al., 1992; Chopelas, 1996) indicate a thermal expansivity closer to $1 \times 10^{-5}\,\mathrm{K}^{-1}$ at the CMB, so this estimate of density contrast should be adjusted to 3%. Additionally, if the initial layer thickness were larger, then a higher entrainment rate could be tolerated. In any case, this density contrast corresponds to $B \sim 3$ based on the temperature drop over the lower boundary layer or $B \sim 1.5$ using the temperature drop over the entire system – both substantially larger than that required to stabilize the layer against rapid overturn. Sleep (1988) also considered the case of an internally convecting layer and concluded that the earlier mentioned estimate is still reasonable.

The entrainment process at the base of the plume (not considered by Sleep, 1988) was included in the high-resolution 2-D numerical models of Zhong and Hager (2003). They found that treating the lateral flow at the bottom of the plume makes some significant differences compared to the 1-D analysis of Sleep (1988), with the 1-D model overestimating entrainment by up to more than a factor of 4 compared to their 2-D calculations. They found that the entrainment rate Q is mainly controlled by the buoyancy ratio B and the radius of the thermal plume r_T but insensitive to the thickness of the dense layer, with a relationship

$$Q \sim B^{-2.48} r_T^{3.80} \qquad [48]$$

Because their model was set up to produce a plume with prescribed parameters, they did not obtain a scaling law for a full convective system. They did, however, apply the scaling to estimate the survival time of a 1000 km thick layer and estimated that more than 90% of a 1000 km thick dense layer can survive for 4.5 Gy if the dense material has a net negative buoyancy of ~1%. It is important to note that this is the 'net' buoyancy (thermal + chemical) and not the chemical buoyancy! For a thermal expansivity of $2.5 \times 10^{-5}\,\mathrm{K}^{-1}$ and a dense material 800 K hotter, the chemical density contrast would have to be 3%. This could be reduced by a factor of ~2 using a more realistic deep mantle thermal expansivity.

Recently, Lin and Van Keken (2006a,b) revisited the transient dynamics of a plume forming from a boundary layer with an included dense chemical layer, first studied by Christensen (1984). The dynamics are discussed in **Section 7.12.3.1.3**. Although the short-lived (250 Ma) nature of their simulations was not intended to study long-term entrainment, they did compare short-term entrainment with existing laws and also found some interesting behavior. In particular, they found two effects that are not accounted for in standard entrainment theory: (i) A very thin layer, that is, much thinner than the TBL, could be entrained very rapidly despite having $B = 2$ or 3. (ii) For $B \sim 1$, a new starting plume head caused a 'pulse' in entrainment, bringing into question the applicability of steady-state entrainment laws for a dynamic, time-dependent mantle. As expected, temperature-dependent viscosity resulted in much lower entrainment, for example, with a factor of 1000, even a layer with $B < 0.5$ was stable. Regarding entrainment rate, their results were consistent with $F = C/B^2$ found by Sleep (1988) with $C = 0.07$ and the scaling law of Davaille (1999b) with $C = 1.1$, although there was some deviation from the latter when $B > 1$, which they suggested is due to the effective B and Ra adapting with time in the laboratory experiments. They estimated that a layer with temperature-dependent viscosity can survive if it is thicker than 75 km and its compositional density contrast is larger than 1.5% assuming thermal expansivity is 3×10^{-5}, which would be reduced to ~0.5% with an Earth-like thermal expansivity.

7.12.3.2.1.3 Summary of layer survival estimates

As several studies discussed earlier have estimated the density contrast required for a dense layer to survive over geologic time in the face of continuous entrainment, it is useful to consider whether these estimates are consistent with each other. In general, the published estimates assume a deep mantle thermal expansivity at least a factor of 2 higher than realistic, so in **Table 2**, they have been rescaled if necessary to a thermal expansivity of $1 \times 10^{-5}\,\mathrm{K}^{-1}$. In general, the rescaled estimates are consistent, with thinner layers increasing the required density contrast and a viscosity contrast (either higher or lower) reducing the required density contrast. Perhaps the exception is Lin and Van Keken (2006a), whose density estimate is very low. This could be because they have a larger viscosity contrast than any other study, and this is certainly worth exploring further. Another factor might be that they consider a single plume with $\Delta T = 750$ K rather than a full convective system as in the laboratory studies, and convective downwellings could help to destabilize the layer. On the other hand, Sleep (1988)

Table 2 Scaled estimates of density contrast required for long-term survival

Study	*Thickness (km)*	$\Delta\rho$	η
Sleep (1988)	100	3.0%	1
Davaille et al. (2002)	100	3.5%	1
Davaille et al. (2002)	100	2.0%	10
Gonnermann et al. (2002)	300	2.0%	1
Namiki (2003)	200	2.75%	0.01
Zhong and Hager (2003)	1000	1.5%	1
Lin and Van Keken (2006a)	>75	>0.5%	0.001

and Zhong and Hager (2003) also considered isolated plumes. In summary, this issue requires investigation in a fully convecting system with large viscosity contrast.

7.12.3.3 Evolution of a Mantle with Ongoing Differentiation

7.12.3.3.1 General evolution

So far, this review has focused on the evolution of a system with preexisting layering. However, while the possibility of primordial layering exists, most of the geochemically observed heterogeneity appears to be related to recycled material, so several models have studied the evolution of a mantle in which heterogeneity is continuously introduced over time, usually to simulate the differentiated components in subducted slabs (Christensen, 1989b; Christensen and Hofmann, 1994; Davies, 2002, 2007; Gurnis, 1986a; Huang and Davies, 2007a,b,c; Kameyama et al., 1996; Nakagawa and Tackley, 2005a,b, 2006, 2010, 2011, 2012, 2013, 2014; Nakagawa et al., 2009, 2010, 2012; Ogawa, 1988, 1993, 1997, 2000a, 2003, 2010, 2013; Tackley et al., 2007; van Thienen et al., 2004; Xie and Tackley, 2004a,b). Some of these have already been discussed to a certain extent, for example, in the context of the effect on residence time.

In this section, models in which active heterogeneity is introduced are discussed. Some of the models track trace elements as well as crust residue differentiation; the trace-element aspects of them are discussed in **Section 7.12.4**. One of the main differences between studies is how they treat the secular evolution of the planet, in which the mantle and core cool and heat-producing elements produce less heat. While some studies attempt to directly include this (e.g., Nakagawa and Tackley, 2005a; Ogawa, 2003; Xie and Tackley, 2004b), others have parameterized the faster earlier evolution as a longer run time at a constant convective vigor (Davies, 2002). Other differences are how crustal production is treated (self-consistent melting criterion or assumed thickness crust) and how plate tectonics is treated (kinematic plates or using a yield-stress approach).

While there are substantial variations in the assumptions and results among different calculations, it is possible to generalize the typical evolution. Here and in subsequent discussions of the deep mantle, 'MORB' refers to subducted MORB that actually has a different mineralogy than basalt due to solid–solid phase transitions; for example, it is eclogite at upper mantle pressures:

1. Initial condition: chemically homogeneous.
2. Vigorous early melting phase, characterized by (i) high magmatic heat transport (the so-called 'magmatic heat pipe' mode discussed in **Section 7.12.3.3.2**), (ii) rapid production of basaltic crust, thick enough that the base of it transitions to eclogite, which could result in delamination or even wholesale sinking of the crust (Johnson et al., 2014; van Thienen et al., 2004), and (iii) buildup of compositional stratification if the crust and residue are able to sink into the mantle and separate at some depth: Harzburgitic residue rises to the top, while eclogitic crust sinks to the bottom, forming a depleted shallow mantle and a deep layer of subducted crust. This rapid formation of a depleted upper mantle was observed in some of the calculations of Davies (2002), Nakagawa and Tackley (2005b), Ogawa (2003), Ogawa and Nakamura (1998), but particularly in the calculation presented by Davies (2006) because of its high convective vigor (internally heated $Ra = 7.7 \times 10^{11}$) designed to represent the early Earth. Davies (2006) argued that this depletion helps plate tectonics to operate early on by preventing the formation of a thick crust; however, a crust that is thick enough to transform to eclogite can help plate tectonics because its high density can initiate subduction-like behavior (e.g., van Thienen et al., 2004).
3. Increasing chemical stratification (depending on density contrasts), possibly including a layer of MORB (i.e., subducted MORB that has undergone phase transformations to high-pressure phases) above the CMB, a depleted shallow mantle, and MORB and harzburgite trapped above and below 660 km (see **Section 7.12.3.3.4**). Increasing lateral heterogeneity as more recycled material gets subducted and stirred. It is possible that the phase changes around 660 km depth (**Section 7.12.3.3.4**) play a much larger role than they do now, because phase changes have more effect at higher convective vigor (Christensen and Yuen, 1985; Ogawa, 2003).
4. Transition to a long-term, slowly evolving equilibrium state, in which a dynamic equilibrium may be set up between segregation and entrainment and between the generation (by melting) and destruction (by mixing and/or remelting) of heterogeneity. The mantle is highly heterogeneous, containing a large fraction of recycled material. At this point, most of the mantle is depleted relative to the starting composition if the subducted crust is able to form a layer in the deep mantle (e.g., Christensen and Hofmann, 1994; Ogawa, 1997; Xie and Tackley, 2004a).
5. Possible switches in the regime can occur, such as remixing of previously formed layers (Ogawa, 1994, 1997). Other possible changes are a reduction in stratification at 660 km depth (Ogawa, 2003) or changes in the plate tectonic regime (e.g., as proposed by Davies, 1992; Sleep, 2000; Vlaar, 1986). The latter occurs to some extent in Ogawa (2007, 2013).

It is worth noting some findings of such calculations. Firstly, layers that form from segregation and settling of dense material (as discussed in **Section 7.12.3.3.3**) tend not to have sharp boundaries as do layers that are introduced a priori (**Figure 7**). This makes it more difficult for plumes to form from their tops (Tackley, 2011).

Second, changes in internal heating rate can cause changes in the regime, for example, between layered (caused by vigorous magmatism and basalt/eclogite settling) and well-mixed as occurred in the calculations of Ogawa (1997) and Ogawa and Nakamura (1998). Dupeyrat et al. (1995) also obtained a switch between layered and well-mixed modes, from a homogeneous start.

Third, shallow mantle depletion can cause some dynamic effects, as found by Dupeyrat et al. (1995) modeling upper mantle convection. A layer of depleted residue building up under the lithosphere reduces convective velocity and increases the wavelength of convective cells. When plates are included, they carry the buoyant residue down to the bottom where it can subsequently rise in the form of diapirs, which increases mixing rate (as observed in many of the previously discussed studies).

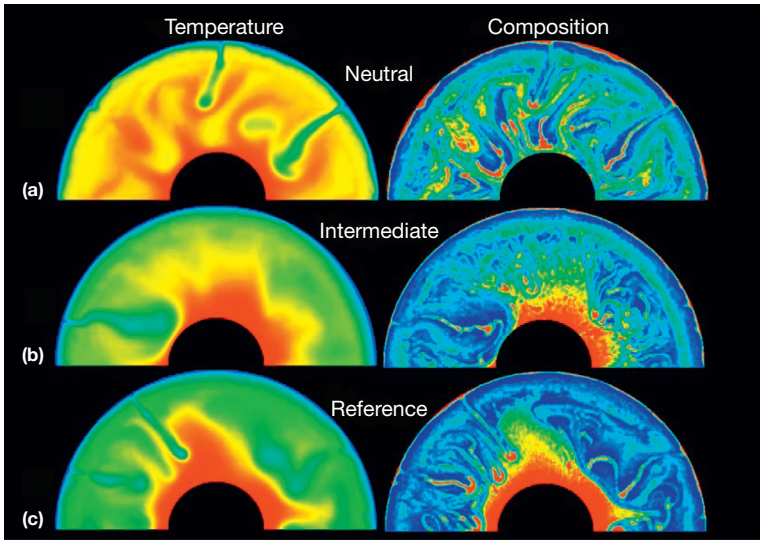

Figure 7 Laterally heterogeneous mantle and 'messy' layering resulting from continuous oceanic differentiation and recycling of MORB and residue for billions of years, from Nakagawa and Tackley (2005a). MORB, red; harzburgite, blue. All models include composition-dependent depth of the transition to perovskite (deeper for MORB) and the same compositional density contrasts in the upper mantle and top of lower mantle. The density contrast of MORB relative to pyrolite at the CMB is either (a) 0%, (b) 1.1%, or (c) 2.2%. When MORB is dense at the CMB, some of it segregates into a layer, which is intermittent in the intermediate-density case. In all cases, the transition zone is enriched and the top of the upper mantle is depleted, due to the different depths of the perovskite phase transition.

7.12.3.3.2 Magmatic heat transport

In models that include secular cooling, extrusive magmatism can be a dominant transport mechanism of heat through the lithosphere at early times. Magmatic heat transport is the sum of energy transport due to latent heat (absorption due to melting in the asthenosphere and then release when the magma solidifies as crust) and energy loss to rapid cooling of the newly formed hot crust at the surface. This 'magmatic heat pipe' mechanism is thought to be the dominant interior heat loss mechanism on Jupiter's moon Io (O'Reilly and Davies, 1981) and tends to result in a cold crust/lithosphere. Parameterized models predicted that it should have been an efficient heat loss mechanism in the early Earth (Davies, 1990). In numerical simulations for Earth by Xie and Tackley (2004b), heat transported by magma was about equally important as conductive heat loss early in the calculation and, later on, subsided to a small fraction of the total heat transport as is the case on present-day Earth. In subsequent simulations of mobile-lid convection for Earth (Nakagawa and Tackley, 2012), episodic-lid convection on Venus (Armann and Tackley, 2012), and stagnant-lid convection on Mars (Keller and Tackley, 2009; Ogawa and Yanagisawa, 2011), magmatic heat transport was found to dominate heat transport at early times. These numerical simulation results are broadly consistent with the parameterization of van Thienen et al. (2005b). This process also acts to buffer mantle temperature, giving a thermostat-like effect (Ogawa and Yanagisawa, 2011). Based on box modeling of xenon isotopes, Coltice et al. (2009) argued that the Earth's early outgassing rate was so high that magmatism was the dominant heat transport mechanism. Recently, Moore and Webb (2013) highlighted magmatic heat piping as being important in the early Earth and made a case that it is consistent with geologic observations.

These models all assume that magmatism is purely extrusive, however. Intrusive magmatism could have quite a different effect, causing a warm, soft crust rather than a cold, hard crust. As intrusive magmatism is generally thought to be more important than extrusive magmatism (Crisp, 1984), its effect on global heat transport and dynamics at early times must be studied in the future.

7.12.3.3.3 Development of a dense layer by gravitational settling of subducted crust

The idea that subducted oceanic crust might settle at the CMB was initially proposed by Hofmann and White (1982) as a way of separating the subducted crust from convective mixing long enough for it to develop the isotopic age observed in OIBs. Long-term storage of subducted oceanic crust may also help explain other geochemical signatures – for example, sulfur isotopes indicating subducted crust older than 2.45 Ga (Cabral et al., 2013). This section discusses constraints on the plausibility of this process, with a focus on MORB. It is also likely that other crustal types have been subducted although in smaller quantities than MORB, for example, Kawai et al. (2009) and Komabayashi et al. (2009) argued that significant amounts of Archean TTG and primordial anorthositic crust have been subducted, with anorthositic crust able to sink to the deep mantle and TTG either becoming trapped in the transition zone (Kawai et al., 2009) or also sinking into the deep mantle (Komabayashi et al., 2009). Tatsumi et al. (2013) found that the residue from the formation of upper continental crust (which is thought to form mainly by partial melting of arc basalts; see **Section 7.12.1.5.2**) is denser than pyrolite at all mantle depths and might therefore contribute to any chemical layering above the CMB.

7.12.3.3.3.1 Subducted MORB density contrast

A key parameter in the process of crustal settling is the density contrast of the MORB composition at the pressure and temperature range of the CMB. Unfortunately, this contrast is still not well known due to uncertainties in the properties of the mineral phases present in MORB at these pressures, although there are ongoing improvements in our knowledge of these. Historically, Ringwood (1990b) proposed that basalt remains 2–4% denser than peridotite throughout the whole mantle, with the exception of the depth range 660–720 km, where it is less dense, the consequences of which are discussed in **Section 7.12.3.3.4**. Subsequently, it was calculated that MORB might actually be less dense than pyrolite at CMB pressures (Kesson et al., 1998; Ono et al., 2001). According to Kesson et al. (1998), MORB is intrinsically 0.9% denser than pyrolite at 1100 km depth but −0.5% (28 kg m^{-3}) less dense than pyrolite at the CMB, while depleted peridotite is less dense than pyrolite at all depths: −0.8 and −0.7% at 1100 km and the CMB, respectively. At face value, this implies that MORB would be positively buoyant at the CMB, but what may matter is the density relative to residue, rather than relative to pyrolite, which is +0.2% (11 kg m^{-3}). This is because it seems likely that 95–99% of the mantle has been processed through MOR melting and thus has been differentiated into residue and MORB, with very little pyrolite remaining. In any case, 11 kg m^{-3} density difference is not enough to have a significant dynamic effect. More recently, Ono et al. (2001) calculated that although MORB is ~100 kg m^{-3} denser at the top of the lower mantle, its density profile intersects an average mantle density at around 1500–2000 km depth in the lower mantle, making MORB neutrally buoyant at ~1600 km depth and positively buoyant at greater depths.

More recent estimates of MORB density are moving back in the direction of it being denser than pyrolite at CMB pressures. From in situ x-ray observations of peridotite and NMORB and K-rich basalts at up to CMB pressures and temperatures, Ono et al. (2005b) estimated that MORB is still 40–80 kg m^{-3} denser than the average mantle at a depth of 1800 km, at which depth they had previously estimated MORB to have ~zero density anomaly (Ono et al., 2001). Guignot and Andrault (2004) refined the equation of state of phases containing Na, K, and Al and calculated MORB to be denser than pyrolite by 100–160 kg m^{-3} at the top of the lower mantle reducing to 25–95 kg m^{-3} at the CMB, which corresponds to 0.45% to 1.7% of the density at the CMB and results in a buoyancy parameter B of 0.2–0.7 (assuming a thermal expansivity of 1.0×10^{-5} K^{-1} and superadiabatic temperature contrast of 2500 K) or 0.4–1.4 (assuming a local temperature contrast of 1200 K). Hirose et al. (2005) measured physical properties of MORB samples at pressures and temperatures up to those near the CMB and found that MORB is substantially denser than PREM throughout the lower mantle and by about 200 kg m^{-3} (3.6%) near the CMB, corresponding to a buoyancy ratio B of 1.4 ($\Delta T = 2500$ K) or 3.0 ($\Delta T = 1200$ K). Most recently, Ricolleau et al. (2010) measured the phase assemblages and densities of a natural MORB sample at up to 89 GPa and then calculated the density profile of MORB for various compositions and temperature profiles. Depending on exact composition, they found that thermally equilibrated MORB is between 0.5% and 2% denser than PREM over the entire lower mantle range.

7.12.3.3.3.2 Regional modeling studies

The laboratory study of Olson and Kincaid (1991) is particularly enlightening because there are no questions of resolution, artificial diffusion, or other issues that plague numerical treatments of composition. They introduced compositionally stratified slabs with equally thick layers of 1% denser and 1% less dense material ($B \sim \pm 0.6$) and initially 3.5 orders of magnitude higher viscosity to the bottom of their tank and found that after a period of warming, the buoyant component of the slab underwent a Rayleigh–Taylor instability in which the low-density 'depleted' material rose through the high-density 'crustal' material, which then remained above the CMB in a 'spoke' pattern and subsequently got entrained over time, as will be discussed later. The scaled time from slab incidence to dense spokes was 1.8 Ga. In this experiment, which has a buoyancy ratio in the range discussed earlier, almost all of the dense 'crust' settled to the CMB, but this may be exaggerated because the 'crust' and 'residue' layers were assumed to be equally thick, whereas in reality, the crustal layer is much thinner.

This case of compositionally stratified slab segments dropping onto a hot CMB was studied using 3-D numerical models by Tackley (2011). The different buoyancies of the high-pressure versions of MORB and harzburgite give the slab a torque that tends to make the MORB side face down. If the slab lands basalt-side down, then MORB can peel off from its underside via fingering instabilities. If the slab lands harzburgite-side down, then MORB can segregate through harzburgite extrusion from the slab sides or by the Rayleigh–Taylor instability observed by Olson and Kincaid (1991). The fraction of MORB that segregates ranges from 0.5–0.7 if a dense layer is already present to 0.25–0.45 if no dense layer is initially present. Slabs spreading above the CMB tend to induce plumes at their edges; these plumes initially contain harzburgitic material, although may entrain basaltic material later on.

7.12.3.3.3.3 Numerical modeling: Prescribed plates

The earliest results on this issue (Gurnis, 1986a) found that with $B = 2$, basaltic tracers that were already separated from the residue component of the slab could aggregate into piles under upwellings for completely internally heated flows; however, with basal heating, they got rapidly swept back into the main flow and did not settle at all if accompanied by complementary depleted tracers. One way of understanding this result is in terms of the Stokes velocity of a sinking blob of crust: At high lower mantle viscosities, this velocity is extremely low, for example, 0.1 mm year^{-1} for a 5 km blob with mantle viscosity = 10^{21} Pa s. If, however, the strong temperature dependence of viscosity of mantle rocks is taken into account, then relatively low viscosities may be present in the hot lower TBL, which allow the crust to settle from the residue fast enough, and several studies that have included this have found significant crustal settling is possible. A similar process has been obtained in numerical experiments, but with a smaller fraction of the crustal material remaining at the CMB. Christensen (1989b) included temperature-dependent viscosity as well as a decrease in thermal expansivity with depth in a calculation with the continuous introduction of slabs containing crust and residue layers, taking care to scale the thickness of the compositional layers in proportion to the thermal thickness of the slab. He found that for a buoyancy ratio ~1,

between 5% and 25% of the basaltic crust settled at the CMB. Again, the observed process was a Rayleigh–Taylor instability of the residue component, leaving behind some fraction of the crust. With constant viscosity, no segregation occurred, consistent with Gurnis (1986a). Interestingly, if a layer of dense crustal material already existed, a larger fraction of the incoming basalt was able to segregate and settle. These calculations were further developed in Christensen and Hofmann (1994) in which it was found that for $B=1.5$, ~14% of the total amount of crust in the mantle was in 'pools' (similar to piles) above the CMB, implying that ~1/6 of the subducted crust initially settled into a layer at the bottom. Higher Rayleigh number decreased the size of the bottom 'pools,' but higher B increased them (e.g., 26% of the total crust for $B=2.25$). Making the viscosity less temperature-dependent reduced the amount of settling, as with previous results. Interestingly, the bottom pools were not 100% crust – rather their crustal content was ~60%. Further testing and extension of such models to higher Ra was done by Brandenburg and van Keken (2007), who confirmed that the trend of less basalt segregation with higher Ra continues to higher Ra up to 2.10^7. This approach, with the addition of force-balanced plates, was subsequently extended to 2-D cylindrical geometry (Brandenburg et al., 2008).

The first such models that had an Earth-like convective vigor were presented by Davies (2002), who assumed a density difference of up to 100 kg m^{-3} but a constant $\alpha=2\times10^{-5}\,K^{-1}$, about a factor of 2 higher than realistic at the CMB. In contrast to the models of Christensen and Hofmann (1994), the model was heated entirely from within, with no hot TBL and hence no low-viscosity region at the bottom (the fraction of basal heating was arguably higher than realistic in the models of Christensen and Hofmann (1994)). Nevertheless, despite the absence of a low-viscosity TBL, a high α, and modest compositional density difference, a significant amount of basalt settled above the CMB, although less than obtained by Christensen and Hofmann (1994). Davies (2002) suggested other mechanisms that assist crustal settling, such as thickening of the crust due to slab buckling (the Stokes velocity increases as size^2), and the fact that the vertical velocity approaches zero toward the lower boundary (making it more difficult for the convective flow to entrain sinking blobs). All these mechanisms may play a role, but given the findings of Christensen (1989b) and Christensen and Hofmann (1994) that temperature-dependent viscosity facilitates crustal settling above the CMB, it is likely that Davies (2002) would have obtained more crustal settling, if the lower boundary region were less viscous. Such calculations were extended to early-Earth conditions (i.e., higher internal temperatures) by Davies (2006, 2007). At high internal temperature, corresponding to a low internal viscosity and high effective Ra, more basalt settling was observed, with a strongly depleted region forming in the upper part of the mantle. As a result of this depleted region, the thickness of early oceanic crust was no higher, or sometimes lower, than that under modern-day conditions.

7.12.3.3.3.4 Modeling studies: Self-consistent plates

The studies discussed in this section so far have controlled the surface velocities (to make them platelike) and the rate at which compositionally distinct material is injected. A number of other studies (e.g., Nakagawa and Tackley, 2005c; Ogawa, 2000a, 2003; Xie and Tackley, 2004a) attempted to treat these aspects self-consistently, with the crustal production rate determined by melting induced when the temperature reaches the solidus and the surface velocities determined by solution of the governing equations, often using a rheology that facilitates a 'platelike' behavior (e.g., Moresi and Solomatov, 1998; Yoshida and Ogawa, 2004; see also **Chapter 7.07**). It is not clear that this makes the resulting calculations more representative of Earth, but they are different from the previously discussed studies in other ways that make it instructive to discuss the results here.

The 2-D box calculations of Ogawa (2003), building on a series of earlier papers (Kameyama et al., 1996; Ogawa, 1988, 1993, 1994, 1997, 2000a,b; Ogawa and Nakamura, 1998), include self-consistent differentiation, a plate treatment involving hysteresis (Yoshida and Ogawa, 2004), and a cooling mantle with decaying heat sources. With MORB having a density anomaly of 120 kg m^{-3} and a somewhat high constant thermal expansivity of $3\times10^{-5}\,K^{-1}$, subducted MORB settles into a layer above the CMB that accumulates with time, while subducted residue undergoes diapir-like instabilities raising it back through the mantle. The basaltic layer has large undulations and typically has a thickness of ~1/4 of the domain depth, which scales to 500 km. Subsequently, the influence of variations in internal heating rate was explored (Fujita and Ogawa, 2009; Ogawa, 2007). High internal heating rates (representative of early Earth) led to unstable basaltic piles and episodic bursts of upwelling that caused chaotic plate motions, whereas lower internal heating rates (representative of recent Earth) led to stable basaltic piles and more stable plate configurations. Such models cause a variety of plume types (Ogawa, 2010).

The 2-D cylindrical calculations of Tackley and Xie (2002), Xie and Tackley (2004a,b), and Nakagawa and Tackley (2004b, 2005a,c) include self-consistent magmatism, temperature- and depth-dependent viscosity and yielding-induced plate tectonics (but with no hysteresis), and decreasing convective vigor due to decaying heat-producing elements and a cooling core. The material properties such as thermal expansivity have reasonable depth dependencies. Various density profiles for the MORB component relative to the residue component in the lower mantle are considered, and the density of the average composition ('pyrolite') is assumed to be a weighted average of the densities of the two end-members, consistent with the small-scale structure being a heterogeneous mixture of the two end-members, but not primitive never-melted pyrolite. These calculations show that even for a relatively small density contrast for MORB in the deep mantle (e.g., 62 kg m^{-3}; Nakagawa and Tackley, 2005a), subducted MORB settles at the base and builds up into large discontinuous 'piles' of material extending up to ~700 km into the mantle. With double this density contrast (123 kg m^{-3}; Nakagawa and Tackley, 2005a; Xie and Tackley, 2004a,b), a continuous undulating layer of dense material is formed, again up to 500–700 km thick. When basalt is neutrally buoyant at CMB pressures, the CMB region is still heterogeneous because subducted crust and residue reside at the bottom for some period, while they heat up sufficiently to be stirred back in to the convective flow (Xie and Tackley, 2004a). If there is crossover in density, with MORB positively buoyant at the CMB, then a layer of depleted

residue can build up above the CMB, with blobs of MORB residing in the mid lower mantle where it is neutrally buoyant (Xie and Tackley, 2004a,b). The effect of initial CMB temperature on the present-day thermal and chemical state of the mantle and core was found to be minimal (Nakagawa and Tackley, 2010) unless the CMB became completely blanketed in MORB, because cases with different initial CMB temperatures follow convergent evolutions. Similarly, initial mantle temperature was also found to have a minimal effect on the present-day structures (Nakagawa and Tackley, 2012), even though there were substantial differences early on.

Recent 2-D Cartesian models with relatively simple physical assumptions (Li and McNamara, 2013) suggest far less basalt settling than observed in the various models discussed earlier. The reconciliation of this is not clear at present. While using a (realistically) thin crust may be one factor, other possible factors are the slabs being much broader than realistic, very strong hot plumes (due to pure basal heating in most cases; i.e., zero internal heating) and a weak dependence of viscosity on temperature. It will be important to understand this by future modeling (see also **Chapter 7.11**).

7.12.3.3.3.5 Differing basalt fractions

In the calculations of Ogawa (2003), Tackley et al. (2005), and subsequent works by the same authors, the basal layer of dense material can become much thicker than observed in the calculations of Brandenburg and van Keken (2007), Christensen and Hofmann (1994), and Davies (2002, 2006, 2007), a major reason being that the total amount of MORB that can be produced by melting of primitive material is higher. Brandenburg and van Keken (2007), Christensen and Hofmann (1994), and Davies (2002) limited the total amount of MORB in the system to 10% or 12.5%, whereas the other authors assumed, based on the fraction of garnet + pyroxene in pyrolite being 30–40%, that up to 30% or 40% basalt fraction can be generated by melting. In fact, Xu et al. (2008) calculated that the amount of MORB it is possible to extract from a pyrolytic composition is 20%, so this is probably a reasonable compromise and has been used in recent studies (e.g., Nakagawa and Tackley, 2010, 2012; Nakagawa et al., 2009, 2010, 2012). In reality, basalt is not the only composition that can be produced by partial melting – pyrolite can melt up to 100% with the bulk composition of the melt changing depending on the degree of melting (e.g., Asimow et al., 2001; McKenzie and Onions, 1992), something that could be accounted for in future models.

7.12.3.3.3.6 More or less basalt settling at higher Ra?

In the calculations of Christensen and Hofmann (1994) and Brandenburg and van Keken (2007), it was observed that the amount of basalt segregation above the CMB decreases with increasing *Ra*. Seemingly in contradiction of this are other results (e.g., Davies, 2007; Nakagawa and Tackley, 2012; Ogawa, 2007) in which the amount of basalt segregation stays similar or increases with increasing *Ra*. A possible reconciliation of these different trends is the different assumptions made about crustal thickness. In Christensen and Hofmann (1994) and Brandenburg and van Keken (2007), crustal thickness is scaled with TBL thickness, so higher *Ra* is accompanied by thinner crust. In contrast, in Davies (2007), Nakagawa and Tackley (2012), and Ogawa (2007), higher *Ra* is generally associated with a thicker crust, because melting is based on a solidus and higher *Ra* typically means a hotter mantle hence deeper melting. Thus, in the latter models, the rate of supply of MORB to the deep mantle increases greatly with *Ra*. Additionally, it seems likely that separation of crust from the slab above the CMB is easier when the crust is thicker and/or the viscosity is lower.

7.12.3.3.3.7 2-D versus 3-D

Most of the previous calculations of long-term mantle evolution are in 2-D, so an important question is whether the results would be much different in 3-D. For example, as discussed in **Section 7.12.3.2.1**, different scaling laws were found (i.e., with different exponents for *B* and *Ra*) for entrainment by 2-D sheets and 3-D plumes in the laboratory experiments of Davaille (1999b). A factor to bear in mind is that toroidal motion, which is thought to increase the mixing rate (**Section 7.12.2.3.4**), is negligible in the deep mantle. For evolution calculations covering the age of the Earth, however, Nakagawa and Tackley (2010) compared simulations computed in full 3-D spherical geometry with identical calculations computed in a 2-D spherical annulus (Hernlund and Tackley, 2008) and found essentially no difference in averaged diagnostics such as mantle and core thermal evolution. In models with imposed plate motions and the continuous introduction of dense basaltic crust by subduction, Huang and Davies (2007a) found essentially the same results in 3-D as Davies (2002) did in 2-D. In regional models of slab–CMB interaction (Tackley, 2011), it was found that 2-D models gave a good guide to the amount of basalt settling in 3-D models. For mixing of passive tracers, Coltice and Schmalzl (2006) found no difference in mixing rates between 2-D and 3-D. Of course, the detailed planform of dense material above the CMB requires 3-D geometry to establish.

7.12.3.3.4 Chemical layering induced by phase transitions

The intriguing possibility exists that one or more phase transitions near or below 660 km depth could enforce or enhance chemical layering. Much research has focused on the effect of a single phase transition – the endothermic spinel to perovskite + magnesiowüstite transition at around 660 km depth, which, according to dynamic models that assume this transition applies to all mantle material, can cause partial layering of thermal convection, with the degree of flow stratification very sensitive to the value of the Clapeyron slope (e.g., Christensen and Yuen, 1985; Machetel and Weber, 1991; Peltier and Solheim, 1992; Tackley et al., 1994; Weinstein, 1993). In reality, however, olivine makes up only ~60% of the mantle mineral assemblage, and the phase changes in the other pyroxene–garnet system occur at different pressures. In particular, in the pyroxene–garnet system, the transition to the perovskite phase occurs with a positive Clapeyron slope and probably at a greater depth in the range 720–750 km. This has two effects: (i) the effect of the combined phase transitions on purely thermal convection is much reduced relative to what would occur if the olivine transitions applied to all mantle material, and (ii) subducted oceanic crust is positively buoyant (less dense than other compositions) in a region from ~660 to 730 km depth, whereas it is negatively buoyant (denser) at other pressures (Irifune and Ringwood, 1993). This has been

suggested to cause the separation of slab components in the vicinity of 660 km, with the accumulation of 'megaliths' (Ringwood, 1991; Ringwood and Irifune, 1988).

Estimates of the depth extent over which this anomalous buoyancy occurs have varied widely: A recent study of Ono et al. (2001) puts it at 660–720 km. A possible intermediate transition to ilmenite (Chudinovskikh and Boehler, 2004) would reverse this picture and increase the layering (van den Berg et al., 2002), but it is doubtful whether ilmenite occurs in a pyrolite composition (S. Ono, personal communication).

7.12.3.3.4.1 A single endothermic phase transition

If a chemical boundary already exists at a similar depth to the 660 km phase transition, Christensen and Yuen (1984) showed that their effects on deflecting a subducting slab and therefore causing flow layering can be added linearly. For the parameters they assumed, flow layering required a 4.5% chemical contrast or a Clapeyron slope of -5 MPa K^{-1} or a linear combination of the two. If chemical stratification does not, however, already exist, can an endothermic phase transition dynamically induce it? For a long-wavelength initial chemical heterogeneity, Weinstein (1992) showed that it can for certain combinations of chemical buoyancy ratio and Clapeyron slope. The endothermic phase was shown to act as a filter, trapping chemically dense material below it and chemically less dense material above it, because the total buoyancy (thermal + chemical) of these types of material is insufficient to overcome the phase change buoyancy. For this mechanism to operate, the required chemical buoyancy contrasts were in the range 1.1–1.5% (assuming thermal expansivity $= 2 \times 10^{-5}$ K^{-1}) – much lower than those required to cause layering on their own. The required Clapeyron slope was, however, larger than realistic, in the range -5 to -8.6 MPa K^{-1}, though this is partly because the calculations were performed at a low convective vigor ($Ra = 10^5$), and would be substantially reduced if an Earth-like vigor could be reached (Christensen and Yuen, 1985). For small-scale heterogeneities introduced by the continuous injection of compositionally layered slabs, Mambole and Fleitout (2002) showed that small but measurable chemical stratification can be introduced by Clapeyron slopes as weak as -1 MPa K^{-1}, with the amount of chemical stratification increasing steadily with the magnitude of the Clapeyron slope. With only the endothermic transition active, the dense component, which is the enriched, subducted MORB, is more prevalent in the lower mantle, while depleted, relatively buoyant material is more prevalent in the upper mantle. This result was confirmed by Nakagawa and Buffett (2005) in the case where the compositional anomalies were generated by melting-induced differentiation and by van Summeren et al. (2009) for the case where compositional anomalies are the result of primordial layering. None of these studies accounted for the change to a positive Clapeyron slope at high temperatures, such as might be relevant to plumes (Hirose, 2002). If the full system of phase transitions is considered, the sense of layering is reversed, as discussed in the succeeding text.

7.12.3.3.4.2 Composition-dependent phase transitions and subducted slabs

An important question is whether the basaltic crust and harzburgitic residue can separate out due to the density inversions that occur around and below 660 km depth, as suggested by Ringwood (1994). Three studies have demonstrated that this does not occur for slabs with a simple rheology, due to the strong viscous coupling between the crust and the rest of the slab (Christensen, 1997; Gaherty and Hager, 1994; Richards and Davies, 1989), whereas van Keken et al. (1996) showed that if a weak layer separates the crust from the rest of the slab, crustal separation may be possible. While Richards and Davies (1989) investigated constant-viscosity slabs, Gaherty and Hager (1994) studied slabs with temperature-dependent viscosity falling vertically onto a viscosity increase at 660 km depth and a local density inversion below this depth, but their model did not include density anomalies due to phase change deflection or net compositional buoyancy of the slab below 660 km, which was an important component of the proposal of Ringwood and Irifune (1988). Thus, Christensen (1997) included these effects as well as a more realistic slab angle associated with trench migration at the subduction zone, with basalt buoyant between 680 and 900 km, but still found that compositional effects are negligible for 100 Myr old plates, and although they could cause younger plates to stagnate at lower trench velocity, they did not prevent eventual slab penetration into the lower mantle. The rheology of the slab is, however, more complicated than simple temperature dependence (Karato et al., 2001). van Keken et al. (1996) considered a slab with an idealized rheological sandwich containing a soft (low-viscosity) layer between the 'hard garnet' crust and the cold viscous slab interior and showed that the crust can separate once the slab passes below 660 km depth, if most of the slab is ten times more viscous than the surrounding material and the weak peridotitic layer is 10 or 100 times less viscous than the rest of the slab. This model underestimates the viscosity of the slab based on simple viscosity laws, but once the peridotitic part of the slab passes through the spinel to perovskite + magnesiowüstite transition, it may be considerably weakened due to transformational superplasticity associated with grain-size reducing by the phase transition (Karato, 1995), whereas the crustal component would not. In summary, with 'conventional' rheology, compositional effects play only a minor role in slab interaction with the 660–800 km region and separation of slab components at 660 km depth is not possible, but if there is substantial weakening of the subcrustal layer due to transformation superplasticity or other effects, then separation of the basaltic crust might occur.

7.12.3.3.4.3 Composition-dependent phase transitions in a convecting system

Regardless of the viability of slab components separating at around 660 km depth, several studies have shown that once slabs reach the bottom TBL and heat up, the compositionally distinct components can indeed separate (e.g., Christensen and Hofmann, 1994; Ogawa, 2000b; Olson and Kincaid, 1991; Tackley, 2011); thus, the question of how already-separated crust and residue components interact with the phase transitions is of great relevance. The stability of a transition layer (consisting of an inseparable mixture of MORB-derived eclogite and harzburgite) that has already formed in the 660 region to thermal convection was studied by Christensen (1988), who found that it could only survive for a few hundred million years, but this model did not allow for separate basalt and

harzburgite components nor the possibility of recharge of these components. Models in which differentiated components are constantly introduced by subduction (Fleitout et al., 2000; Ogawa, 2000a) show the development of a strong compositional gradient across the 660, with depleted harzburgitic material accumulating at the top of the lower mantle, enriched basaltic material accumulating at the bottom of the upper mantle, and a chemical gradient present throughout the entire mantle, as evident in many later calculations (e.g., Armann and Tackley, 2012; Davies, 2008; Nakagawa et al., 2009; Ogawa, 2007; Tackley and Xie, 2002; Xie and Tackley, 2004a,b). This entrapment of distinct components typically does not occur when a downwelling first encounters the region, but rather after the crust and residue components have separated in the deep mantle and are subsequently circulating as 'blobs.' That the chemical and flow stratification is due mainly to the different depths of the perovskite transition in garnet and olivine systems rather than Clapeyron slope effects was demonstrated by Tackley et al. (2005). Nakagawa and Buffett (2005) found that slab penetration into the lower mantle is accompanied by an upwelling counterflow of depleted material in the area surrounding the slab, which is a mechanism for generating depleted regions in the upper mantle.

Multicomponent phase transitions are not the only mechanism that can cause an accumulation of subducted basalt above 660 km: Davies (2002, 2006) showed that a low-viscosity (high Rayleigh number) upper mantle in combination with a viscosity jump at 660 km depth can also cause this.

In summary, it is quite likely that local chemical stratification exists across the 660 km interface caused by differing depths of the perovskite transition in the olivine and pyroxene–garnet systems. There is, however, still uncertainty as to these depths. This local chemical stratification around 660–720 km is a prediction that could be tested seismically, which would help to determine whether the currently estimated depths of these phase transitions are indeed correct. For additional information on phase transitions, see **Chapter 2.08**.

7.12.3.3.4.4 Postperovskite phase transition

A factor that decreases the stability of a deep, dense layer is the recently discovered postperovskite phase transition (Murakami et al., 2004; Oganov and Ono, 2004). The positive Clapeyron slope of this transition acts to slightly destabilize the lower TBL (Nakagawa and Tackley, 2004a) and any resulting chemical layering (Nakagawa and Tackley, 2005b; Tackley et al., 2007). The destabilization effect is however relatively small and seems to be lower than the uncertainties in MORB density discussed earlier and uncertainties due to composition dependence of the PPV transition (e.g., Murakami et al., 2005; Ono et al., 2005a). In any case, because dense material tends to accumulate under hot upwellings, and the positive Clapeyron slope leads to an anticorrelation between the phase transition depth and temperature, the occurrence of a thick PPV layer is anticorrelated with the occurrence of thick pile of dense material (e.g., Nakagawa and Tackley, 2006). If the CMB is in the postperovskite stability field, then a continuous but varying-thickness layer of postperovskite is expected. However, because of the rapid increase of temperature with depth in the lower TBL, it is possible that the CMB is in the perovskite stability field, which would result in a double crossing of the perovskite to postperovskite phase boundary, and postperovskite not occurring at all in hot regions (Hernlund et al., 2005; see also **Chapter 7.11**).

7.12.3.3.4.5 Self-consistent mineralogical treatments

Instead of parameterizing each individual phase transition, another approach is to calculate the stable mineral assemblage as a function of pressure, temperature, and composition using free-energy minimization and then calculate the resulting density and other physical properties (e.g., Connolly, 2005; Xu et al., 2008). Nakagawa et al. (2012) found that the resulting dynamics and structures were similar to those using a simpler parameterization provided that the latter takes both olivine and nonolivine components into account. Such an approach is a useful framework for evaluating the effect of variations in composition (the exact MORB composition was found to be important by Nakagawa et al. (2009)) and for naturally generating seismic velocity structures for comparison with seismological models (Nakagawa et al., 2010).

7.12.3.3.5 The effect of chemical layering on core heat flow and planetary thermal evolution

As was noted early on (e.g., Christensen and Hofmann, 1994), the presence of a compositionally dense layer above the CMB reduces the heat flow out of the core. This reduction can be dramatic if the dense layer completely covers the core and should be taken into account in thermal evolution calculations (e.g., McNamara and Van Keken, 2000). Unfortunately, when the layer undulates greatly and is discontinuous, such that some patches of the core are not covered, the appropriate parameterization of core heat flux is unknown, so numerical simulation becomes the preferred approach.

A long-standing paradox in modeling Earth's thermal evolution is explaining how the heat flux out of the core can stay large enough over billions of years to maintain the geodynamo, without growing the inner core to a much larger size than observed. Parameterized models of core–mantle evolution in which no complexities are present predict a final inner core size that is much larger than that observed (e.g., Labrosse, 2003; Labrosse et al., 1997; Nimmo et al., 2004). As the heat conducted out of the core is determined by what is happening in the mantle, the time history of CMB heat flow is an important quantity to investigate using numerical models, both from the point of view of understanding core evolution and in providing an additional constraint on mantle models.

Nakagawa and Tackley (2004b) used a thermochemical convection model similar to those already presented but with a parameterized core heat balance based on Buffett et al. (1992, 1996) to show that the presence of a layer of dense material above the CMB, either primordial or arising from segregated crust, substantially reduces the CMB heat flow, hence inner core growth, something also shown by models in which the dense layer is parameterized (Costin and Butler, 2006). A problem is CMB heat flow can be reduced so much that it is insufficient to facilitate dynamo action and can even become zero or negative. Because of this, a discontinuous layer, rather than a global layer, was found to be the most promising scenario. Nakagawa and Tackley (2005a) subsequently found that it is difficult to match the constraints of correct inner core

size and enough heat flow out of the core, unless there is radioactive potassium in the core (e.g., Nimmo et al., 2004); in that case, viable evolution solutions were obtained, with a trade-off found between crustal density and core K content. Subsequently, it was found that initial core temperature (Nakagawa and Tackley, 2010) and initial mantle temperature (Nakagawa and Tackley, 2012) make little difference to the present-day core and mantle state.

The recent finding that the thermal conductivity of the core is two to three times higher than previously thought (de Koker et al., 2012; Gomi et al., 2013; Pozzo et al., 2012) makes it more difficult to explain core thermal evolution because a much higher core heat flow (at least ~12 TW) is needed for a geodynamo to exist. The higher core conductivity does not influence mantle dynamics, but it does severely restrict the range of parameters for which a successful core evolution can be obtained (Nakagawa and Tackley, 2013). Having a primordial layer in addition to subsequent basaltic segregation may be necessary to obtain a successful evolution (Nakagawa and Tackley, 2014).

As was discussed in an earlier section, chemical layering has a strong influence on plume temperature and dynamics. A systematic study of the effect of chemical layering on plume heat flux, plume excess temperature, and upper mantle temperature was conducted by Zhong (2006) in 3-D spherical geometry, assuming a sharp chemical interface and a global layer and moderately temperature-dependent viscosity. The possible range of parameters (layer depth and internal heating rates) was constrained by comparing to observations. The preferred model is one in which the dense layer is relatively thin (<350 km) and the internal heating rate in the upper layer is approximately three times higher than that inferred for the MORB source region, which, curiously, is similar to the heating deficit inherent in the 'heat–helium paradox' (Ballentine et al., 2002).

7.12.3.4 On the accuracy of numerical thermochemical convection calculations

A fundamental problem with treating chemical variations numerically is the negligible diffusivity of chemical variations, which leads to the possibility of sharp interfaces and very narrow lamella (e.g., less than one grid spacing), both of which are very difficult to treat numerically. Two major classes of method are used in the mantle dynamics community to track compositional variations: field-based approaches on a fixed (Eulerian) grid and Lagrangian markers/tracers/particles that are advected through the grid. Various benchmark tests of these have been performed in the mantle convection community (Tackley and King, 2003; van Keken et al., 1997). See **Chapter 7.05** for further discussion.

Field-based approaches have the advantage of computational speed and little additional computational complexity but the disadvantages of numerical diffusion, which smears out sharp features, and numerical dispersion, which causes artifacts like overshoots and ripples. Other research communities that employ computational fluid dynamics techniques (e.g., the atmospheric science community) face similar problems, and there is much ongoing research into improving advection methods, a small sampling of which is Muller (1992), Smolarkiewicz and Margolin (1998), Xu-Dong and Osher (1996), and Yabe et al. (2002). In the mantle dynamics community, the relatively straightforward interface-sharpening scheme of Lenardic and Kaula (1993) can yield a dramatic improvement in the advection of interfaces (e.g., Tackley and King, 2003).

Tracer-based approaches have the advantage of minimal numerical diffusion (a small amount does exist because of finite error in updating each tracer's position), thus the apparent ability to represent discontinuities and sub grid-scale features, but the disadvantage that one needs 5–50 times as many tracers as grid points to prevent statistical noise from unduly influencing the solution (e.g., Christensen and Hofmann, 1994; Tackley and King, 2003), which adds a considerable computational burden. This noise arises because in order to calculate the buoyancy caused by compositional variations, some averaging must be done over tracers in the vicinity of each grid or nodal point. It has been found that taking a local average of the C value of each tracer (as exemplified by the 'ratio method') is far less noisy than methods that rely on a number count of tracers (the so-called absolute method), regardless of the underlying numerical scheme (Tackley and King, 2003). Another type of tracer method tracks only the interface between two compositions and is thus far more computationally efficient than methods where tracers exist everywhere (e.g., Lin and Van Keken, 2006a; Schmalzl and Loddoch, 2003), though it is not suited for continuously varying chemical fields and the computational needs increase up to exponentially with time as the interface becomes more complex, unless interface simplification algorithms are applied (Schmalzl and Loddoch, 2003).

Benchmarks of these various methods for cases with an active compositional layer (Tackley and King, 2003; van Keken et al., 1997) indicate a sensitivity of the results to the details of the method being used, including a strong sensitivity of the entrainment rate of a stable compositional layer to resolution (both grid and number of tracers) (Tackley and King, 2003). This means that the various numerical results reviewed in this section may not be quantitatively accurate in the amount of entrainment that exists as a function of density contrast except in calculations where the grid is greatly refined in the region of entrainment (e.g., Lin and Van Keken, 2006a; Zhong and Hager, 2003). However, convergence tests suggest that they are qualitatively correct in the general planforms and features that arise. This is an issue that will require more attention in the future, particularly as more calculations are performed in 3-D.

7.12.4 Convection Models Tracking Trace-Element Evolution

7.12.4.1 Noble Gases

7.12.4.1.1 Helium and argon

The evolution of noble gases in a mantle that includes outgassing and radiogenic ingrowth but not major-element differentiation was studied by van Keken and Ballentine (1998, 1999). These studies investigated various proposed mechanisms for maintaining a relatively undegassed lower mantle over billions of years, finding that neither high deep mantle

viscosity, a strongly endothermic phase transition at 660 km depth, nor temperature-dependent viscosity is capable of causing a relatively undegassed deep mantle, in contrast to earlier modeling at lower convective vigor (Gurnis and Davies, 1986a). They did find that the observed total amount of ^{40}Ar outgassing is consistent with whole-mantle convection over geologic history, although the convective vigor in their models was constant with time. In that case, 50% degassing of radiogenic ^{40}Ar implies ~70% degassing of primitive isotopes.

van Keken et al. (2001) extended the analysis to the heat–helium imbalance (**Section 7.12.1.6.1**), tracking the relationship between the rate of helium outgassing and the heat flux. Large fluctuations in the helium outgassing were obtained, but only the most extreme fluctuations would explain the 'heat–helium' issue as it is currently understood, that is, with a ^{4}He concentration 3.5 times higher than current estimates (Ballentine et al., 2002).

The helium ratio evolution caused by subduction of differentiated oceanic plates was studied by Ferrachat and Ricard (2001), who tracked the evolution of oceanic crust and residue and showed that if oceanic crust segregates at the CMB, a large region of recycled oceanic lithosphere with high ^{3}He/^{4}He can form above it. However, in their model, compositional variations were also purely passive, that is, not influencing the flow, whereas models that account for the density anomalies of differentiated components (discussed later) have found that the depleted material, which in this case carries the high ^{3}He/^{4}He signature, tends to rise.

7.12.4.1.2 Origin of ^{3}He/^{4}He

The origin of the high ^{3}He/^{4}He end-member is discussed in **Section 7.12.1.6.1**. The two most commonly hypothesized origins have both been the foci of numerical investigations: Samuel and Farnetani (2003) and Deschamps et al. (2011) demonstrated the dynamic viability of the 'primitive' explanation, while Ferrachat and Ricard (2001) and Xie and Tackley (2004a) demonstrated the viability of the 'recycled' explanation. In any case, it is important to recall that the ratio of ^{3}He/^{4}He constantly decreases with time due to radiogenic ingrowth of ^{4}He from U and Th decay. Elemental fractionation between He and (U+Th) upon melting and outgassing of He to the atmosphere influence He/(U+Th) in the crust and residue, which over time can then develop ^{3}He/^{4}He different from primitive material. Thus, the present-day distribution of He isotope ratios reflects a combination of ingrowth, fractionation, and outgassing.

7.12.4.1.2.1 Primitive helium

Samuel and Farnetani (2003) used a fully dynamic convection model (e.g., with no imposed surface velocities) to demonstrate that a thick basal layer of primitive material, consistent with the proposal of Kellogg et al. (1999) and van der Hilst and Karason (1999), is capable of generating ^{3}He/^{4}He histograms similar to those observed for MORB and OIB. Isotopes of U, Th, K, and He were tracked in three different components: primitive, subducted MORB, and subducted residue, with the primitive layer being the 'mass balance' reservoir of U, Th, and K as well as the high ^{3}He/^{4}He component. Partitioning of trace elements between crust and residue was based on an assumed melt fraction. With a compositional density contrast of 2.4% (100 kg m^{-3}), depth-dependent thermal expansivity, temperature-dependent viscosity, and a primitive layer making up 25% of the mantle volume, it was found that ^{3}He/^{4}He values in MORB cluster in the observed range, whereas OIB samples, which were associated with plumes forming from the layer interface, display a much wider spread because they contain a heterogeneous mixture of the three different components. Heterogeneity dispersed more rapidly in the upper layer than in the lower layer due to the higher convective vigor there. Lower layer material was entrained into the upper layer much more rapidly than upper layer into the lower layer: after 2.1 Gy, the percentages were 25% and 3%, respectively. Deschamps et al. (2011) performed 3-D simulations of mantle convection with a relatively small primitive dense layer giving a good match to probabilistic seismic tomography (Deschamps and Tackley, 2009) and showed that the amount of entrainment into plumes is in the range required to give the observed helium ratios of OIBs; therefore, the models are consistent with the seismological and geochemical constraints considered.

7.12.4.1.2.2 Recycled helium

As discussed in **Section 7.12.4.1.1**, Ferrachat and Ricard (2001) found that a high ^{3}He/^{4}He repository of subducted residue built up in the deep mantle in a steady-state flow with no compositional buoyancy. Studies that do include compositional buoyancy find, however, that the depleted residue tends to rise to the shallow mantle, as in the preliminary calculations of Tackley and Xie (2002), in which high ^{3}He/^{4}He residue aggregates near the top due to its buoyancy, where it is sampled by mid-ocean ridge volcanism. Thus, Xie and Tackley (2004a) investigated the possibility that active (buoyant) compositional variations caused by crustal production may play an important role in the evolution of noble gas isotopes and the generation and maintenance of distinct end-members, using numerical convection models with a self-consistent melting criterion and platelike dynamics. The distribution of ^{3}He/^{4}He ratios in the modeled MORB source region was found to be highly dependent on the density contrasts between the different components (primitive, residue, and basalt) and compatibility of He relative to U and Th. While in most cases the ^{3}He/^{4}He was scattered to too-high values, two parameter combinations were identified that led to a 'realistic' MORB-like distribution of ^{3}He/^{4}He (i.e., clustered around 8–10 times atmospheric): (i) He less compatible than U, Th, and crust dense in the deep mantle; in this case, the shallow mantle contained a large proportion of depleted residue, which had MORB-like ^{3}He/^{4}He, and the high ^{3}He/^{4}He component was primitive material. (ii) He equally compatible as U, Th, and crust buoyant in the deep mantle; in this case, subducted crust in the shallow mantle brought the ^{3}He/^{4}He into the correct range; both primitive material and residue had the same 'primitive' ^{3}He/^{4}He.

These calculations demonstrate that a MORB-like shallow mantle ^{3}He/^{4}He and the existence of a high ^{3}He/^{4}He end-member are consistent with whole-mantle convection from a homogeneous start but with the ambiguity of two alternative explanations. Indeed, there may be a continuum of 'successful' solutions in (partition coefficient and buoyancy) space, which would require the consideration of additional constraints to constrain further. These calculations did not attempt to

distinguish between MORB and OIB melting signatures. Thus, more investigations are necessary, preferably in 3-D.

There has also been progress on understanding helium ratios using conceptual or box models discussed later (Section 7.12.5.1).

7.12.4.2 Other Isotopes (U, Pb, Nd, and Sm) and the Origin of HIMU

The hypothesis that segregation and sequestering of subducted MORB is responsible for the HIMU component and related Pb–Pb isochron (Hofmann and White (1982)) was investigated in pioneering calculations by Christensen and Hofmann (1994) using a numerical mantle convection model that included tracking of crust residue differentiation and isotopes of trace elements U, Pb, Sm, and Nd, which partitioned between the crust and residue on melting. The model was partly heated from within and partly from below and had a kinematic time-dependent platelike upper boundary condition. As discussed earlier, a fraction of the subducted crust segregated into a layer above the CMB, and with some parameter combinations, realistic Pb–Pb isotope diagrams and 'ages' were obtained. The isotope age depended on the length of time subducted MORB resided near the CMB. However, the authors found it necessary to run the calculations for only 3.6 Gy instead of the full age of the Earth; otherwise, the isotopic age was too high, contrary to previous expectations from mixing time estimates (reviewed in Section 7.12.2.6.4) that it would be difficult to obtain a large enough age. This would be appropriate if the mantle were completely mixed 3.6 Gy before present. Furthermore, their model mantle had a constant convective vigor (e.g., velocities and rate of melting), rather than, as discussed earlier, a vigor that decreases with time as the mantle temperature and radiogenic heat production decrease.

The calculations of Xie and Tackley (2004b) followed a similar approach to those of Christensen and Hofmann (1994), but with a convective vigor that decreases with time due to secular cooling and the decay of heat-producing elements, and the investigation of 4.5 Gy run times as well as 3.6 Gy. Technical differences were the use of a viscoplastic rheology to allow platelike behavior of the lithosphere (Moresi and Solomatov, 1998), rather than kinematic velocity boundary conditions, and a more self-consistent treatment of melting and crustal generation based on comparing the temperature to a solidus. The higher convective vigor early in the calculations plus the longer evolution resulted in a lot of differentiation early in the modeled evolution, which resulted in Pb–Pb ages that are much too large (3.39 Gy for the reference case). This large age is not surprising, because the rate of melting is very high early in the evolution, so early differentiating material dominates the isotopic signature. Additionally, early differentiated material has developed a more radiogenic signature so influences the least squares fit more than recently differentiated material. This finding is consistent with previous attempts at modeling lead isotope ratios starting from 4.5 Gy ago that obtained unrealistically high slopes in $^{207}Pb/^{204}Pb$–$^{206}Pb/^{204}Pb$ space (Allegre et al., 1980; Armstrong and Hein, 1973). It is also consistent with the numerical models of Davies (2002), in which although Pb–Pb ages were not calculated, they found mean ages (since melting) of ~2.7 Gy for MORB. Christensen and Hofmann (1994) attributed this 'too old' problem to the rapid decay of ^{235}U into ^{207}Pb in the early stage of the model, also finding that the early differentiation has a strong effect on the isotopic signatures at the end of the run. Thus, they chose to start their models 3.6 Gy ago with uniform Pb composition, which assumes that any earlier differentiation in the mantle has been completely homogenized by the convection.

Several possible explanations for this 'too old' discrepancy between models and data were investigated by Xie and Tackley (2004b). These are that HIMU material may not have been subducted into the mantle prior to 2.0–2.5 Gy BP, that melting is not rapid enough in the model (i.e., too low processing rate meaning too high residence time), that stretching of heterogeneities is inadequately represented, that the 'sampling volume' over which isotopic ratios are calculated is incorrect, that the deep mantle density of crustal material is incorrect, and that the Pb–Pb slope is made artificially large by noise associated with tracer discretization. The most successful and straightforward explanation was found to be the first (i.e., that HIMU was not subducted in the late Archean), which is discussed in more detail in the succeeding text, but it is worth briefly discussing the others. Regarding the melting-induced processing rate, this was found to be within the range of possibilities for the Earth (see discussion in Section 7.12.1.5.3). A parameterized box model indicated that only the most extreme assumptions would lead to a low enough residence time. Inadequate treatment of stretching highlights a problem with tracer treatments: whereas in reality a tracer should get exponentially stretched into a long tendril that extends over an area much wider than the sampling volume, thereby reducing its contribution to the isotopic signature of a melt, in fact, it remains as a localized entity. Xie and Tackley (2004b) tested one approximation of this: tracking the integrated strain as in Kellogg and Turcotte (1990) and McKenzie (1979) and then ignoring high-strain tracers when calculating the isotopic signature of a sampling volume. This was found to reduce the Pb–Pb somewhat, but not enough to match observations. Changing the sampling volume over which heterogeneities are averaged does not change the Pb–Pb slope, only the amount of scatter.

One possible reason for the ~1.8 Ga Pb–Pb age is that HIMU material did not enter the mantle before 2.0–2.5 Gy ago, for which there are two possible explanations. One of these is that higher subduction zone temperatures in the past may have caused essentially all Pb, U, and other trace elements to be stripped from the subducted crust by melting (Martin, 1986). Supporting this explanation are eclogite xenoliths from the upper mantle under Western Africa that are highly depleted in incompatible elements and have been interpreted as the melting residue of Archean subducted crust (Barth et al., 2001). Another possible explanation is that the HIMU endmember was not produced prior to the rise in atmospheric oxygen about 2.2 Gy ago. In this latter scenario, HIMU is produced by addition of continental U to oceanic crust by hydrothermal circulation at ridges (Elliott et al., 1999; Michard and Albarède, 1985), with efficient stripping of U from continents being accomplished by an oxygen-rich atmosphere oxidizing U to its 6+ state (Holland, 1984, 1994). This is not the only process that has been proposed to

produce HIMU: the other is preferential stripping of Pb (relative to U) from the subducted crust to the overlying mantle in subduction zones (Chauvel et al., 1995; Hofmann, 1988; Newsom et al., 1986). It is possible that both of these processes may operate. In the numerical model of Xie and Tackley (2004b), as in that of Christensen and Hofmann (1994), HIMU was produced by artificially changing the partition coefficients of U and Pb so that they fractionate on melting. In order to evaluate the effect of it not being produced prior to some point in the past, Xie and Tackley (2004b) ran cases in which the U and Pb partition coefficients are set equal for the first part of the model run and then changed to their default values at a specified point in the past. Setting the transition to 2.5 Gy before present caused a Pb–Pb isotopic age of 1.75 Gy, whereas setting it to 2.0 Gy before present caused an isotopic age of 1.4 Gy. Thus, from a modeling perspective, a lack of HIMU production prior to 2–2.5 Gy ago is an appealing mechanism for explaining the effective age of the Pb–Pb isotope diagrams, although it needs to be shown that this fits other isotope systems as well.

A mathematical analysis of the relationship between the probability distribution of heterogeneity age (i.e., time since last melting) and that of the pseudoisochron age was conducted by Rudge (2006), superseding an earlier box model approach by Allegre and Lewin (1995). He obtained simple relationships between mean remelting time and isochron age for a constant melting rate, which closely fit the Pb–Pb pseudoisochron ages in the numerical simulations of Christensen and Hofmann (1994). His more general theory was also able to fit the isochron ages of the time-dependent melting histories in the simulations and calculations of Xie and Tackley (2004b). An important finding is that for constant melting rate, the Pb–Pb pseudoisochron age is substantially higher than the mean time before remelting – in particular fitting a 2.0 Gy Pb–Pb pseudoisochron age with a constant melting rate over the Earth's history requires a time interval of only 0.5 Gy before material remelts, much shorter than seems reasonable (**Section 7.12.1.5.3**).

7.12.4.3 Extension to Include Continental Differentiation

This style of modeling was further developed by Brandenburg et al. (2008) who added Rb–Sr and Re–Os isotope systems to the U–Th–Pb and Sm–Nd included the previously mentioned studies. An additional feature of their model was the extraction of trace elements to the continental crust, which was parameterized in what the authors described as an ad hoc process. Extraction of continental crust was found necessary in order to obtain reasonable fits to data in all isotope systems. It was also necessary to change the continental crust extraction efficiency for U and Pb at 2.25 Gy before present to match Pb–Pb systematics, similar to as discussed in the previous paragraph. Interestingly, they found that ancient oceanic crust (subducted long in the past) adds an EM-I-like component, while more recently subducted oceanic crust adds a HIMU component.

'Box' modeling of the distribution of isotope ratios by sampling a heterogeneous system was performed by Kellogg (2004) and Kellogg et al. (2002, 2007) using a new type of 'box model' that allows the distribution of isotope ratios to be calculated in addition to the mean values (Allegre and Lewin, 1995). The method was used to successfully match Rb–Sr and Sm–Nd isotope ratio diagrams by differentiation and recycling in the upper mantle–continental crust system (i.e., no oceanic recycling) and subsequently extended to include the U–Th–Pb system in Kellogg (2004) and Kellogg et al. (2007). In the latter model, a lower continental crust was added but the lower mantle remained primitive. It was found that matching lead isotopes required considering recycled MORB and again a change regarding relative U and Pb behavior at 2.3 Gy before present.

From the earlier two studies, it is clear that both differentiation associated with oceanic crust production and differentiation associated with continental crust production must be considered in order for all isotope ratios to be consistent with observed ones.

The convection models of Walzer and Hendel (1997a,b, 1999, 2008) included only the melting-induced formation of the continental crust, without treating the massive differentiation caused by oceanic crust formation. Trace-element ratios of crust and residue were constrained to be those in the geochemical literature (e.g., Hofmann, 1988) rather than calculated based on partition coefficients. While the models display some interesting dynamic characteristics, they are geochemically predetermined to match observations and thus cannot provide predictions about the origin of geochemical heterogeneities.

7.12.4.4 Isotopic Variations at Hotspots and Transport by Plumes

Spatial and temporal isotopic variations within a hot-spot chain were not addressed in the previously mentioned studies, but are a notable feature of hot-spot volcanism (White, 2010); for example, the Hawaiian chain displays two isotopically distinct tracks of volcanoes often referred to as the 'Loa' and 'Kea' chains. A key question is whether this difference is caused by isotopic heterogeneity in the region feeding the presumed plume above the CMB or caused by processes in the region where the plume interacts with the lithosphere (see **Chapter 7.10**).

Investigating the feasibility of the plume source region explanation, Farnetani and Hofmann (2010) modeled in 3-D the propagation of heterogeneities from the lower TBL above the CMB up the plume conduit to the melting region beneath Hawaii, building on an earlier, 2-D axisymmetric study (Farnetani and Hofmann, 2009; see also **Section 7.12.1.4**). Blobs in the source region become filaments as they are advected up the plume. A straightforward mapping was found between isotopic heterogeneity in the shallow region and in the source region. Filaments of 10 km radius cause isotopic changes on timescale 400 ky. Subsequently, Farnetani et al. (2012) showed how a large-scale gradient in Pb isotopes above the CMB corresponding to the DUPAL anomaly maps to shallow structure. According to these modeling results, it is possible to directly link geochemical maps of OIBS to the structure and composition of the lowermost mantle.

Helium ratios display a different variation, in that the highest $^{3}He/^{4}He$ signature is observed at the most recently formed volcano, Lō'ihi. Hofmann et al. (2011) argued that this is due to processes occurring within the plume conduit at transition

zone depths. Specifically, they proposed that carbonatite melting in the transition zone followed by rapid ascent of the melt relative to the tilted plume displaces the higher ^{3}He/^{4}He signature toward the leading edge of the plume.

Investigating the 'shallow processes' explanation, Bianco et al. (2008) modeled plume–lithosphere interaction and melting of a plume with two geochemical components, 10% enriched (EC) and 90% depleted (DC), and found that two geochemically distinct trends (reminiscent of the 'Loa' and 'Kea' trends) could be generated by different amounts of melting, with no chemical zoning of the plume being necessary. This was further developed to include the effects of preexisting small-scale convection by Ballmer et al. (2011), who found that the interaction of the plume with small-scale convection-related washboard topography on the base of the lithosphere caused asymmetrical spreading and melting of the plume and hence in geochemistry of the erupted lavas, as well as temporal variations in the flux or erupted material (see **Chapter 7.10** for further discussion).

7.12.5 New Concepts and Future Outlook

7.12.5.1 Revisiting Noble Gas Constraints

7.12.5.1.1 Ar and He budget

Noble gas constraints were reviewed in **Section 7.12.1.6.1**. As discussed in that section, the '50% ^{40}Ar degassing' constraint is straightforward to match with whole-mantle convection, even with substantially higher processing rates in the past. A much more troubling constraint from the point of view of whole-mantle convection models is that the argon concentration in the MORB source is much lower than it would be if the Ar thought to be in the mantle were evenly distributed, which has been taken as evidence of layered convection with the lower layer containing the 'missing' argon. Along similar lines is the 'heat–helium imbalance,' that is, the concentration of He in the MORB source region seems to be too low relative to concentrations of U and Th. Recently, Ballentine et al. (2002) noted that both of these constraints are based on fluxes of ^{3}He through the oceans that represent an average over 1000 years, and if the true long-term average were a factor of 3.5 higher, both constraints would be removed. He argues that two other indicators of ^{3}He concentration in the MORB source – the concentration in the 'popping rock' and the estimate of carbon concentration in MORBs based on graphite–melt equilibrium – give estimates of ^{3}He concentration up to several times higher than obtained from the He flux through the oceans. On the other hand, Saal et al. (2002) obtained rather lower ^{3}He concentrations by considering carbon concentrations in undegassed melt inclusions. Numerical models of convection that track the relevant isotopes (van Keken et al., 2001) obtain considerable variation in the outgassing rate over timescales much longer than 1000 years.

The 'standard' reconciliation of the heat–helium imbalance invokes the concept that He and heat have different transport mechanisms, that is, heat is transported across a TBL at 660 km depth, whereas He is not. Castro et al. (2005) found that a similar concept occurs to He transport in continental aquifers, which, when applied to the oceans, suggests that the He flux into the ocean may be much lower than the flux out of the mantle, due to the action of seawater circulating through the oceanic crust (see Albarède (2005a) for further discussion).

The 'missing ^{40}Ar' constraint would also be eased if the total amount of ^{40}K in the mantle were lower than commonly assumed, which is based on BSE abundances (e.g., McDonough and Sun, 1995) combined with the K/U ratio observed in MORB (Jochum et al., 1983). It has been shown that this difficulty could be resolved if the amount of ^{40}K in the mantle were a factor ~2 than commonly estimated (Albarède, 1998; Davies, 1999), which would be the case if the K/U ratio were lower than that observed in MORB, perhaps due to fractionation of K from U (Albarède, 1998) or because the Earth is nonchondritic (Campbell and O'Neill, 2012; Lyubetskaya and Korenaga, 2007b). Lassiter (2004) suggested that K/U could be significantly lower than normally assumed, if the K depletion of oceanic crust in subduction zones is taken into account. Then, subducted MORB in the mantle would have a relatively low K/U, lowering the mantle average.

As a result of these various arguments, it seems plausible that the 'missing ^{40}Ar' and 'heat–helium imbalance' constraints are less robust than previously thought.

7.12.5.1.2 High ^{3}He/^{4}He

Although the high ^{3}He/^{4}He end-member (FOZO/C) is often assumed to be primitive and undegassed, several authors (e.g., Albarède, 1998; Anderson, 1998; Coltice et al., 2000b; Coltice and Ricard, 1999, 2002; Ferrachat and Ricard, 2001) have suggested that it could instead be generated by recycling, as was discussed in detail in **Section 7.12.1.6.1** and investigated by the numerical models of Ferrachat and Ricard (2001) and Xie and Tackley (2004a) discussed in **Section 7.12.4.1**. If high ^{3}He/^{4}He is caused by low [U + Th] rather than high [^{3}He], then an inverse correlation is expected between [U + Th] and ^{3}He/^{4}He, and such a correlation was found in the data plotted by Coltice and Ricard (1999). Meibom et al. (2003) pointed out that the unfiltered ^{3}He/^{4}He dataset for MORB has a Gaussian distribution similar to that for ^{187}Os/^{188}Os and proposed that both are due to mixing of radiogenic and nonradiogenic components (associated with basalt and residue respectively) with varying amounts of partial melting. They proposed that residue can retain substantial He due to the capture of He-rich bubbles in magma chambers. Further reinforcing this interpretation is a recent compilation of OIB isotope data, which shows that high ^{3}He source has the same isotopic and major-element composition as depleted mantle and therefore represents already-melted material (Class and Goldstein, 2005). Hauri et al. (1994) had earlier concluded that the FOZO represented differentiated material. Class and Goldstein (2005) found an inverse correlation between ^{3}He/^{4}He and Th abundance consistent with FOZO being a mixture of a small amount (~2%) primitive material plus ingrown ^{4}He. Based on the difference between plumes and OIBs, they inferred that the amount of time the high ^{3}He/^{4}He material has remained separate from the rest of the mantle is ~1–2 Gy. Heber et al. (2007) measured lower partition coefficients for noble gases in olivine and clinopyroxene than previously measured; however, they still concluded that residue from previously melted material could account for the high ^{3}He/^{4}He material.

The recycled-helium explanation is not universally accepted, however. Gonnermann and Mukhopadhyay (2007)

presented a new model for nonequilibrium degassing of CO_2, H_2O, and noble gases that explains the helium concentration paradox (i.e., low [^{3}He] in high ^{3}He/^{4}He samples). By this mechanism, the OIB source can have a large, primitive He concentration if it has more CO_2, while the MORB source has less CO_2. In the context of mantle convection, Gonnermann and Mukhopadhyay (2009) showed using a 'box' model that the lower mantle can retain relatively high ^{3}He/^{4}He despite convection and processing, including slab penetration, provided the flux of material into the lower mantle is low, at 0.5–1 lower mantle masses over the Earth's history. However, from a dynamic perspective, this amount must be regarded as impossibly low, as it is not only slabs that penetrate but also the general large-scale circulation.

Another recent proposal is that the high ^{3}He/^{4}He endmember is carried by refractory rocks, as a result of He and Ne diffusing into such rocks early in the Earth's history (Albarede, 2008). Such refractory material would be less sampled by melting and possibly less stretched and mixed.

7.12.5.2 Improved Recipes for Marble Cakes and Plum Puddings

7.12.5.2.1 Two recipes

7.12.5.2.1.1 Heterogeneous assemblage

Extreme compositional heterogeneity of the mantle, building on the 'marble cake' proposal of Allegre and Turcotte (1986), is a common theme in recent attempts to explain mantle geochemistry and contrasts with earlier views of a relatively homogeneous upper mantle, with the necessary OIB heterogeneity supplied by plumes from the deep mantle. The proposed mantle assemblage typically consists of a mostly depleted residue with approximately few % primitive material, ~10–20% recycled MORB, and approximately few % recycled sediment (derived from continental crust) and possibly continental lithosphere and/or OIB.

7.12.5.2.1.2 Two-assemblage recipe

One possible recipe is that the assemblage in the MORB source region is different from that in the plume (hence OIB) source region, but both assemblages are derived mostly by recycling processes. This is consistent with the proposal of Christensen and Hofmann (1994) and Hofmann and White (1982) that HIMU and perhaps EM components arise from subducted crust that has segregated into a layer above the CMB. This recycled deep layer can also be the location for storing incompatible elements that are 'missing' according to mass budget calculations (Coltice and Ricard, 1999) and have higher concentrations in MORB than in primitive material, requiring a smaller storage area. The high ^{3}He/^{4}He component might be caused by strips of former oceanic lithosphere (Coltice and Ricard, 1999, 2002) as discussed in the previous section. In the marble cake of Coltice and Ricard (1999, 2002), this subducted lithosphere forms a layer above D″, accounting for different MORB and OIB signatures, but it is not clear that such a layer would be stable. A deep layer of residue was obtained in the numerical calculations of Ferrachat and Ricard (2001), but compositional density contrasts were not accounted for in those calculations, and when they are, residue tends to rise into the upper part of the mantle (e.g., Ogawa, 2003; Tackley and Xie, 2002; Xie and Tackley, 2004a).

7.12.5.2.1.3 Single-assemblage recipe

Another possible recipe is that OIB and MORB result from the same statistical distribution with their geochemical differences due entirely to melting processes, with the details of the melting processes varying in different proposals. In the original proposal (Allegre and Turcotte, 1986), enriched plums exist in a depleted matrix, and the higher heterogeneity of OIBs was ascribed to smaller sampling region and lower degrees of melt. More recent proposals tend to emphasize the heterogeneity of the entire mixture, with no~uniform residue. Based on modeling the evolution of the distribution of trace-element ratios in the differentiating continental crust–depleted mantle system, Kellogg (2004) proposed something of an inversion of this model, with depleted 'plums' consisting the residue from continental crust extraction, and a 'matrix' with a C/FOZO composition consisting of small-scale strips of everything else. Meibom and Anderson (2004) and Meibom et al. (2003) proposed that MORB and OIB derive from the same source region (statistical upper mantle assemblage (SUMA); the composition of the lower mantle was not specified) with the geochemical differences due to different statistical sampling of this highly heterogeneous source region – essentially, smaller melt fractions. A whole mantle consisting mainly of residue and strips of subducted crust was also favored by Helffrich and Wood (2001), who used various constraints to estimate plausible fractions of the different components that satisfy global heat budget constraints: for the mantle, their model contained between 10% and 24% recycled oceanic crust, with the rest mostly sterile mantle (i.e., zero heat-producing elements) and recycled continental material making up to 0.4%. The viability of this class of model is strongly supported by the modeling of Ito and Mahoney (2005a,b, 2006) who calculated the melting of a heterogeneous 4- or 5-component mantle and found that in most cases, OIBs and MORBs could be drawn from the same source distribution, although different OIBs require different proportions of the components.

The single-assemblage model has been the basis of various proposals discussed in the following sections.

7.12.5.2.2 Two-stage melting

It was proposed by Phipps Morgan and Morgan (1999), that the OIB and MORB signatures can be explained by two-stage melting of a heterogeneous 'plum pudding' source region. In this model, the OIB source is 'normal' mantle that includes lots of enriched basalt-pyroxenite veins, while the MORB source is produced from this by depletion associated with hot-spot melting. Thus, the initial stage of melting is associated with plumes producing OIBs with low-degree melting. The once-depleted plume material fills the asthenosphere, constituting the MORB source; subsequent second-stage melting underneath spreading centers produces the depleted MORB signature. A parameterized box model was presented to demonstrate the success of this model in explaining geochemical data. While this two-stage model is not widely accepted, it is useful to summarize the outcome of the parameterized model because the heterogeneous mixture of different components

could have wider applicability. The model mantle contains the following components: PRIM (primitive material), ORES (residue from OIB melting), MRES (residue from MORB melting), recycled components ZOIB, ZMORB, and ZCONT, and the continental crust. The rate of oceanic floor production is 2.7 km^2 $year^{-1}$ at the present day and increases in the past as (heat production)^2. By the end of the calculation, 95% of mantle has passed through MOR processing, and the proportions of the components are PRIM = 5%, ZCONT + ZOIB = 2%, ZMORB = 20%, ORES = 5%, and MRES = 62.5%, with continental crust being 0.5% . A Rb–Sr pseudoage of 1.3 Ga is obtained, which is much younger than whole-mantle pseudoisochron of 3.5 Ga because it represents the average time between OIB melting and MORB melting. Phipps Morgan and Morgan (1999) also presented an explanation for the Pb kappa conundrum (Th/U of MORB is 2.5, whereas lead ratios imply it should be 4) based on the different compatibilities of Th and U and for the heat–He imbalance based on He being outgassed mainly by hot spots and continental flood basalts (as previously suggested by Kellogg and Wasserburg (1990)), which leads to the prediction that atmospheric He concentrations should be elevated after flood basalt events.

7.12.5.2.3 Source statistics and component fractions

A series of papers (Anderson, 2000, 2001; Meibom and Anderson, 2004; Meibom et al., 2003; Meibom et al., 2002; Meibom et al., 2005) studied the statistical distributions of isotope ratios in MORB and OIB environments and found that they support the idea that the upper mantle consists of a multiple-length-scale mixture of different 'plums' with no uniform matrix, from long-term recycling of crustal and sedimentary components. Helium ratio distributions for the 'unfiltered' MORB dataset were plotted by Anderson (2000, 2001) and found to be drawn from the same statistical distribution as OIB helium ratios but with smaller standard deviation, which was argued to be related to averaging over larger sampling regions and degrees of melting consistent with the central limit theorem in which "independent averaging of samples from any given distribution will approach a Gaussian distribution with a variance that becomes smaller as the sample volume increases" (Meibom et al., 2002). This random sampling model was subsequently found to be consistent with the observed Gaussian distribution of $^{187}Os/^{188}Os$ in mantle-derived grains, implying random sampling between ancient radiogenic and unradiogenic mantle with relatively high degrees of partial melting (Meibom et al., 2002). The similarity between Os ratio distributions and He ratio distributions was discussed in Meibom et al. (2003) and argued to be evidence for the same processes acting on both systems, with Meibom and Anderson (2004) further analyzing ratios of Pb, Sr, and Nd, pointing out the Gaussian shape reflects the dominance of the homogenization during sampling process by partial melting and magma chamber mixing, rather than the nature of the source region. They argued that the dominant length scales are in the range 100 m to 100 km, rather than the cm to meter scale implicit in the original marble cake proposal (Allegre and Turcotte, 1986), and that therefore the efficiency of convective stirring is limited, with the dominant homogenization processes occurring during the melting and magmatic stages. There are also larger-scale variations related to different plate tectonic histories.

A length-scale constraint comes from the Os analysis of mantle-derived grains in Meibom et al. (2002): as a single grain is derived from about 1 m^3 of mantle, this is the minimum length scale of heterogeneity, and it is consistent with observations of Os variations in abyssal peridotites on length scales 10–100 m (Brandon et al., 2000; Parkinson et al., 1998). An age constraint comes from the least radiogenic Os ratio they found, which indicates a depletion age of 2.6 Gy.

Quantitative modeling of the distribution of isotope ratios by sampling a heterogeneous system was performed by Kellogg et al. (2002) using a new type of 'box model' that allows the distribution of isotope ratios to be calculated in addition to the mean values (Allegre and Lewin, 1995), as a function of melt fraction, sampling zone size, and evolution. Essentially, each melting event produces new 'subreservoirs,' which are stretched with time, evolve isotopically, and can be statistically sampled at a particular length scale. The results showed that indeed, as the sampling length scale or melt fraction is increased, isotope ratio distributions tend toward a Gaussian distribution, as discussed earlier. The method was used to successfully match Rb–Sr and Sm–Nd isotope ratio diagrams by differentiation and recycling in the upper mantle–continental crust system and subsequently extended to include the U–Th–Pb system in Kellogg (2004) and Kellogg et al. (2007). In the latter model, a lower continental crust was added, but the lower mantle remained primitive. It was found that matching lead isotopes required considering recycled MORB and again a change regarding relative U and Pb behavior at 2.3 Gyr before present. Preliminary results were obtained for a whole-mantle system including the oceanic differentiation cycle (Kellogg, 2004).

A simpler mathematical model of mantle isotopic variability was developed by Rudge et al. (2005). Their model considered the mantle to be a single reservoir that experiences ongoing melting events with a certain average time between remelting events. They found that the best fit to the isotopic scatter was obtained with remelting timescale of 1.4–2.4 Ga and melt fraction of around 0.5%, the latter of which is similar to Kellogg (2004) and Kellogg et al. (2002), although the latter study was intended to represent continental formation melting. This did not, however, fit Pb isotopic data.

7.12.5.2.4 Melting of a heterogeneous source

To understand the geochemical signature of erupted magmas and how it is related to the composition and heterogeneity of the source region, it is necessary to understand the trace- and major-element composition that is obtained when a heterogeneous mixture is partially melted.

When a source region that is heterogeneous in major-element chemistry is partially melted, the enriched pyroxenite material melts at a lower temperature than depleted residue, which means that low degrees of melting will preferentially sample the enriched material, while high degrees of melting will average over the whole assemblage (Sleep, 1984). Whether this can quantitatively account for the differences between MORB and OIB compositions has not, until recently, been quantitatively assessed. Note that this preferential sampling of enriched components is different from the proposal of Anderson (2001) and Meibom and Anderson (2004), in which the same material would be melted in MORB and OIB environments but with smaller melt fraction producing greater variability with the

same mean. Based on quantitative modeling of trace-element distributions, Kellogg et al. (2002) found that OIB and MORB cannot be produced from the same distribution simply by differences in sample volume (with smaller samples being more heterogeneous): differences in the melting processes and/or source regions are necessary.

If the depleted matrix (DM) and pyroxenite (PX) veins are at small enough length scales to be in thermal equilibrium, Phipps Morgan (2001) found that melting of the PX is greatly enhanced by heat flowing from the surrounding matrix. The details depend on the temperature–pressure gradient of PX solidus relative to DM solidus, consistent with other calculations (Hirschmann et al., 1999) and confirming the prediction of Sleep (1984).

Katz and Rudge (2011) considered the influence of the size and topology of fertile heterogeneities. They found an enhancement of melting by up to a factor of 2 for small ($<$1 km) heterogeneities, which is less than predicted by Sleep (1984) because of a more sophisticated petrologic and mathematical model.

Complicating interpretations of hot-spot melting is that different basalts from the same hot spot do not generate the same composition, but rather elongate tubelike fields (Hart et al., 1992), a traditional interpretation of which is a mixing line between two end-member components present in the source region. Phipps Morgan (1999) found, however, that such linear arrays are naturally generated by progressive melting of a heterogeneous source mixture and remain linear independent of the number of distinct isotopic components in the initial source mixture.

The earlier analyses are for equilibrium melting. Disequilibrium melting of a heterogeneous source was considered by Rudge et al. (2011), who found a generalization that reduces to the familiar batch and fractional melting models in the appropriate limits.

Some laboratory experiments emphasize the difference between melting MORB and melting pyroxenite. Kogiso et al. (2003) presented experiments showing that it is possible to generate OIB major-element composition by melting pyroxenite but not by melting MORB. Pertermann (2003) performed experiments of melting pyroxenite with a basaltic composition. They found that it starts melting 35–50 km deeper than peridotite and generates much more magma than the original amount of pyroxenite, estimating that there must be $\sim<2\%$ pyroxenite in the MORB source. One origin for pyroxenite is melting of MORB followed by reaction with surrounding peridotite (Sobolev et al., 2005).

Length-scale issues were considered by Kogiso et al. (2004). For the case of pyroxenite heterogeneities melting in a peridotite matrix, they investigated the conditions necessary for the melt to retain its isotopic heterogeneity. Segregation of the melt must occur faster than diffusive equilibration of the melt with surrounding solid. They calculated that pyroxenite bodies submeter to a few meters wide can retain and produce melts with distinctive geochemical signatures under typical mantle melting conditions.

7.12.5.2.5 Can OIB and MORB be produced by the same statistical assemblage?

From the considerations in the previous section, it is possible to consider the resulting signature when a heterogeneous mixture is melted in different environments – in particular, underneath spreading centers (MORB) versus underneath the lithosphere (OIBs). See **Chapter 7.10** for a review of some of the relevant observations and explanations. Different (OIB vs. MORB) melting environments will cause both major-element and trace-element variations, and correlation of major and trace elements in OIBs indicates that some of the isotopic variation can be explained by variations in melting (Jackson and Dasgupta, 2008).

7.12.5.2.5.1 Modeling basalt compositions

Calculations with up to five components were performed by Ito and Mahoney (2005a,b, 2006), who quantitatively modeled the different trace-element compositions that arise as a result of differing OIB and MORB environments. Two key differences arise between OIB and MORB melting environments as a result of the differing mantle flow. Whereas flow beneath a spreading center rises at a roughly constant velocity to the surface, the vertical flow caused by plumes impinging on the base of a rigid lithosphere decreases toward the base of the lithosphere tens of kilometers deep. Hence, the total amount of decompression melting that takes place in OIB environments is typically less, but even if the temperature is high enough to make it the same, the depth distribution of OIB melting is concentrated toward greater depths, whereas that of MORB melting is constant with depth. As the enriched components are assumed to melt at lower temperature (greater depth) due to their different lithologies and (sometimes) enrichment in volatiles, they make up a larger proportion of OIB-type melts, whereas MORB melting is diluted to a much larger extent by the depleted component, leading to a more enriched signature for OIBs. The details of the trace element are sensitive to the exact composition of enriched components in the melting zone, particularly for OIB melting.

Ito and Mahoney (2005a) studied melting of a heterogeneous mantle consisting of three components: DM = depleted mantle (similar to the DMM of Hart et al. (1992)), PX = pyroxenite (essentially subducted MORB and carrying the HIMU signature), and EM = enriched mantle (similar to EM1 and EM2). They calculated the trace-element signature (La/Sm, Sr, Nd, and Pb) of the resulting melt assuming perfect melt homogenization, as a function of the proportions of PX and EM (keeping DM fixed at 90%), the thickness of lithosphere, and the potential temperature. Their results reproduce many of the features observed in MORB and OIB data, particularly the difference between OIBs erupting over old (thick) seafloor and those erupting over young seafloor: over young seafloor, the compositions of hot-spot islands are less variable and overlap with MORB observations, whereas over old seafloor, trace-element compositions are more enriched and highly variable due to sensitivity to exact proportions of PX and EM, and temperature, in the source region. Their results are also able to reproduce some features of 'arrays' in ratio–ratio space, the trajectories of which are often curved and have corners due to the transition from melting one component to melting another. Because the observed isotope ratios of each hot spot typically cover a wide range (an elongated 'array'), the 'fit' must focus on fitting the scatter rather than precise values. Incomplete magma mixing during ascent, which is not treated, may cause melt batches to have more extreme isotopic signatures. Evidence for pressure being the most important sampling

parameter is in correlated major-element, trace-element, and isotope compositions in postglacial Icelandic basalts (Stracke et al., 2003), as well as other oceanic basalts (Jackson and Dasgupta, 2008).

This analysis was then applied to specific island chains in Ito and Mahoney (2005b), with the goal of answering the question of whether two distinct sources are needed to explain OIB and MORB. The authors used a simple grid search scheme to determine the range of mantle sources that can fit 13 specific hot-spot island chains based on correlations in Sr, Nd, Pb isotopes space and then calculated the isotopic composition you would get if melting each one below mid-ocean ridges. The variables are mantle temperature excess, mass fractions of components, and isotopic compositions of EM and PX. Most model OIB compositions produce MORB that is indistinguishable from observed MORB compositions, suggesting that the whole mantle could be made of the same statistical assemblage. The proportion of different components was different for different OIBs, indicating large-scale heterogeneity. However, some predicted MORB compositions lie outside the range of observed normal MORB data. The fit to MORB is optimal when DM fractions are 85–95%, with the rest being PX and EM. Regarding abundances of enriched components, on average, PX is slightly more abundant than EM (by a factor 1.17). Regarding the global budget issue, they calculated that if the upper bound for U and Th in continents and upper bound for U and Th in model are assumed, an additional primitive or otherwise enriched source is not necessary, though in that case, only 30% of the mantle + core heat budget is radiogenic.

This approach was extended to include He in Ito and Mahoney (2006), with the addition of a high $^{3}He/^{4}He$ component corresponding to C (Hanan and Graham, 1996) or FOZO (Hart et al., 1992; Hilton et al., 1999) and basically the same as HRDM (Stuart et al., 2003). It was found that OIB and MORB can arise out of the same heterogeneous source region if three conditions are met: (i) The high $^{3}He/^{4}He$ component starts melting deeper than DM, (ii) DM is $>=85\%$ of the mantle, and (iii) the concentration of He in C/FOZO is comparable to that in DM. The models are successful in matching the low variation in MORB $^{3}He/^{4}He$. The requirement for C/FOZO to have the same He concentration as DM implies that it is not primitive but has already melted and reinforces the findings of Class and Goldstein (2005) and earlier proposals and evidence discussed earlier (Albarède, 1998; Coltice and Ricard, 1999). In this view, C/FOZO keeps a high He ratio due to strong depletion in U and Th while retaining relatively high ^{3}He, perhaps in olivine-rich lithologies (Meibom et al., 2005; Parman et al., 2005), or by mixing with primitive material. Ito and Mahoney (2006) removed the requirement for this component to be distributed differently (e.g., located in the deep mantle) – it can be part of the general upper mantle assemblage as proposed by Meibom and Anderson (2004). Still, C/FOZO and DM are distinct components despite their similarity in major and trace elements other than He, so it needs to be established how such similar material can evolve two quite different He ratios.

Such a multicomponent melting treatment was incorporated into a 3-D numerical model of small-scale sublithospheric convection by Ballmer et al. (2010), who found that variations in the fractions of pyroxenite and enriched peridotitic components occurred naturally as a function of seafloor age and match observations of various chains in the western and southern Pacific. Additionally, complex age–distance relationships were displayed.

A simplified version of this, with only two components (10% enriched (EC) and 90% depleted (DC)), was applied to plume–lithosphere interaction underneath the Hawaiian chain (Bianco et al., 2008) and further developed to include the effects of preexisting small-scale convection by Ballmer et al. (2011), with some success at explaining isotopic heterogeneity as discussed in **Section 7.12.4.4**.

7.12.5.2.6 Basal Magma Ocean

A plausible mechanism that may have influenced the Earth's chemical and thermal evolution is the crystallization of a 'basal magma ocean' (Labrosse et al., 2007). In this scenario, the early magma ocean encompassing the entire mantle crystallized from the middle rather than the bottom as previously thought (Abe, 1997; Solomatov and Stevenson, 1993b), resulting in both shallow and BMOs. While the shallow magma ocean would have cooled and solidified rapidly as per previous analyses, the BMO would take a relatively long time to cool because heat transport is limited by the solid mantle. Thus, the deep mantle would have been partly molten for much of the Earth's history, with some pockets of remnant partial melt left at the present day in the form of ULVZs, as discussed in **Section 7.12.3.1.5**. There are several implications and consequences to such an evolution.

One is that heat-producing elements would partition into the melt; thus, the BMO would act as a reservoir of incompatible elements over the Earth's history, helping with the budget problems discussed in **Section 7.12.1.4**. This includes noble gases: Coltice et al. (2011) showed that under certain conditions, solid cumulates crystallizing from the BMO could explain the primitive-like He and Ne signatures in hot spots. A complexity here is that solid–melt partitioning depends on which solid minerals are present: if Ca-perovskite is present, then large-ion lithophile elements prefer to partition into that (Corgne et al., 2005; Hirose et al., 2004). However, Ca-perovskite is the first phase to melt.

Another is that as the BMO crystallized, the resulting solid would be relatively dense and might therefore remain above the CMB, being responsible for (or a component in) the dense piles discussed in other sections. Over time, fractional crystallization would have changed the composition of the remaining liquid and of the solid that progressively crystallized, such that the crystallizing solid would have become increasingly iron-rich and therefore dense.

The influence on the core would be profound early on. If the deep mantle is molten or mostly molten, then it will convect very rapidly and the TBL above the CMB will have only a very small temperature drop (Ulvrová et al., 2012), as does the TBL at the outside of the outer core. This means that the molten core and molten deep mantle will rapidly adjust to the same potential temperature and there will be a substantial TBL at the point where the mantle changes from mostly liquid to mostly solid, from which hot plumes could form. Furthermore, the large concentration of incompatible heat-producing elements in the BMO might lead to a slow cooling rate. The BMO would also strongly influence (essentially eliminate)

lateral variations of CMB heat flux. Another intriguing possibility is that a dynamo could be generated in the long-lived BMO rather than in the core itself (Ziegler and Stegman, 2013), something that might be able to drive a dynamo for about 2 billion years.

The main requirement for a BMO to be possible is that melt be denser than solid in the deepest mantle. A requirement for a complete magma ocean to solidify from the middle rather than from the bottom is that the melt adiabat intersects the liquidus in the midmantle, rather than at the base. Several researchers have been investigating whether these two requirements are true.

Regarding melt density, melt is normally less dense than solid if it has the same composition but could be denser than solid if the melt is enriched in Fe relative to the solid. Whether the latter is true for the lower mantle composition at CMB pressures is currently unclear. Nomura et al. (2011) found that for $(Mg,Fe)SiO_3$, melt is denser than the coexisting solid due to Fe partitioning, and de Koker et al. (2013) found this to be the case in the $MgO–SiO_2$ system, consistent with earlier experimental results for Mg_2SiO_4 (Mosenfelder et al., 2007). However, the experiments of Andrault et al. (2012) on a composition that includes aluminum indicate that Fe is insufficiently partitioned into the melt for it to be denser; the difference to the earlier results is attributed to the presence of aluminum.

Regarding melt adiabat and liquidus, it is now well established that for molten silicate, the Grüneisen parameter increases with pressure (de Koker et al., 2013; Mosenfelder et al., 2007, 2009; Stixrude et al., 2009), implying that the adiabatic gradient might increase with pressure, but for the liquidus (and solidus) curves, there is some disagreement. While several groups find a curved liquidus/solidus (de Koker et al., 2013; Fiquet et al., 2010; Mosenfelder et al., 2009; Stixrude et al., 2009), implying that a point of intersection might occur in midmantle, Andrault et al. (2011) found straight curves, which would intersect the melt adiabat at the CMB. These differences need to be resolved.

More research needs to be done to on these physical properties to understand the viability of a BMO.

7.12.5.2.7 Internal differentiation: 'Upside-down' and 'hybrid pyroxenite'

Melting-induced differentiation inside the mantle, that is, without the formation of crust, may also play an important role. One such type of internal differentiation was described by Sobolev et al. (2005): ascending MORB-derived eclogite partially melts; the melt starts migrating through host peridotite and reacts with it to form pyroxenite. Because pyroxenite has a higher solidus than MORB, it solidifies, although it could subsequently melt upon rising further. Such a mechanism is supported by measurements on Hawaiian rocks and was later used to calculate the amount of MORB in the source region for both MORBs and OIBs by Sobolev et al. (2007).

This mechanism was argued by Davies (2009) to be important in the Earth's trace-element budget and isotopic evolution. For this to be the case, some of the 'hybrid pyroxenite' must avoid remelting, thereby trapping trace elements in the residual zone, and be advected back into the deep mantle, where some of it should settle above the CMB due its higher density. This was subsequently applied to the noble gas budget (Davies, 2010), for which a key point is that during this internal differentiation, noble gases are not lost to the atmosphere, as they are with external differentiation (i.e., crustal formation).

The previously mentioned process could have happened throughout the Earth's history. Another internal differentiation process termed 'upside-down differentiation' is argued to have occurred in the early Earth by Lee et al. (2010). Due to the mantle being hotter than today, partial melting could have occurred much deeper in the upper mantle than it does today. Melt that formed deep in the hot, early upper mantle could have segregated downward rather than upward, then solidified, and sunk into the deepest mantle to form a primitive layer.

7.12.5.3 Water: Influence on Convection and the Transition Zone Water Filter

As discussed in **Section 7.12.1.10**, water is a potentially very important constituent in the Earth's mantle due to its effect on rheology (e.g., Hirth and Kohlstedt, 1996, although recently, this has been disputed Fei et al., 2013), and it is cycled between the interior and the biosphere/exosphere. In order for water to be carried into the deep mantle, it must first be incorporated into slabs and then escape dehydration processes as the slab sinks and warms; for a detailed review of these, see Faccenda (2014). Understanding dehydration of the slab requires detailed modeling incorporating complex phase diagrams (Arcay et al., 2005; Gerya and Yuen, 2003; Ruepke et al., 2004; van Keken et al., 2002, 2011). The latest such models (van Keken et al., 2011) predict that about 1/3 of the water bound in slabs makes it to 240 km depth, corresponding to about one ocean mass of water over the age of the Earth. Water that is lost from the slab plays an important role in transporting trace elements from the subducting slab to the mantle wedge region (Elliott, 2003) as well as causing melting that generates new crust. Recent analysis indicates that subducted seawater accounts for about 50% of the unbound water presently in the convecting mantle (Holland and Ballentine, 2006).

There have been several parameterized convection studies of the influence of water on global mantle evolution, all of which have found that it has a large influence. McGovern and Schubert (1989) found a negative feedback that stabilizes volatile content and cooling rate on a timescale of 100s Myr. Further developing this model, Sandu et al. (2011) also found a negative feedback that causes the final amount of water to be relatively independent of the initial amount and also the possibility that the overall balance switched from degassing to regassing as the Earth cooled. Crowley et al. (2011) analyzed the complex interaction between temperature and water feedbacks, finding possible states to be warming + degassing or cooling + regassing, with other combinations not compatible. In the future, these predictions of parameterized models should be verified in full convection models. So far, water cycling has only been incorporated into two global convection modeling studies (Fujita and Ogawa, 2013; Richard et al., 2002), neither of which attempted to deal with the complexities of subduction zones or to determine the influence of water on the Earth's evolution. The studies come to opposite conclusions regarding the distribution of water: Richard et al.

(2002) found it to be quite uniform (although they assumed more rapid hydrogen diffusion than might be realistic (Shaw et al., 2012)), while Fujita and Ogawa (2013) found it to be quite nonuniform.

It has also been proposed that water plays an important role in trace-element transport in the transition zone region. Due to different solubilities of water in different minerals, the transition zone between 410 and 660 km depth is capable of containing 10–30 times higher water concentrations than the mantle above or below it (Hirschmann, 2006a). This led to the idea (Bercovici and Karato, 2003) that some water may be trapped in the transition zone, and with it, incompatible trace elements. If so, this provides a way of maintaining a mantle that is layered in trace elements but still undergoing whole-mantle convection.

The high water content of enriched transition zone material rising through the 410 km discontinuity would cause it to partially melt, and the incompatible trace elements would enter the melt, leaving a depleted solid in the MORB source region. A requirement for this melt to be trapped is that it should be denser than the surrounding solid, in which case a melt layer would build up above 410 km, with the production of new melt being balanced by entrainment and solidification of melt near downwelling slabs. This mechanism applies to the slow passive upwelling return flow characteristic of a mainly internally heated system. Plumes from the water-poor lower mantle could, however, escape being stripped of their trace elements because they have a relatively low water content and move through the transition zone too quickly for water to diffuse into them. Thus, plumes in the upper mantle appear enriched relative to the filtered MORB. Material traveling in the opposite direction and entering the lower mantle across the 660 km discontinuity would likely be too cold to melt, but water could enter a free phase at grain boundaries and percolate back into the transition zone.

While appealing in its simplicity and ability to reconcile geochemical layering and whole-mantle convection, several aspects of the proposal require testing, as is presently happening. The existence of a partial melt layer above 410 km should be testable seismically, and some studies have indeed indicated such a zone (e.g., Courtier and Revenaugh, 2007; Jasbinsek and Dueker, 2007; Revenaugh and Sipkin, 1994; Song et al., 2004; Tauzin et al., 2010) or a possibly related abrupt change in anisotropy (Yuan and Beghein, 2013). An analysis of electrical conductivity of the relevant phases compared to that inferred in the mantle implies the predicted amount of water in the transition zone (Huang et al., 2005, 2006), although this has been questioned (Hirschmann, 2006b). Further discussions of water transport in the mantle can be found in Hirschmann (2006a).

Various research has been performed on dynamic aspects of this proposal, some of which is discussed in Karato et al. (2006). Leahy and Bercovici (2004) calculated the convective consequences of concentrating heat-producing elements in the transition zone and/or lower mantle, finding that the exact distribution has a minor influence on the flow except in the extreme case where all heat-producing elements are concentrated in the transition zone. Details of the spreading and entrainment (back into the transition zone) of the melt layer above 410 km were calculated by Leahy and Bercovici (2007) with the model extended to include reactive infiltration of hydrous melt into solid by Leahy and Bercovici (2010): melt layers with a thickness in excess of 10 km were found for a wide range of parameters. The influence of the melt–solid density crossover has a strong influence on the stability of such a melt layer (Youngs and Bercovici, 2009), with the crossover needing to be above the 410 km layer for it to be stable there. Water may be released from a slab that resides in the transition zone for some time (Richard et al., 2006), and the released water may cause small-scale convection above the slab due to buoyancy and low viscosity of the hydrated material (Richard and Bercovici, 2009).

Mineral properties such as the density of melt above 410 km depth, the partition coefficients or relevant trace elements at this pressure, and the diffusivity of hydrogen need to be better known. A geochemical prediction of the model is that at steady state, the average isotopic composition of the convecting upper mantle must be almost the same as that of the lower mantle, with modifications for radiogenic ingrowth, which implies that noble gas residence times in the upper mantle must be very long (C. J. Ballentine, personal communication, 2007).

7.12.5.4 Outlook and Future Directions

7.12.5.4.1 Can geochemical and geophysical observations be reconciled with current paradigms?

Recent advances in paradigms and modeling approaches bring us closer to an integrated model that is consistent with both geochemical and geophysical constraints. Indeed, the large number of uncertain parameters associated with the various physical processes that may be important (early differentiation possibly leading to layering (**Section 7.12.1.5.1**), crustal settling above the CMB (**Section 7.12.3.3.3**), partial layering around 660 km (**Section 7.12.3.3.4**), transition zone-water filter (**Section 7.12.5.3**), BMO (**Section 7.12.5.2.5**), internal differentiation (**Section 7.12.5.2.6**), reactions with the core (**Section 7.12.1.5.4**), shallow melting of a heterogeneous source (**Section 7.12.5.2.4**), and continental extraction and recycling (**Section 7.12.4.3**)) combined with the uncertain BSE composition (chondritic vs. nonchondritic (**Sections 7.12.1.2** and **7.12.1.6.3**) and noble gas abundances (**Section 7.12.5.1**)) likely leads to nonuniqueness and multiple solutions. Indeed, the discussions of the various geochemical paradoxes in earlier sections indicate multiple plausible hypotheses. More data and improved modeling will be key to resolving this.

Likely characteristics of a successful geodynamic–geochemical model are the following:

- Whole-mantle convection, perhaps with a dense layer near the base and some partial/intermittent stratification around 660 km depth.
- Almost all of the mantle (i.e., 95–99%) has been processed through mid-ocean ridge melting and so presumably been degassed of most primordial noble gases. This is consistent with the constraint of only ~50% degassing of radiogenic ^{40}Ar (**Section 7.12.1.6.1**).
- The mantle is compositionally heterogeneous at all scales, from thousands of km to centimeters (**Sections 7.12.1.7** and **7.12.2.7**).
- The turbulent (exponential) mixing regime, with a whole-mantle mixing time (to ~10 s cm scale lengths) of ~3 Gy at

present-day rates (Section 7.12.2.6.4). The upper mantle that is not much better mixed than the lower mantle (Sections 7.12.2.4.2 and 7.12.2.5). ('Upper mantle' mixing time estimates are meaningless in whole-mantle convection.)
- A residence time of ~6 Gy based on present-day rates (Sections 7.12.1.5.3 and 7.12.2.5), with faster processing in the past.

Less certain, but looking increasingly feasible are the following:

- Many OIBs may arise from a statistically similar heterogeneous source as MORB through differences in melting processes (Section 7.12.5.2.4). At the same time, there are some lateral and radial variations in the statistical assemblage.
- Some vertical stratification of incompatible trace elements due to either gravitational stratification of major elements (early enriched layer, subducted crust or other dense differentiation products settling above the CMB, and composition-dependent phase transitions around 660 km), effects of water (the transition zone water filter), or melting (BMO, internal differentiation processes).
- A nonchondritic BSE composition, resolving several geochemical paradoxes (Campbell and O'Neill, 2012).

Regarding possible dense material above the CMB, several of the previous mechanisms could have operated, leading to a heterogeneous assemblage of dense differentiated products – the basal mélange (BAM) (Tackley, 2012).

7.12.5.4.2 Quantitative modeling approaches

Recent years have seen the improvement of several modeling approaches that are capable of generating model geochemical data to compare to observations. These include improved 'box models' that treat the statistical distribution of isotope ratios as well as their mean values (Section 7.12.5.2.3), improved methods for calculating the trace-element signatures that arise from melting in different environments (Section 7.12.5.2.3), and numerical thermochemical convection models that track trace elements and make quantitative predictions about trace-element distributions and evolution as well as the seismic structure of the mantle (Sections 7.12.4.1–7.12.4.3). These different methods are complementary and can be combined to enhance understanding. Several modeling challenges remain in the future. The global numerical models presently do not include continent formation, because the relevant processes are poorly understood, and also cannot resolve the complex mass transport occurring in subduction zones, which is an important part of this. Global numerical models cannot treat the smaller scales, which must therefore be done using a statistical approach or local models.

Acknowledgments

The author thanks Chris Ballentine and Nicolas Coltice for thoughtful reviews on the original version of this chapter, David Bercovici for his editorial comments and organization, and Yanick Ricard for providing Figure 4.

References

Abe Y (1997) Thermal and chemical evolution of the terrestrial magma ocean. *Physics of the Earth and Planetary Interiors* 100: 27–39.
Agranier A, Blichert-Toft J, Graham DW, Debaille V, Schiano P, and Albarède F (2005) The spectra of isotopic heterogeneities along the Mid-Atlantic Ridge. *Earth and Planetary Science Letters* 238: 96–109.
Albarède F (1998) Time-dependent models of U–Th–He and K–Ar evolution and the layering of mantle convection. *Chemical Geology* 145: 413–429.
Albarède F (2001) Radiogenic ingrowth in systems with multiple reservoirs: Applications to the differentiation of the mantle-crust system. *Earth and Planetary Science Letters* 189: 59–73.
Albarède F (2005a) Helium feels the heat in Earth's mantle. *Science* 310: 1777–1778.
Albarède F (2005b) The survival of mantle geochemical heterogeneities. In: van der Hilst RD, Bass JD, Matas J, and Trampert J (eds.) *Earth's Deep Mantle: Structure, Composition, and Evolution*, pp. 27–46. Washington, DC: American Geophysical Union.
Albarede F (2008) Rogue mantle helium and neon. *Science* 319: 943–945.
Albarède F and van der Hilst RD (2002) Zoned mantle convection. *Philosophical Transactions of the Royal Society A* 360: 2569–2592.
Allegre CJ (1997) Limitation on the mass exchange between the upper and lower mantle: The evolving convection regime of the Earth. *Earth and Planetary Science Letters* 150: 1–6.
Allegre CJ, Brevart O, Dupre B, and Minster JF (1980) Isotopic and chemical effects produced in a continuously differentiating convecting Earth mantle. *Philosophical Transactions of the Royal Society A* 297: 447–477.
Allegre CJ, Hart SR, and Minster JF (1983a) Chemical structure and evolution of the mantle and continents determined by inversion of Nd and Sr isotopic data. I. Theoretical methods. *Earth and Planetary Science Letters* 66: 177–190.
Allegre CJ, Hofmann A, and O'Nions K (1996) The argon constraints on mantle structure. *Geophysical Research Letters* 23: 3555–3557.
Allegre CJ and Lewin E (1995) Isotopic systems and stirring times of the Earths mantle. *Earth and Planetary Science Letters* 136: 629–646.
Allegre CJ, Moreira M, and Staudacher T (1995) $^{4}He/^{3}He$ dispersion and mantle convection. *Geophysical Research Letters* 22: 2325–2328.
Allegre CJ, Sarda P, and Staudacher T (1993) Speculations about the cosmic origin of He and Ne in the interior of the earth. *Earth and Planetary Science Letters* 117: 229–233.
Allegre CJ, Staudacher T, Sarda P, and Kurz MD (1983b) Constraints on evolution of Earth's mantle from rare gas systematics. *Nature* 303: 762–766.
Allegre CJ and Turcotte DL (1986) Implications of a 2-component marble-cake mantle. *Nature* 323: 123–127.
Anderson DL (1993) He-3 from the mantle – Primordial signal or cosmic dust. *Science* 261: 170–176.
Anderson DL (1995) Lithosphere, asthenosphere, and perisphere. *Reviews of Geophysics* 33: 125–149.
Anderson DL (1998) A model to explain the various paradoxes associated with mantle noble gas geochemistry. *Proceedings of the National Academy of Sciences of the United States of America* 95: 9087–9092.
Anderson DL (2000) The statistics of helium isotopes along the global spreading ridge system and the central limit theorem. *Geophysical Research Letters* 27: 77–82.
Anderson DL (2001) A statistical test of the two reservoir model for helium isotopes. *Earth and Planetary Science Letters* 193: 77–82.
Anderson OL, Oda H, and Isaak D (1992) A model for the computation of thermal expansivity at high compression and high temperatures – MgO as an example. *Geophysical Research Letters* 19: 1987–1990.
Andrault D, Bolfan-Casanova N, Nigro GL, Bouhifd MA, Garbarino G, and Mezouar M (2011) Solidus and liquidus profiles of chondritic mantle: Implication for melting of the Earth across its history. *Earth and Planetary Science Letters* 304: 251–259.
Andrault D, Petitgirard S, Lo Nigro G, et al. (2012) Solid-liquid iron partitioning in Earth's deep mantle. *Nature* 487: 354–357.
Antolik M, Gu YJ, Ekstrom G, and Dziewonski AM (2003) J362D28: A new joint model of compressional and shear velocity in the Earth's mantle. *Geophysical Journal International* 153: 443–466.
Arcay D, Tric E, and Doin M-P (2005) Numerical simulations of subduction zones. Effect of slab dehydration on the mantle wedge dynamics. *Physics of the Earth and Planetary Interiors* 149: 133–153.

Armann M and Tackley PJ (2012) Simulating the thermo-chemical magmatic and tectonic evolution of Venus' mantle and lithosphere: Two-dimensional models. *Journal of Geophysical Research* 117: E12003, http://dx.doi.org/12012JE004231/12012JE004231.

Armstrong RL and Hein SM (1973) Computer simulation of Pb and Sr isotope evolution of the Earth's crust and upper mantle. *Geochimica et Cosmochimica Acta* 37: 1–18.

Asimow PD, Hirschmann MM, and Stolper EM (2001) Calculation of peridotite partial melting from thermodynamic models of minerals and melts, IV. Adiabatic decompression and the composition and mean properties of mid-ocean ridge basalts. *Journal of Petrology* 42: 963–998.

Ballentine CJ (2002) Geochemistry – Tiny tracers tell tall tales. *Science* 296: 1247–1248.

Ballentine CJ and Barford DN (2000) The origin of air-like noble gases in MORB and OIB. *Earth and Planetary Science Letters* 180: 39–48.

Ballentine CJ, Marty B, Lollar BS, and Cassidy M (2005) Neon isotopes constrain convection and volatile origin in the Earth's mantle. *Nature* 433: 33–38.

Ballentine CJ, van Keken PE, Porcelli D, and Hauri EH (2002) Numerical models, geochemistry and the zero-paradox noble-gas mantle. *Philosophical Transactions of the Royal Society A: Mathematical, Physical and Engineering Sciences* 360: 2611–2631.

Ballmer MD, Ito G, van Hunen J, and Tackley PJ (2010) Small-scale sublithospheric convection reconciles geochemistry and geochronology of 'superplume' volcanism in the western and south Pacific. *Earth and Planetary Science Letters* 290: 224–232.

Ballmer MD, Ito G, van Hunen J, and Tackley PJ (2011) Spatial and temporal variability in Hawaiian hotspot volcanism induced by small-scale convection. *Nature Geoscience* 4: 457–460.

Barth MG, Rudnick RL, Horn I, et al. (2001) Geochemistry of xenolithic eclogites from west Africa, part I: A link between low MgO eclogites and Archean crust formation. *Geochimica et Cosmochimica Acta* 65: 1499–1527.

Batchelor GK (1952) The effect of homogeneous turbulence on material lines and surfaces. *Proceedings of the Royal Society A* 213: 349–366.

Batchelor GK (1959) Small-scale variation of convected quantities like temperature in a turbulent fluid. *Journal of Fluid Mechanics* 5: 113–133.

Becker TW, Kellogg JB, and O'Connell RJ (1999) Thermal constraints on the survival of primitive blobs in the lower mantle. *Earth and Planetary Science Letters* 171: 351–365.

Benz W and Cameron AGW (1990) Terrestrial effects of the giant impact. In: Newsom HE and Jones JH (eds.) *Origin of the Earth*, pp. 61–68. New York: Oxford University Press.

Bercovici D and Karato S (2003) Whole-mantle convection and the transition-zone water filter. *Nature* 425: 39–44.

Bianco TA, Ito G, van Hunen J, Ballmer MD, and Mahoney JJ (2008) Geochemical variation at the Hawaiian hot spot caused by upper mantle dynamics and melting of a heterogeneous plume. *Geochemistry, Geophysics, Geosystems* 9: Q11003.

Boehler R, Chopelas A, and Zerr A (1995) Temperature and chemistry of the core-mantle boundary. *Chemical Geology* 120: 199–205.

Bolton H and Masters G (2001) Travel times of P and S from the global digital seismic networks: Implications for the relative variation of P and S velocity in the mantle. *Journal of Geophysical Research: Solid Earth* 106: 13527–13540.

Bower DJ, Gurnis M, and Seton M (2013) Lower mantle structure from paleogeographically constrained dynamic Earth models. *Geochemistry, Geophysics, Geosystems* 14: 44–63.

Bower DJ, Wicks JK, Gurnis M, and Jackson JM (2011) A geodynamic and mineral physics model of a solid-state ultralow-velocity zone. *Earth and Planetary Science Letters* 303: 193–202.

Boyet M and Carlson RW (2005) 142Nd evidence for early (>4.53 Ga) global differentiation of the silicate Earth. *Science* 309: 576–581.

Boyet M and Carlson RW (2006) A new geochemical model for the Earth's mantle inferred from ^{146}Sm-^{142}Nd systematics. *Earth and Planetary Science Letters* 250: 254–268.

Brandenburg JP, Hauri EH, van Keken PE, and Ballentine CJ (2008) A multiple-system study of the geochemical evolution of the mantle with force-balanced plates and thermochemical effects. *Earth and Planetary Science Letters* 276: 1–13.

Brandenburg JP and van Keken PE (2007) Deep storage of oceanic crust in a vigorously convecting mantle. *Journal of Geophysical Research* 112: B06403. http://dx.doi.org/10.1029/2006JB004813.

Brandon A, Snow JE, Walker RJ, Morgan JW, and Mock TD (2000) ^{190}Pt-^{186}Os and ^{187}Re-^{187}Os systematics of abyssal peridotites. *Earth and Planetary Science Letters* 177: 319–335.

Brandon AD and Walker RJ (2005) The debate over core-mantle interaction. *Earth and Planetary Science Letters* 232: 211–225.

Brandon AD, Walker RJ, Morgan JW, Norman MD, and Prichard HM (1998) Coupled 186Os and 187Os evidence for core-mantle interaction. *Science* 280: 1570–1573.

Brandon AD, Walker RJ, Puchtel IS, Becker H, Humayun M, and Revillon S (2003) 186Os-187Os systematics of Gorgona Island komatiites: Implications for early growth of the inner core. *Earth and Planetary Science Letters* 206: 411–426.

Buffett BA, Garnero EJ, and Jeanloz R (2000) Sediments at the top of Earth's core. *Science* 290: 1338–1342.

Buffett BA, Huppert HE, Lister JR, and Woods AW (1992) Analytical model for solidification of the Earths core. *Nature* 356: 329–331.

Buffett BA, Huppert HE, Lister JR, and Woods AW (1996) On the thermal evolution of the Earth's core. *Journal of Geophysical Research* 101: 7989–8006.

Bull AL, McNamara AK, and Ritsema J (2009) Synthetic tomography of plume clusters and thermochemical piles. *Earth and Planetary Science Letters* 278: 152–162.

Bunge HP, Richards MA, and Baumgardner JR (1997) A sensitivity study of 3-dimensional spherical mantle convection at 10^8 Rayleigh number – Effects of depth-dependent viscosity, heating mode, and an endothermic phase change. *Journal of Geophysical Research* 102: 11991–12007.

Bunge HP, Richards MA, Lithgowbertelloni C, Baumgardner JR, Grand SP, and Romanowicz BA (1998) Time scales and heterogeneous structure in geodynamic Earth models. *Science* 280: 91–95.

Burke K, Steinberger B, Torsvik TH, and Smethurst MA (2008) Plume generation zones at the margins of large low shear velocity provinces on the core–mantle boundary. *Earth and Planetary Science Letters* 265: 49–60.

Burke K and Torsvik TH (2004) Derivation of Large Igneous Provinces of the past 200 million years from long-term heterogeneities in the deep mantle. *Earth and Planetary Science Letters* 227: 531–538.

Cabral RA, Jackson MG, Rose-Koga EF, et al. (2013) Anomalous sulphur isotopes in plume lavas reveal deep mantle storage of Archaean crust. *Nature* 496: 490–493.

Caffee MW, Hudson GB, Velsko C, Huss GR, Alexander EC, and Chivas AR (1999) Primordial noble gases from Earth's mantle: Identification of a primitive volatile component. *Science* 285: 2115–2118.

Campbell IH and O'Neill HS (2012) Evidence against a chondritic Earth. *Nature* 483: 553–558.

Caracas R and Cohen RE (2005) Effect of chemistry on the stability and elasticity of the perovskite and post-perovskite phases in the $MgSiO_3$–$FeSiO_3$–Al_2O_3 system and implications for the lowermost mantle. *Geophysical Research Letters* 32: L16310, http://dx.doi.org/16310.11029/12005gl023164.

Carlson RW (1987) Geochemical evolution of the crust and mantle. *Reviews of Geophysics* 25: 1011–1020.

Carlson RW (1994) Mechanisms of Earth differentiation – Consequences for the chemical-structure of the mantle. *Reviews of Geophysics* 32: 337–361.

Carlson RW and Boyet M (2008) Composition of the Earth's interior: The importance of early events. *Philosophical Transactions. Series A, Mathematical, Physical, and Engineering Sciences* 366: 4077–4103.

Caro G (2011) Early silicate earth differentiation. *Annual Review of Earth and Planetary Sciences* 39: 31–58.

Castillo P (1988) The Dupal anomaly as a trace of the upwelling lower mantle. *Nature* 336: 667–670.

Castle JC and van der Hilst RD (2003a) Searching for seismic scattering off mantle interfaces between 800 km and 2000 km depth. *Journal of Geophysical Research* 108: 2095. http://dx.doi.org/10.1029/2001JB000286.

Castle JC and van der Hilst RD (2003b) Using ScP precursors to search for mantle structures beneath 1800 km depth. *Geophysical Research Letters* 30: 1422. http://dx.doi.org/10.1029/2002GL016023.

Castro MC, Patriarche D, and Goblet P (2005) 2-D numerical simulations of groundwater flow, heat transfer and 4He transport – Implications for the He terrestrial budget and the mantle helium-heat imbalance. *Earth and Planetary Science Letters* 237: 893–910.

Chase CG (1981) Oceanic island Pb: Two-stage histories and mantle evolution. *Earth and Planetary Science Letters* 52: 277–284.

Chauvel CS, Goldstein SL, and Hofmann AW (1995) Hydration and dehydration of oceanic crust controls Pb evolution in the mantle. *Chemical Geology* 126: 65–75.

Chauvel C, Lewin E, Carpentier M, Arndt NT, and Marini J-C (2008) Role of recycled oceanic basalt and sediment in generating the Hf-Nd mantle array. *Nature Geoscience* 1: 64–67.

Chopelas A (1996) Thermal expansivity of lower mantle phases Mgo and $MgSiO_3$ perovskite at high-pressure derived from vibrational spectroscopy. *Physics of the Earth and Planetary Interiors* 98: 3–15.

Christensen U (1984) Instability of a hot boundary layer and initiation of thermo-chemical plumes. *Annales Geophysicae* 2: 311–319.

Christensen U (1988) Is subducted lithosphere trapped at the 670-km discontinuity? *Nature* 336: 462–463.

Christensen U (1989a) Mixing by time-dependent convection. *Earth and Planetary Science Letters* 95: 382–394.
Christensen UR (1989b) Models of mantle convection – One or several layers. *Philosophical Transactions of the Royal Society A* 328: 417–424.
Christensen U (1990) Mixing by time-dependent mantle convection – Reply. *Earth and Planetary Science Letters* 98: 408–410.
Christensen UR (1997) Influence of chemical buoyancy on the dynamics of slabs in the transition zone. *Journal of Geophysical Research* 102: 22435–22444.
Christensen UR and Hofmann AW (1994) Segregation of subducted oceanic crust in the convecting mantle. *Journal of Geophysical Research* 99: 19867–19884.
Christensen UR and Yuen DA (1984) The interaction of a subducting lithospheric slab with a chemical or phase-boundary. *Journal of Geophysical Research* 89: 4389–4402.
Christensen UR and Yuen DA (1985) Layered convection induced by phase transitions. *Journal of Geophysical Research* 90: 10291–10300.
Chudinovskikh L and Boehler R (2004) MgSiO/sub 3/ phase boundaries measured in the laser-heated diamond cell. *Earth & Planetary Science Letters* 219: 285–296.
Cizkova H, Cadek O, Van Den Berg AP, and Vlaar NJ (1999) Can lower mantle slab-like seismic anomalies be explained by thermal coupling between the upper and lower mantles? *Geophysical Research Letters* 26: 1501–1504.
Class C and Goldstein SL (2005) Evolution of helium isotopes in the Earth's mantle. *Nature* 436: 1107–1112.
Coltice N (2005) The role of convective mixing in degassing the Earth's mantle. *Earth and Planetary Science Letters* 234: 15–25.
Coltice N, Albarède F, and Gillet P (2000a) ^{40}K-^{40}Ar constraints on recycling continental crust into the mantle. *Science* 288: 845–847.
Coltice N, Ferrachat S, and Ricard Y (2000b) Box modeling the chemical evolution of geophysical systems: Case study of the Earth's mantle. *Geophysical Research Letters* 27: 1579–1582.
Coltice N, Marty B, and Yokochi R (2009) Xenon isotope constraints on the thermal evolution of the early Earth. *Chemical Geology* 266: 4–9.
Coltice N, Moreira M, Hernlund J, and Labrosse S (2011) Crystallization of a basal magma ocean recorded by Helium and Neon. *Earth and Planetary Science Letters* 308: 193–199.
Coltice N and Ricard Y (1999) Geochemical observations and one layer mantle convection. *Earth and Planetary Science Letters* 174: 125–137.
Coltice N and Ricard Y (2002) On the origin of noble gases in mantle plumes. *Philosophical Transactions of the Royal Society A: Mathematical, Physical and Engineering Sciences* 360: 2633–2648.
Coltice N and Schmalzl J (2006) Mixing times in the mantle of the early Earth derived from 2-D and 3-D numerical simulations of convection. *Geophysical Research Letters* 33: L23304. http://dx.doi.org/10.1029/2006GL027707.
Condie KC and Kröner A (2013) The building blocks of continental crust: Evidence for a major change in the tectonic setting of continental growth at the end of the Archean. *Gondwana Research* 23: 394–402.
Connolly JAD (2005) Computation of phase equilibria by linear programming: A tool for geodynamic modeling and an application to subduction zone decarbonation. *Earth and Planetary Science Letters* 236: 524–541.
Corgne A, Liebske C, Wood BJ, Rubie DC, and Frost DJ (2005) Silicate perovskite-melt partitioning of trace elements and geochemical signature of a deep perovskitic reservoir. *Geochimica et Cosmochimica Acta* 69: 485–496.
Corrsin S (1961) The reactant concentration spectrum in turbulent mixing with a first order reaction. *Journal of Fluid Mechanics* 11: 407–416.
Costin SO and Butler SL (2006) Modelling the effects of internal heating in the core and lowermost mantle on the Earth's magnetic history. *Physics of the Earth and Planetary Interiors* 157: 55–71.
Cottrell E and Kelley KA (2013) Redox heterogeneity in mid-ocean ridge basalts as a function of mantle source. *Science* 340: 1314–1317.
Courtier AM and Revenaugh J (2007) Deep upper-mantle melting beneath the Tasman and Coral Seas detected with multiple ScS reverberations. *Earth and Planetary Science Letters* 259: 66–76.
Creager KC and Jordan TH (1984) Slab penetration into the lower mantle. *Journal of Geophysical Research* 89: 3031–3049.
Creager KC and Jordan TH (1986) Slab penetration into the lower mantle beneath the Mariana and other island arcs of the Northwest Pacific. *Journal of Geophysical Research – B: Solid Earth and Planets* 91: 3573–3589.
Crisp JA (1984) Rates of magma emplacement and volcanic output. *Journal of Volcanology and Geothermal Research* 20: 177–211.
Crowley JW, Gérault M, and O'Connell RJ (2011) On the relative influence of heat and water transport on planetary dynamics. *Earth and Planetary Science Letters* 310: 380–388.
Cserepes L and Rabinowicz M (1985) Gravity and convection in a 2-layer mantle. *Earth and Planetary Science Letters* 76: 193–207.
Cserepes L, Rabinowicz M, and Rosembergborot C (1988) Three-dimensional infinite Prandtl number convection in one and two layers with implications for the Earth's gravity-field. *Journal of Geophysical Research – B: Solid Earth and Planets* 93: 12009–12025.
Dasgupta R (2013) Ingassing, storage, and outgassing of terrestrial carbon through geologic time. *Reviews in Mineralogy and Geochemistry* 75: 183–229.
Dasgupta R and Hirschmann MM (2010) The deep carbon cycle and melting in Earth's interior. *Earth and Planetary Science Letters* 298: 1–13.
Dasgupta R, Mallik A, Tsuno K, Withers AC, Hirth G, and Hirschmann MM (2013) Carbon-dioxide-rich silicate melt in the Earth's upper mantle. *Nature* 493: 211–215.
Davaille A (1999a) Simultaneous generation of hotspots and superswells by convection in a heterogeneous planetary mantle. *Nature* 402: 756–760.
Davaille A (1999b) Two-layer thermal convection in miscible viscous fluids. *Journal of Fluid Mechanics* 379: 223–253.
Davaille A, Girard F, and Le BM (2002) How to anchor hotspots in a convecting mantle? *Earth and Planetary Science Letters* 203: 621–634.
Davies GF (1980) Thermal histories of convective Earth models and constraints on radiogenic heat production in the Earth. *Journal of Geophysical Research* 85: 2517–2530.
Davies GF (1981) Earth's neodymium budget and structure and evolution of the mantle. *Nature* 290: 208–213.
Davies GF (1983) Viscosity structure of a layered convecting mantle. *Nature* 301: 592–594.
Davies GF (1984) Geophysical and isotopic constraints on mantle convection – An interim synthesis. *Journal of Geophysical Research* 89: 6017–6040.
Davies GF (1988) Ocean bathymetry and mantle convection. 1. Large-scale flow and hotspots. *Journal of Geophysical Research – B: Solid Earth and Planets* 93: 10467–10480.
Davies GF (1990) Heat and mass transport in the early Earth. In: Newsome HE and Jones JH (eds.) *Origin of the Earth*, pp. 175–194. New York: Oxford University Press.
Davies GF (1992) On the emergence of plate-tectonics. *Geology* 20: 963–966.
Davies GF (1999) Geophysically constrained mantle mass flows and the ^{40}Ar budget: A degassed lower mantle? *Earth and Planetary Science Letters* 166: 149–162.
Davies GF (2002) Stirring geochemistry in mantle convection models with stiff plates and slabs. *Geochimica et Cosmochimica Acta* 66: 3125–3142.
Davies GF (2006) Depletion of the early Earth's upper mantle and the viability of early plate tectonics. *Earth and Planetary Science Letters* 243: 376–382.
Davies GF (2007) Controls on density stratification in the early mantle. *Geochemistry, Geophysics, Geosystems* 8: Q04006.
Davies GF (2008) Episodic layering of the early mantle by the 'basalt barrier' mechanism. *Earth and Planetary Science Letters* 275: 382–392.
Davies GF (2009) Reconciling the geophysical and geochemical mantles: Plume flows, heterogeneities, and disequilibrium. *Geochemistry, Geophysics, Geosystems* 10: Q10008.
Davies GF (2010) Noble gases in the dynamic mantle. *Geochemistry, Geophysics, Geosystems* 11: Q03005, http://dx.doi.org/02009GC002801/02009GC002801.
Davies DR, Goes S, Davies JH, Schuberth BSA, Bunge HP, and Ritsema J (2012) Reconciling dynamic and seismic models of Earth's lower mantle: The dominant role of thermal heterogeneity. *Earth and Planetary Science Letters* 353: 253–269.
Davies GF and Gurnis M (1986) Interaction of mantle dregs with convection – Lateral heterogeneity at the core-mantle boundary. *Geophysical Research Letters* 13: 1517–1520.
de Koker N, Karki BB, and Stixrude L (2013) Thermodynamics of the MgO-SiO_2 liquid system in Earth's lowermost mantle from first principles. *Earth and Planetary Science Letters* 361: 58–63.
de Koker N, Steinle-Neumann G, and Vlcek V (2012) Electrical resistivity and thermal conductivity of liquid Fe alloys at high P and T, and heat flux in Earth's core. *Proceedings of the National Academy of Sciences of the United States of America* 109: 4070–4073.
Debaille V, O'Neill C, Brandon AD, et al. (2013) Stagnant-lid tectonics in early Earth revealed by 142Nd variations in late Archean rocks. *Earth and Planetary Science Letters* 373: 83–92.
Delano JW (2001) Redox history of the Earth's interior since similar to 3900 Ma: Implications for prebiotic molecules [Review]. *Origins of Life and Evolution of Biospheres* 31: 311–341.
Deparis V, Legros H, and Ricard Y (1995) Mass anomalies due to subducted slabs and simulations of plate motion since 200 My. *Physics of the Earth and Planetary Interiors* 89: 271–280.
Deschamps F, Kaminski E, and Tackley PJ (2011) A deep mantle origin for the primitive signature of ocean island basalt. *Nature Geoscience* 4: 879–882.

Deschamps F and Tackley PJ (2008) Searching for models of thermo-chemical convection that explain probabilistic tomography I. Principles and influence of rheological parameters. *Physics of the Earth and Planetary Interiors* 171: 357–373.

Deschamps F and Tackley PJ (2009) Searching for models of thermo-chemical convection that explain probabilistic tomography II – Influence of physical and compositional parameters. *Physics of the Earth and Planetary Interiors* 176: 1–18.

Deschamps F, Trampert J, and Tackley PJ (2007) Thermo-chemical structure of the lower mantle: Seismological evidence and consequences for geodynamics. In: Yuen DA, Maruyama S, Karato SI, and Windley BF (eds.) *Superplume: Beyond Plate Tectonics*, pp. 293–320. Dordrecht: Springer.

Dhuime B, Hawkesworth CJ, Cawood PA, and Storey CD (2012) A change in the geodynamics of continental growth 3 billion years ago. *Science* 335: 1334–1336.

Dixon ET, Honda M, McDougall I, Campbell IH, and Sigurdsson I (2000) Preservation of near-solar isotopic ratios in Icelandic basalts. *Earth and Planetary Science Letters* 180: 309–324.

Dobson DP and Brodholt JP (2005) Subducted banded iron formations as a source of ultralow-velocity zones at the core-mantle boundary. *Nature* 434: 371–374.

Drake MJ and Righter K (2002) Determining the composition of the Earth [Review]. *Nature* 416: 39–44.

du Vignaux NM and Fleitout L (2001) Stretching and mixing of viscous blobs in Earth's mantle. *Journal of Geophysical Research: Solid Earth* 106: 30893–30908.

Dubrovinsky L, Annersten H, Dubrovinskaia N, et al. (2001) Chemical interaction of Fe and Al_2O_3 as a source of heterogeneity at the Earth's core-mantle boundary. *Nature* 412: 527–529.

Dubrovinsky L, Dubrovinskaia N, Langenhorst F, et al. (2003) Iron-silica interaction at extreme conditions and the electrically conducting layer at the base of Earth's mantle. *Nature* 421: 58–61.

Dupeyrat L, Sotin C, and Parmentier EM (1995) Thermal and chemical convection in planetary mantles. *Journal of Geophysical Research – B: Solid Earth and Planets* 100: 497–520.

Dupre B and Allegre CJ (1983) Pb-Sr variation in Indian Ocean basalts and mixing phenomena. *Nature* 303: 142–146.

Dziewonski AM, Lekic V, and Romanowicz BA (2010) Mantle anchor structure: An argument for bottom up tectonics. *Earth and Planetary Science Letters* 299: 69–79.

Elkins-Tanton LT (2008) Linked magma ocean solidification and atmospheric growth for Earth and Mars. *Earth and Planetary Science Letters* 271: 181–191.

Elkins-Tanton LT, Parmentier EM, and Hess PC (2003) Magma ocean fractional crystallization and cumulate overturn in terrestrial planets: Implications for Mars. *Meteoritics and Planetary Science* 38: 1753–1771.

Elliott TR (2003) Tracers of the Slab. In: Eiler JM (ed.) *Inside the Subduction Factory*, pp. 23–45. Washington, DC: American Geophysical Union.

Elliott T, Zindler A, and Bourdon B (1999) Exploring the kappa conundrum: The role of recycling in the lead isotope evolution of the mantle. *Earth and Planetary Science Letters* 169: 129–145.

Faccenda M (2014) Water in the slab: A trilogy. *Tectonophysics* 614: 1–30.

Farley KA, Natland JH, and Craig H (1992) Binary mixing of enriched and undegassed (primitive?) mantle components (He, Sr, Nd, Pb) in samoan lavas. *Earth and Planetary Science Letters* 111: 183–199.

Farley KA and Neroda E (1998) Noble gases in the Earth's mantle. *Annual Review of Earth and Planetary Sciences* 26: 189–218.

Farnetani CG (1997) Excess temperature of mantle plumes – The role of chemical stratification across D″. *Geophysical Research Letters* 24: 1583–1586.

Farnetani CG and Hofmann AW (2009) Dynamics and internal structure of a lower mantle plume conduit. *Earth and Planetary Science Letters* 282: 314–322.

Farnetani CG and Hofmann AW (2010) Dynamics and internal structure of the Hawaiian plume. *Earth and Planetary Science Letters* 295: 231–240.

Farnetani CG, Hofmann AW, and Class C (2012) How double volcanic chains sample geochemical anomalies from the lowermost mantle. *Earth and Planetary Science Letters* 359–360: 240–247.

Farnetani CG, Legras B, and Tackley PJ (2002) Mixing and deformations in mantle plumes. *Earth and Planetary Science Letters* 196: 1–15.

Farnetani DG and Richards MA (1995) Thermal entrainment and melting in mantle plumes. *Earth and Planetary Science Letters* 136: 251–267.

Farnetani CG and Samuel H (2003) Lagrangian structures and stirring in the Earth's mantle. *Earth and Planetary Science Letters* 206: 335–348.

Farnetani CG and Samuel H (2005) Beyond the thermal plume paradigm. *Geophysical Research Letters* 32: L07311. http://dx.doi.org/10.1029/2005GL022360.

Fei H, Wiedenbeck M, Yamazaki D, and Katsura T (2013) Small effect of water on upper-mantle rheology based on silicon self-diffusion coefficients. *Nature* 498: 213–215.

Ferrachat S and Ricard Y (1998) Regular vs. chaotic mantle mixing. *Earth and Planetary Science Letters* 155: 75–86.

Ferrachat S and Ricard Y (2001) Mixing properties in the Earth's mantle: Effects of the viscosity stratification and of oceanic crust segregation. *Geochemistry, Geophysics, Geosystems* 2: 1013. http://dx.doi.org/10.1029/2000GC000092.

Fiquet G, Auzende AL, Siebert J, et al. (2010) Melting of peridotite to 140 gigapascals. *Science* 329: 1516–1518.

Fleitout L, Mambole A, and Christensen U (2000) Phase changes around 670 km depth and segregation in the Earth's mantle. *Eos, Transactions American Geophysical Union* 81, Fall Meeting Suppl., Abstract T12E-11.

Foley SF, Buhre S, and Jacob DE (2003) Evolution of the Archaean crust by delamination and shallow subduction. *Nature* 421: 249–252.

Forte AM and Mitrovica JX (2001) Deep-mantle high-viscosity flow and thermochemical structure inferred from seismic and geodynamic data. *Nature* 410: 1049–1056.

Fujita K and Ogawa M (2009) Basaltic accumulation instability and chaotic plate motion in the earliest mantle inferred from numerical experiments. *Journal of Geophysical Research* 114: B10402.

Fujita K and Ogawa M (2013) A preliminary numerical study on water-circulation in convecting mantle with magmatism and tectonic plates. *Physics of the Earth and Planetary Interiors* 216: 1–11.

Fukao Y (1992) Seismic tomogram of the earths mantle – Geodynamic implications. *Science* 258: 625–630.

Fukao Y, Obayashi M, Inoue H, and Nenbai M (1992) Subducting slabs stagnant in the mantle transition zone. *Journal of Geophysical Research: Solid Earth* 97: 4809–4822.

Gable CW, O'Connell RJ, and Travis BJ (1991) Convection in 3 dimensions with surface plates – Generation of toroidal flow. *Journal of Geophysical Research* 96: 8391–8405.

Gaherty JB and Hager BH (1994) Compositional vs thermal buoyancy and the evolution of subducted lithosphere. *Geophysical Research Letters* 21: 141–144.

Galer SJG and O'Nions RK (1986) Magmagenesis and the mapping of chemical and isotopic variations in the mantle. *Chemical Geology* 56: 45–61.

Garnero EJ (2004) A new paradigm for Earth's core-mantle boundary. *Science* 304: 834–836. http://dx.doi.org/10.1126/science.1097849.

Garnero EJ and Helmberger DV (1995) A very slow basal layer underlying large-scale low-velocity anomalies in the lower mantle beneath the pacific – Evidence from core phases. *Physics of the Earth and Planetary Interiors* 91: 161–176.

Garnero EJ and Helmberger DV (1996) Seismic detection of a thin laterally varying boundary-layer at the base of the mantle beneath the central Pacific. *Geophysical Research Letters* 23: 977–980.

Gerya TV and Yuen DA (2003) Rayleigh-Taylor instabilities from hydration and melting propel 'cold plumes' at subduction zones. *Earth and Planetary Science Letters* 212: 47–62.

Glatzmaier GA and Schubert G (1993) 3-Dimensional spherical-models of layered and whole mantle convection. *Journal of Geophysical Research* 98: 21969–21976.

Goarant F, Guyot F, Peyronneau J, and Poirier JP (1992) High-pressure and high-temperature reactions between silicates and liquid iron alloys, in the diamond anvil cell, studied by analytical electron microscopy. *Journal of Geophysical Research* 97: 4477–4487.

Gomi H, Ohta K, Hirose K, et al. (2013) The high conductivity of iron and thermal evolution of the Earth's core. *Physics of the Earth and Planetary Interiors* 224: 88–103.

Gonnermann HM, Manga M, and Jellinek AM (2002) Dynamics and longevity of an initially stratified mantle. *Geophysical Research Letters* 29: 1399, http://dx.doi.org/1310.1029/2002GL014851.

Gonnermann HM and Mukhopadhyay S (2007) Non-equilibrium degassing and a primordial source for helium in ocean-island volcanism. *Nature* 449: 1037–1040.

Gonnermann HM and Mukhopadhyay S (2009) Preserving noble gases in a convecting mantle. *Nature* 459: 560–563.

Graham DW (2002) Noble gas isotope geochemistry of mid-ocean ridge and ocean island basalts; characterization of mantle source reservoirs. In: Porcelli D, Wieler R, and Ballentine CJ (eds.) *Noble Gases in Geochemistry and Cosmochemistry, Reviews in Mineralogy and Geochemistry*, pp. 247–318. Washington, DC: Mineralogical Society of America.

Graham DW, Blichert-Toft J, Russo CJ, Rubin KH, and Albarède F (2006) Cryptic striations in the upper mantle revealed by hafnium isotopes in southeast Indian ridge basalts. *Nature* 440: 199–202.

Graham D, Lupton J, Albarède F, and Condomines M (1990) Extreme temporal homogeneity of Helium isotopes at Piton de la Fournaise, Reunion Island. *Nature* 347: 545–548.

Graham DW, Lupton JE, Spera FJ, and Christie DM (2001) Upper-mantle dynamics revealed by helium isotope variations along the Southeast Indian Ridge. *Nature* 409: 701–703.

Grand SP (1994) Mantle shear structure beneath the america and surrounding oceans. *Journal of Geophysical Research: Solid Earth* 99: 11591–11621.
Griffiths RW (1986) Dynamics of mantle thermals with constant buoyancy or anomalous internal heating. *Earth and Planetary Science Letters* 78: 435–446.
Guignot N and Andrault D (2004) Equations of state of Na-K-Al host phases and implications for MORB density in the lower mantle. *Physics of the Earth and Planetary Interiors* 143–144: 107–128.
Gurnis M (1986a) The effects of chemical density differences on convective mixing in the Earth's mantle. *Journal of Geophysical Research* 91: 1407–1419.
Gurnis M (1986b) Quantitative bounds on the size spectrum of isotopic heterogeneity within the mantle. *Nature* 323: 317–320.
Gurnis M (1986c) Stirring and mixing in the mantle by plate-scale flow – Large persistent blobs and long tendrils coexist. *Geophysical Research Letters* 13: 1474–1477.
Gurnis M and Davies GF (1986a) The effect of depth-dependent viscosity on convective mixing in the mantle and the possible survival of primitive mantle. *Geophysical Research Letters* 13: 541–544.
Gurnis M and Davies GF (1986b) Mixing in numerical-models of mantle convection incorporating plate kinematics. *Journal of Geophysical Research – B: Solid Earth and Planets* 91: 6375–6395.
Hager BH, Clayton RW, Richards MA, Comer RP, and Dziewonski AM (1985) Lower mantle heterogeneity, dynamic topography and the geoid. *Nature* 313: 541–546.
Hager BH and Richards MA (1989) Long-wavelength variations in Earths geoid – Physical models and dynamical implications. *Philosophical Transactions of the Royal Society A* 328: 309–327.
Hanan BB and Graham DW (1996) Lead and helium isotope evidence from oceanic basalts for a common deep source of mantle plumes. *Science* 272: 991–995.
Hansen U and Yuen DA (1988) Numerical simulations of thermal-chemical instabilities at the core mantle boundary. *Nature* 334: 237–240.
Hansen U and Yuen DA (1989) Dynamical influences from thermal-chemical instabilities at the core-mantle boundary. *Geophysical Research Letters* 16: 629–632.
Hansen U and Yuen DA (2000) Extended-Boussinesq thermal-chemical convection with moving heat sources and variable viscosity. *Earth and Planetary Science Letters* 176: 401–411.
Harrison TM (2009) The hadean crust: Evidence from >4 Ga zircons. *Annual Review of Earth and Planetary Sciences* 37: 479–505.
Harrison TM, Blichert-Toft J, Mueller W, Albarade F, Holden P, and Mojzsis SJ (2005) Heterogeneous hadean hafnium: Evidence of continental crust at 4.4 to 4.5 Gyr. *Science* 310: 1947–1950.
Harrison D, Burnard P, and Turner G (1999) Noble gas behaviour and composition in the mantle: Constraints from the Iceland plume. *Earth and Planetary Science Letters* 171: 199–207.
Hart SR (1984) A large-scale isotope anomaly in the Southern Hemisphere mantle. *Nature* 309: 753–757.
Hart SR, Hauri EH, Oschmann JA, and Whitehead JA (1992) Mantle plumes and entrainment: Isotopic evidence. *Science* 256: 517–520.
Hauri E (2002) SIMS analysis of volatiles in silicate glasses: 2. Isotopes and abundances in Hawaiian melt inclusions. *Chemical Geology* 183: 115–141.
Hauri EH, Whitehead JA, and Hart SR (1994) Fluid dynamic and geochemical aspects of entrainment in mantle plumes. *Journal of Geophysical Research, Solid Earth* 99: 24275–24300.
Hawkesworth CJ and Kemp AIS (2006) Evolution of the continental crust. *Nature* 443: 811–817.
He Y and Wen L (2009) Structural features and shear-velocity structure of the "Pacific Anomaly". *Journal of Geophysical Research* 114: B02309.
Heber VS, Brooker RA, Kelley SP, and Wood BJ (2007) Crystal-melt partitioning of noble gases (helium, neon, argon, krypton, and xenon) for olivine and clinopyroxene. *Geochimica et Cosmochimica Acta* 71: 1041–1061.
Hedlin MAH and Shearer PM (2000) An analysis of large-scale variations in small-scale mantle heterogeneity using global seismographic network recordings of precursors to PKP. *Journal of Geophysical Research* 105: 13655–13673.
Hedlin MAH, Shearer PM, and Earle PS (1997) Seismic evidence for small-scale heterogeneity throughout the Earth's mantle. *Nature* 387: 145–150.
Helffrich GR and Wood BJ (2001) The Earth's mantle [Review]. *Nature* 412: 501–507.
Hernlund JW and Jellinek AM (2010) Dynamics and structure of a stirred partially molten ultralow-velocity zone. *Earth and Planetary Science Letters* 296: 1–8.
Hernlund JW and Tackley PJ (2007) Some dynamical consequences of partial melting in Earth's deep mantle. *Physics of the Earth and Planetary Interiors* 162: 149–163.
Hernlund JW and Tackley P (2008) Modeling mantle convection in the spherical annulus. *Physics of the Earth and Planetary Interiors* 171: 48–54.
Hernlund JW, Thomas C, and Tackley PJ (2005) A doubling of the post-perovskite phase boundary and structure of the Earth's lowermost mantle. *Nature* 434: 882–886.
Herzberg C and Rudnick R (2012) Formation of cratonic lithosphere: An integrated thermal and petrological model. *Lithos* 149: 4–15.
Hilton DR, Gronvold K, Macpherson CG, and Castillo PR (1999) Extreme $^{3}He/^{4}He$ ratios in northwest Iceland: Constraining the common component in mantle plumes. *Earth and Planetary Science Letters* 173: 53–60.
Hilton DR and Porcelli D (2003) Noble gases as mantle tracers. In: Carlson RW (ed.) *Treatise on Geochemistry. The Mantle and Core*, vol. 2, pp. 277–318. Amsterdam: Elsevier.
Hirose K (2002) Phase transitions in pyrolitic mantle around 670-km depth: Implications for upwelling of plumes from the lower mantle. *Journal of Geophysical Research* 107. http://dx.doi.org/10.1029/2001JB000597.
Hirose K and Kushiro I (1993) Partial melting of dry peridotites at high pressures: Determination of compositions of melts segregated from peridotite using aggregates of diamond. *Earth and Planetary Science Letters* 114: 477–489.
Hirose K, Shimizu N, van Westeren W, and Fei Y (2004) Trace element partitioning in Earth's lower mantle and implications for geochemical consequences of partial melting at the core-mantle boundary. *Physics of the Earth and Planetary Interiors* 146: 249–260.
Hirose K, Takafuji N, Sata N, and Ohishi Y (2005) Phase transition and density of subducted MORB crust in the lower mantle. *Earth and Planetary Science Letters* 237: 239–251.
Hirschmann MM (2006a) Water, melting, and the deep Earth H_2O cycle. *Annual Review of Earth and Planetary Sciences* 34: 629–653.
Hirschmann MM (2006b) A wet mantle conductor? *Nature* 439: E3.
Hirschmann MM, Asimow PD, Ghiorso MS, and Stolper EM (1999) Calculation of peridotite partial melting from thermodynamic models of minerals and melts. III. Controls on isobaric melt production and the effect of water on melt production. *Journal of Petrology* 40: 831–851.
Hirth G and Kohlstedt DL (1996) Water in the oceanic upper-mantle – Implications for rheology, melt extraction and the evolution of the lithosphere. *Earth and Planetary Science Letters* 144: 93–108.
Hoffman NRA and McKenzie DP (1985) The destruction of geochemical heterogeneities by differential fluid motions during mantle convection. *Geophysical Journal of the Royal Astronomical Society* 82: 163–206.
Hofmann AW (1988) Chemical differentiation of the Earth: The relationship between mantle, continental crust, and oceanic crust. *Earth and Planetary Science Letters* 90: 297–314.
Hofmann AW (1997) Mantle geochemistry: The message from oceanic volcanism. *Nature* 385: 219–229.
Hofmann AW (2003) Sampling mantle heterogeneity through oceanic basalts: Isotopes and trace elements. In: Carlson RW (ed.) *Treatise on Geochemistry*, pp. 61–101. Oxford: Elsevier.
Hofmann AW, Farnetani CG, Spiegelman M, and Class C (2011) Displaced helium and carbon in the Hawaiian plume. *Earth and Planetary Science Letters* 312: 226–236.
Hofmann AW and Hart SR (1978) An assessment of local and regional isotopic equilibrium in the mantle. *Earth and Planetary Science Letters* 38: 44–62.
Hofmann AW and White WM (1982) Mantle plumes from ancient oceanic-crust. *Earth and Planetary Science Letters* 57: 421–436.
Hoink T, Schmalzl J, and Hansen U (2006) Dynamics of metal-silicate separation in a terrestrial magma ocean. *Geochemistry, Geophysics, Geosystems* 7: Q09008. http://dx.doi.org/10.1029/2006GC001268.
Holland HD (1984) *The Chemical Evolution of the Atmosphere and Oceans*. Princeton, NJ: Princeton University Press.
Holland HD (1994) Early proterozoic atmospheric change. In: Bengtson S (ed.) *Early Life on Earth*, pp. 237–244. New York: Columbia University Press.
Holland G and Ballentine CJ (2006) Seawater subduction controls the heavy noble gas composition of the mantle. *Nature* 441: 186–191.
Honda M, McDougall I, Patterson DB, Doulgeris A, and Clague DA (1999) Noble gases in submarine pillow basalt glasses from Loihi and Kilauea, Hawaii: A solar component in the Earth. *Geochimica et Cosmochimica Acta* 57: 859–874.
Hopp J and Trieloff M (2005) Refining the noble gas record of the Reunion mantle plume source: Implications on mantle geochemistry. *Earth and Planetary Science Letters* 240: 573–588.
Huang J and Davies GF (2007a) Geochemical processing in a three-dimensional regional spherical shell model of mantle convection. *Geochemistry, Geophysics, Geosystems* 8: Q11006. http://dx.doi.org/10.1029/2007GC001625.
Huang J and Davies GF (2007b) Stirring in three-dimensional mantle convection models and implications for geochemistry: 2. Heavy tracers. *Geochemistry, Geophysics, Geosystems* 8: Q07004.

Huang J and Davies GF (2007c) Stirring in three-dimensional mantle convection models and implications for geochemistry: Passive tracers. *Geochemistry, Geophysics, Geosystems* 8: Q03017.

Huang X, Xu Y, and Karato S (2005) Water content in the transition zone from electrical conductivity of wadsleyite and ringwoodite. *Nature* 434: 746–749.

Huang X, Xu Y, and Karato S (2006) A wet mantle conductor? Reply. *Nature* 439: E3–E4.

Humayun M, Qin L, and Norman MD (2004) Geochemical evidence for excess iron in the mantle beneath Hawaii. *Science* 306: 91–94.

Hunt DL and Kellogg LH (2001) Quantifying mixing and age variations of heterogeneities in models of mantle convection: Role of depth-dependent viscosity. *Journal of Geophysical Research* 106: 6747–6760.

Irifune T and Ringwood AE (1993) Phase-transformations in subducted oceanic-crust and buoyancy relationships at depths of 600-800 km in the mantle. *Earth and Planetary Science Letters* 117: 101–110.

Ishii M and Tromp J (1999) Normal-mode and free-air gravity constraints on lateral variations in velocity and density of Earth's mantle. *Science* 285: 1231–1235.

Ishii M and Tromp J (2004) Constraining large-scale mantle heterogeneity using mantle and inner-core sensitive normal modes. *Physics of the Earth and Planetary Interiors* 146: 113–124.

Ito G and Mahoney JJ (2005a) Flow and melting of a heterogeneous mantle: 1. Method and importance to the geochemistry of ocean island and mid-ocean ridge basalts. *Earth and Planetary Science Letters* 230: 29–46.

Ito G and Mahoney JJ (2005b) Flow and melting of a heterogeneous mantle: 2. Implications for a chemically nonlayered mantle. *Earth and Planetary Science Letters* 230: 47–63.

Ito G and Mahoney JJ (2006) Melting a high $^{3}He/^{4}He$ source in a heterogeneous mantle. *Geochemistry, Geophysics, Geosystems* 7: Q05010, http://dx.doi.org/05010.01029/02005GC001158.

Iwamori H and Albarede F (2008) Decoupled isotopic record of ridge and subduction zone processes in oceanic basalts by independent component analysis. *Geochemistry, Geophysics, Geosystems* 9: Q04033.

Iwamori H, Albaréde F, and Nakamura H (2010) Global structure of mantle isotopic heterogeneity and its implications for mantle differentiation and convection. *Earth and Planetary Science Letters* 299: 339–351.

Jackson MG, Carlson RW, Kurz MD, Kempton PD, Francis D, and Blusztajn J (2010) Evidence for the survival of the oldest terrestrial mantle reservoir. *Nature* 466: 853–856.

Jackson MG and Dasgupta R (2008) Compositions of HIMU, EM1, and EM2 from global trends between radiogenic isotopes and major elements in ocean island basalts. *Earth and Planetary Science Letters* 276: 175–186.

Jacobsen SB and Wasserburg GJ (1979) The mean age of mantle and crustal reservoirs. *Journal of Geophysical Research* 84: 7411–7427.

Jasbinsek J and Dueker K (2007) Ubiquitous low-velocity layer atop the 410-km discontinuity in the northern Rocky Mountains. *Geochemistry, Geophysics, Geosystems* 8: Q10004.

Jellinek AM and Manga M (2002) The influence of a chemical boundary layer on the fixity and lifetime of mantle plumes. *Nature* 418: 760–763.

Jochum K, Hofmann AW, Ito E, Seufert HM, and White WM (1983) K, U and Th in mid-ocean ridge basalt glasses and heat production, K/U and K/Rb in the mantle. *Nature* 306: 431–436.

Johnson TE, Brown M, Kaus BJP, and VanTongeren JA (2014) Delamination and recycling of Archaean crust caused by gravitational instabilities. *Nature Geoscience* 7: 47–52.

Jordan TH, Puster P, Glatzmaier GA, and Tackley PJ (1993) Comparisons between seismic Earth structures and mantle flow models based on radial correlation functions. *Science* 261: 1427–1431.

Jull M and Kelemen PB (2001) On the conditions for lower crustal convective instability. *Journal of Geophysical Research* 106: 6423.

Kameyama M, Fujimoto H, and Ogawa M (1996) A thermo-chemical regime in the upper mantle in the early Earth inferred from a numerical model of magma-migration in a convecting upper mantle. *Physics of the Earth and Planetary Interiors* 94: 187–215.

Kanda RVS and Stevenson DJ (2006) Suction mechanism for iron entrainment into the lower mantle. *Geophysical Research Letters* 33: L02310. http://dx.doi.org/10.1029/2005GL025009.

Kaneshima S and Helffrich G (1999) Dipping low-velocity layer in the mid-lower mantle: Evidence for geochemical heterogeneity. *Science* 283: 1888–1891.

Kaneshima S and Helffrich G (2009) Lower mantle scattering profiles and fabric below Pacific subduction zones. *Earth and Planetary Science Letters* 282: 234–239.

Karato S (1995) Interaction of chemically stratified subducted oceanic lithosphere with the 660 km discontinuity. *Proceedings of the Japan Academy. Series B, Physical and Biological Sciences* 71: 203–207.

Karato S, Bercovici D, Leahy G, Richard G, and Jing Z (2006) The transition zone water filter model for global material circulation: Where do we stand? In: Jacobsen SD and van der Lee S (eds.) *Earth's Deep Water Cycle*. *AGU Monograph Series*, vol. 168, pp. 289–314. Washington, DC: American Geophysical Union.

Karato S and Murthy VR (1997) Core formation and chemical-equilibrium in the Earth. 1. Physical considerations. *Physics of the Earth and Planetary Interiors* 100: 61–79.

Karato S, Riedel MR, and Yuen DA (2001) Rheological structure and deformation of subducted slabs in the mantle transition zone: Implications for mantle circulation and deep earthquakes. *Physics of the Earth and Planetary Interiors* 127: 83–108.

Karato S, Wang ZC, Liu B, and Fujino K (1995) Plastic-deformation of garnets – Systematics and implications for the rheology of the mantle transition zone. *Earth and Planetary Science Letters* 130: 13–30.

Karato S and Wu P (1993) Rheology of the upper mantle – A synthesis. *Science* 260: 771–778.

Kasting JF, Eggler DH, and Raeburn SP (1993a) Mantle redox evolution and the oxidation state of the Archean atmosphere. *Journal of Geology* 101: 245–257.

Kasting JF, Whitmore DP, and Reynolds RT (1993b) Habitable zones around main sequence stars. *Icarus* 101: 108–128.

Katz RF and Rudge JF (2011) The energetics of melting fertile heterogeneities within the depleted mantle. *Geochemistry, Geophysics, Geosystems* 12: Q0AC16.

Kawai K, Tsuchiya T, Tsuchiya J, and Maruyama S (2009) Lost primordial continents. *Gondwana Research* 16: 581–586.

Keller T and Tackley PJ (2009) Towards self-consistent modelling of the Martian dichotomy: The influence of low-degree convection on crustal thickness distribution. *Icarus* 202: 429–443.

Kellogg LH (1997) Growing the Earth's D″ layer: Effect of density variations at the core-mantle boundary. *Geophysical Research Letters* 24: 2749–2752.

Kellogg JB (2004) *Towards and Understanding of Chemical and Isotopic Heterogeneity in the Earth's Mantle*. Cambridge, MA: Harvard University.

Kellogg LH, Hager BH, and van der Hilst RD (1999) Compositional stratification in the deep mantle. *Science* 283: 1881–1884.

Kellogg JB, Jacobsen SB, and O'Connell RJ (2002) Modeling the distribution of isotopic ratios in geochemical reservoirs. *Earth and Planetary Science Letters* 204: 183–202.

Kellogg JB, Jacobsen SB, and O'Connell RJ (2007) Modeling lead isotopic heterogeneity in mid-ocean ridge basalts. *Earth and Planetary Science Letters* 262: 328–342.

Kellogg LH and Stewart CA (1991) Mixing by chaotic convection in an infinite Prandtl number fluid and implications for mantle convection. *Physics of Fluids A: Fluid Dynamics* 3: 1374–1378.

Kellogg LH and Turcotte DL (1986) Homogenization of the mantle by convective mixing and diffusion. *Earth and Planetary Science Letters* 81: 371–378.

Kellogg LH and Turcotte DL (1990) Mixing and the distribution of heterogeneities in a chaotically convecting mantle. *Journal of Geophysical Research* 95: 421–432.

Kellogg LH and Wasserburg GJ (1990) The role of plumes in mantle helium fluxes. *Earth and Planetary Science Letters* 99: 276–289.

Kennett BLN and Gorbatov A (2004) Seismic heterogeneity in the mantle – Strong shear wave signature of slabs from joint tomography. *Physics of the Earth and Planetary Interiors* 146: 87–100.

Kennett BLN, Widiyantoro S, and Vanderhilst RD (1998) Joint seismic tomography for bulk sound and shear-wave speed in the earths mantle. *Journal of Geophysical Research, Solid Earth* 103: 12469–12493.

Kesson SE, Gerald JDF, and Shelley JM (1998) Mineralogy and dynamics of a pyrolite lower mantle. *Nature* 393: 252–255.

Klein EM, Langmuir CH, Zindler A, Staudigel H, and Hamelin H (1988) Isotope evidence of a mantle convection boundary at the Australian-Antarctic Discordance. *Nature* 333: 623–629.

Knittle E and Jeanloz R (1989) Simulating the core-mantle boundary – An experimental study of high-pressure reactions between silicates and liquid iron. *Geophysical Research Letters* 16: 609–612.

Knittle E and Jeanloz R (1991) Earths core-mantle boundary – Results of experiments at high-pressures and temperatures. *Science* 251: 1438–1443.

Kogiso T, Hirschmann MM, and Frost DJ (2003) High-pressure partial melting of garnet pyroxenite: Possible mafic lithologies in the source of ocean island basalts. *Earth and Planetary Science Letters* 216: 603–617.

Kogiso T, Hirschmann MM, and Reiners PW (2004) Length scales of mantle heterogeneities and their relationship to ocean island basalt geochemistry. *Geochimica et Cosmochimica Acta* 68: 345–360.

Komabayashi T, Maruyama S, and Rino S (2009) A speculation on the structure of the D″ layer: The growth of anti-crust at the core-mantle boundary through the subduction history of the Earth. *Gondwana Research* 15: 342–353.

Korenaga J (2003) Energetics of mantle convection and the fate of fossil heat. *Geophysical Research Letters* 30: 1437.
Kramers JD and Tolstikhin IN (1997) Two terrestrial lead isotope paradoxes, forward transport modelling, core formation and the history of the continental crust. *Chemical Geology* 139: 75–110.
Kumagai I, Davaille A, Kurita K, and Stutzmann E (2008) Mantle plumes: Thin, fat, successful, or failing? Constraints to explain hot spot volcanism through time and space. *Geophysical Research Letters* 35: L16301. http://dx.doi.org/10.1029/2008GL035079.
Kump LR, Kasting JF, and Barley ME (2001) Rise of atmospheric oxygen and the "upside-down" Archean mantle. *Geochemistry, Geophysics, Geosystems* 2: U1–U10. http://dx.doi.org/10.1029/2000GC000114.
Kurz MD, Jenkins WJ, Hart SR, and Clague D (1983) Helium isotopic variations in volcanic rocks from Loihi seamount and the island of Hawaii. *Earth and Planetary Science Letters* 66: 388–406.
Kyvalova H, Cadek O, and Yuen DA (1995) Correlation analysis between subduction in the last 180 Myr and lateral seismic structure of the lower mantle: Geodynamical implications. *Geophysical Research Letters* 22: 1281–1284.
Labrosse S (2003) Thermal and magnetic evolution of the Earth's core. *Physics of the Earth and Planetary Interiors* 140: 127–143.
Labrosse S, Hernlund JW, and Coltice N (2007) A crystallising dense magma ocean at the base of Earth's mantle. *Nature* 450: 866–869.
Labrosse S, Poirier JP, and Le Mouel JL (1997) On cooling of the Earth's core. *Physics of the Earth and Planetary Interiors* 99: 1–17.
Lassak TM, McNamara AK, Garnero EJ, and Zhong S (2010) Core-mantle boundary topography as a possible constraint on lower mantle chemistry and dynamics. *Earth and Planetary Science Letters* 289: 232–241.
Lassak TM, McNamara AK, and Zhong S (2007) Influence of thermochemical piles on topography at Earth's core-mantle boundary. *Earth and Planetary Science Letters* 261: 443–455.
Lassiter JC (2004) Role of recycled oceanic crust in the potassium and argon budget of the Earth: Toward a resolution of the "missing argon" problem. *Geochemistry, Geophysics, Geosystems* 5: Q11012, http://dx.doi.org/11010.11029/12004GC000711.
Lay T and Garnero EJ (2004) Core-mantle boundary structures and processes. In: Sparks RSJ and Hawkesworth CJ (eds.) *The State of the Planet: Frontiers and Challenges in Geophysics*. Washington, DC: AGU, http://dx.doi.org/10.1029/1150GM1004.
Lay T, Garnero EJ, and Williams Q (2004) Partial melting in a thermo-chemical boundary layer at the base of the mantle. *Physics of the Earth and Planetary Interiors* 146: 441–467.
Le Bars M and Davaille A (2002) Stability of thermal convection in two superimposed miscible viscous fluids. *Journal of Fluid Mechanics* 471: 339–363.
Le Bars M and Davaille A (2004a) Large interface deformation in two-layer thermal convection of miscible viscous fluids. *Journal of Fluid Mechanics* 499: 75–110.
Le Bars M and Davaille A (2004b) Whole layer convection in a heterogeneous planetary mantle. *Journal of Geophysical Research* 109: B03403, http://dx.doi.org/03410.01029/02003JB002617.
Leahy GM and Bercovici D (2004) The influence of the transition zone water filter on convective circulation in the mantle. *Geophysical Research Letters* 31. http://dx.doi.org/10.1029/2004GL021206.
Leahy GM and Bercovici D (2007) On the dynamics of a hydrous melt layer above the transition zone. *Journal of Geophysical Research* 112. http://dx.doi.org/10.1029/2006JB004631.
Leahy GM and Bercovici D (2010) Reactive infiltration of hydrous melt above the mantle transition zone. *Journal of Geophysical Research* 115: B08406.
Lecuyer C and Ricard Y (1999) Long-term fluxes and budget of ferric iron: Implication for the redox states of the Earth's mantle and atmosphere. *Earth and Planetary Science Letters* 165: 197–211.
Lee CA, Luffi P, and Chin EJ (2011) Building and destroying continental mantle. *Annual Review of Earth and Planetary Sciences* 39: 59–90.
Lee C-T, Luffi P, Hoink T, Li J, Dasgupta R, and Hernlund J (2010) Upside-down differentiation and generation of a 'primordial' lower mantle. *Nature* 463: 930–933.
Lee C-TA, Shen B, Slotnick BS, et al. (2013) Continental arc-island arc fluctuations, growth of crustal carbonates, and long-term climate change. *Geosphere* 9: 21–36.
Lenardic A and Kaula WM (1993) A numerical treatment of geodynamic viscous-flow problems involving the advection of material interfaces. *Journal of Geophysical Research: Solid Earth* 98: 8243–8260.
Li M and McNamara AK (2013) The difficulty for subducted oceanic crust to accumulate at the Earth's core-mantle boundary. *Journal of Geophysical Research, Solid Earth* 118: 1807–1816.
Lin S-C and Van Keken PE (2006a) Dynamics of thermochemical plumes: 1. Plume formation and entrainment of a dense layer. *Geochemistry, Geophysics, Geosystems* 7. http://dx.doi.org/10.1029/2005GC001071.
Lin S-C and Van Keken PE (2006b) Dynamics of thermochemical plumes: 2. Complexity of plume structures and its implications for mapping of mantle plumes. *Geochemistry, Geophysics, Geosystems* 7. http://dx.doi.org/10.1029/2005GC001072.
Lithgow-Bertelloni C, Richards MA, Ricard Y, O'Connell RJ, and Engebretson DC (1993) Toroidal-poloidal partitioning of plate motions since 120 Ma. *Geophysical Research Letters* 20: 375–378.
Luo S-N, Ni S, and Helmberger DV (2001) Evidence for a sharp lateral variation of velocity at the core-mantle boundary from multipathed PKPab. *Earth and Planetary Science Letters* 189: 155–164.
Lyubetskaya T and Korenaga J (2007a) Chemical composition of Earth's primitive mantle and its variance, 1, Method and results. *Journal of Geophysical Research* 112. http://dx.doi.org/10.1029/2005JB004223.
Lyubetskaya T and Korenaga J (2007b) Chemical composition of Earth's primitive mantle and its variance, 2, Implications for global geodynamics. *Journal of Geophysical Research* 112(B3). http://dx.doi.org/10.1029/2005JB004224.
Machetel P and Weber P (1991) Intermittent layered convection in a model mantle with an endothermic phase-change at 670 km. *Nature* 350: 55–57.
Malvern LE (1969) *Introduction to the Mechanics of a Continuous Medium*. Englewood Cliffs, NJ: Prentice Hall.
Mambole A and Fleitout L (2002) Petrological layering induced by an endothermic phase transition in the Earth's mantle – Art. no. 2044. *Geophysical Research Letters* 29: 2044.
Manga M (1996) Mixing of heterogeneities in the mantle – Effect of viscosity differences. *Geophysical Research Letters* 23: 403–406.
Manga M and Jeanloz R (1996) Implications of a metal-bearing chemical-boundary layer in D″ for mantle dynamics. *Geophysical Research Letters* 23: 3091–3094.
Mao WL, Mao HK, Sturhahn W, et al. (2006) Iron-rich postperovskite and the origin of ultralow-velocity zones. *Science* 312: 564–565.
Martin H (1986) Effect of steeper archean geothermal gradient on geochemistry of subduction zone magmas. *Geology* 14: 753–756.
Masters G, Laske G, Bolton H, and Dziewonski A (2000) The relative behavior of shear velocity, bulk sound speed, and compressional velocity in the mantle: Implications for chemical and thermal structure. In: Karato S, Forte AM, Liebermann RC, Masters G, and Stixrude L (eds.) *Geophysical Monograph on Mineral Physics and Seismic Tomography from the Atomic to the Global Scale*, pp. 63–87. Washington, DC: American Geophysical Union.
Matsuda JMS, Ozima M, Ito K, Ohtaka O, and Ito E (1993) Noble gas partitioning between metal and silicate under high pressures. *Science* 259: 788–790.
McDonough WF and Sun S-S (1995) The composition of the Earth. *Chemical Geology* 120: 223–253.
McGovern PJ and Schubert G (1989) Thermal evolution of the Earth – Effects of volatile exchange between atmosphere and interior. *Earth and Planetary Science Letters* 96: 27–37.
McKenzie D (1979) Finite deformation during fluid flow. *Geophysical Journal of the Royal Astronomical Society* 58: 689–715.
McKenzie D and Onions RK (1992) Partial melt distributions from inversion of rare-earth element concentrations (J Petrol, Vol 32, Pg 1021, 1991). *Journal of Petrology* 33: 1453.
McNamara AK, Garnero EJ, and Rost S (2010) Tracking deep mantle reservoirs with ultra-low velocity zones. *Earth and Planetary Science Letters* 299: 1–9.
McNamara AK and Van Keken PE (2000) Cooling of the Earth: A parameterized convection study of whole versus layered models. *Geochemistry, Geophysics, Geosystems* 1: 1027. http://dx.doi.org/10.1029/2000GC000045.
McNamara AK and Zhong S (2004a) The influence of thermochemical convection on the fixity of mantle plumes. *Earth and Planetary Science Letters* 222: 485–500.
McNamara AK and Zhong S (2004b) Thermochemical structures within a spherical mantle: Superplumes or piles? *Journal of Geophysical Research* 109: B07402. http://dx.doi.org/10.1029/2003JB00247.
McNamara AK and Zhong S (2005) Thermochemical piles beneath Africa and the Pacific Ocean. *Nature* 437: 1136–1139.
Megnin C, Bunge HP, Romanowicz B, and Richards MA (1997) Imaging 3-D spherical convection models – What can seismic tomography tell us about mantle dynamics. *Geophysical Research Letters* 24: 1299–1302.
Meibom A and Anderson DL (2004) The statistical upper mantle assemblage. *Earth and Planetary Science Letters* 217: 123–139.
Meibom A, Anderson DL, Sleep NH, et al. (2003) Are high He-3/He-4 ratios in oceanic basalts an indicator of deep-mantle plume components? Earth Planet. *Science Letters* 208: 197–204.

Meibom A, Sleep NH, Chamberlain CP, et al. (2002) Re-Os isotopic evidence for long-lived heterogeneity and equilibration processes in the Earth's upper mantle. *Nature* 419: 705–708.

Meibom A, Sleep NH, Zahnle K, and Anderson DL (2005) Models for noble gases in mantle geochemistry: Some observations and alternatives. In: *Plumes, Plates, and Paradigms*, pp. 347–363, Geological Society of America Special Paper 388.

Melosh HJ (1990) Giant impacts and the thermal state of the early Earth. In: Newsom HE and Jones JH (eds.) *Origin of the Earth*. New York: Oxford University Press.

Metcalfe G, Bina CR, and Ottino JM (1995) Kinematic considerations for mantle mixing. *Geophysical Research Letters* 22: 743–746.

Michard A and Albarède F (1985) Hydrothermal uranium uptake at ridge crests. *Nature* 317: 61–88.

Montague NL and Kellogg LH (2000) Numerical models for a dense layer at the base of the mantle and implications for the geodynamics of D″. *Journal of Geophysical Research* 105: 11101–11114.

Montague NL, Kellogg LH, and Manga M (1998) High Rayleigh number thermo-chemical models of a dense boundary layer in D″. *Geophysical Research Letters* 25: 2345–2348.

Montelli R, Nolet G, Dahlen FA, Masters G, Engdahl ER, and Hung SH (2004) Finite-frequency tomography reveals a variety of plumes in the mantle. *Science* 303: 338–343.

Moore WB and Webb AAG (2013) Heat-pipe Earth. *Nature* 501: 501–505.

Moreira M, Breddam K, Curtice J, and Kurz MD (2001) Solar neon in the Icelandic mantle: New evidence for an undegassed lower mantle. *Earth and Planetary Science Letters* 185: 15–23.

Moresi L and Solomatov V (1998) Mantle convection with a brittle lithosphere – Thoughts on the global tectonic styles of the Earth and Venus. *Geophysical Journal International* 133: 669–682.

Mosca I, Cobden L, Deuss A, Ritsema J, and Trampert J (2012) Seismic and mineralogical structures of the lower mantle from probabilistic tomography. *Journal of Geophysical Research* 117: B06304.

Mosenfelder JL, Asimow PD, and Ahrens TJ (2007) Thermodynamic properties of Mg_2SiO_4 liquid at ultra-high pressures from shock measurements to 200 GPa on forsterite and wadsleyite. *Journal of Geophysical Research* 112: B06208, http://dx.doi.org/06210.01029/02006jb004364.

Mosenfelder JL, Asimow PD, Frost DJ, et al. (2009) The $MgSiO_3$ system at high pressure: Thermodynamic properties of perovskite, postperovskite, and melt from global inversion of shock and static compression data. *Journal of Geophysical Research* 114: B01203, http://dx.doi.org/01210.01029/02008jb005900.

Muller R (1992) The performance of classical versus modern finite-volume advection schemes for atmospheric modeling in a one-dimensional test-bed. *The Monthly Weather Review* 120: 1407–1415.

Murakami M, Hirose K, Kawamura K, Sata N, and Ohishi Y (2004) Post-perovskite phase transition in $MgSiO_3$. *Science* 304: 855–858.

Murakami M, Hirose K, Sata N, and Ohishi Y (2005) Post-perovskite phase transition and mineral chemistry in the pyrolitic lowermost mantle. *Geophysical Research Letters* 32. http://dx.doi.org/10.1029/2004GL021956.

Murphy DT, Kamber BS, and Collerson KD (2003) A refined solution to the first terrestrial Pb-isotope paradox. *Journal of Petrology* 44: 39–53.

Murthy VR and Karato S (1997) Core formation and chemical-equilibrium in the earth. 2. Chemical consequences for the mantle and core. *Physics of the Earth and Planetary Interiors* 100: 81–95.

Nakagawa T and Buffett BA (2005) Mass transport mechanism between the upper and lower mantle in numerical simulations of thermochemical mantle convection with multicomponent phase changes. *Earth and Planetary Science Letters* 230: 11–27.

Nakagawa T and Tackley PJ (2004a) Effects of a perovskite-post perovskite phase change near the core-mantle boundary on compressible mantle convection. *Geophysical Research Letters* 31: L16611. http://dx.doi.org/10.1029/2004GL020648.

Nakagawa T and Tackley PJ (2004b) Effects of thermo-chemical mantle convection on the thermal evolution of the Earth's core. *Earth and Planetary Science Letters* 220: 107–119.

Nakagawa T and Tackley PJ (2005a) Deep mantle heat flow and thermal evolution of Earth's core in thermo-chemical multiphase models of mantle convection. *Geochemistry, Geophysics, Geosystems* 6: Q08003. http://dx.doi.org/10.1029/2005GC000967.

Nakagawa T and Tackley PJ (2005b) The interaction between the post-perovskite phase change and a thermo-chemical boundary layer near the core-mantle boundary. *Earth and Planetary Science Letters* 238: 204–216.

Nakagawa T and Tackley PJ (2005c) Three-dimensional numerical simulations of thermo-chemical multiphase convection in Earth's mantle. In: *Proceedings of the Third MIT Conference on Computational Fluid and Solid Mechanics*.

Nakagawa T and Tackley PJ (2006) Three-dimensional structures and dynamics in the deep mantle: Effects of post-perovskite phase change and deep mantle layering. *Geophysical Research Letters* 33: L12S11. http://dx.doi.org/10.1029/2006GL025719.

Nakagawa T and Tackley PJ (2010) Influence of initial CMB temperature and other parameters on the thermal evolution of Earth's core resulting from thermo-chemical spherical mantle convection. *Geochemistry, Geophysics, Geosystems* 11: Q06001. http://dx.doi.org/10.1029/2010GC003031.

Nakagawa T and Tackley PJ (2011) Effects of low-viscosity post-perovskite on thermo-chemical convection in a 3-D spherical shell. *Geophysical Research Letters* 38: L04309. http://dx.doi.org/10.1029/2010GL046494.

Nakagawa T and Tackley PJ (2012) Influence of magmatism on mantle cooling, surface heat flow and Urey ratio. *Earth and Planetary Science Letters* 329–330: 1–10.

Nakagawa T and Tackley PJ (2013) Implications of high core thermal conductivity on Earth's coupled mantle and core evolution. *Geophysical Research Letters* 40: 2652–2656.

Nakagawa T and Tackley PJ (2014) Influence of combined primordial layering and recycled MORB on the coupled thermal evolution of Earth's mantle and core. *Geochemistry, Geophysics, Geosystems* 15: 619–633. http://dx.doi.org/10.1002/2013GC005128.

Nakagawa T, Tackley PJ, Deschamps F, and Connolly JAD (2009) Incorporating self-consistently calculated mineral physics into thermo-chemical mantle convection simulations in a 3D spherical shell and its influence on seismic anomalies in Earth's mantle. *Geochemistry, Geophysics, Geosystems* 10. http://dx.doi.org/10.1029/2008GC002280.

Nakagawa T, Tackley PJ, Deschamps F, and Connolly JAD (2010) The influence of MORB and harzburgite composition on thermo-chemical mantle convection in a 3-D spherical shell with self-consistently calculated mineral physics. *Earth and Planetary Science Letters* 296: 403–412.

Nakagawa T, Tackley PJ, Deschamps F, and Connolly JAD (2012) Radial 1-D seismic structures in the deep mantle in mantle convection simulations with self-consistently calculated mineralogy. *Geochemistry, Geophysics, Geosystems* 13: Q11002. http://dx.doi.org/10.1029/2012GC004325.

Namiki A (2003) Can the mantle entrain D″? *Journal of Geophysical Research* 108: 2487. http://dx.doi.org/10.1029/2002JB002315.

Newsom HE, White WM, Jochum KP, and Hofmann AW (1986) Siderophile and chalcophile element abundances in oceanic basalts. *Earth and Planetary Science Letters* 80: 299–313.

Ni SV, Helmberger D, and Tromp J (2005) Three-dimensional structure of the African superplume from waveform modelling. *Geophysical Journal International* 161: 283–294.

Ni S, Tan E, Gurnis M, and Helmberger DV (2002) Sharp sides to the African superplume. *Science* 296: 1850–1852.

Nimmo F, Price GD, Brodholt J, and Gubbins D (2004) The influence of potassium on core and geodynamo evolution. *Geophysical Journal International* 156: 363–376.

Nomura R, Ozawa H, Tateno S, et al. (2011) Spin crossover and iron-rich silicate melt in the Earth/'s deep mantle. *Nature* 473: 199–202.

Oganov AR and Ono S (2004) Theoretical and experimental evidence for a post-perovskite phase of $MgSiO_3$ in Earth's D″ layer. *Nature* 430: 445–448.

Ogawa M (1988) Numerical experiments on coupled magmatism-mantle convection system – Implications for mantle evolution and archean continental crusts. *Journal of Geophysical Research – B: Solid Earth and Planets* 93: 15119–15134.

Ogawa M (1993) A numerical-model of a coupled magmatism mantle convection system in venus and the Earths mantle beneath archean continental crusts. *Icarus* 102: 40–61.

Ogawa M (1994) Effects of chemical fractionation of heat-producing elements on mantle evolution inferred from a numerical-model of coupled magmatism mantle convection system. *Physics of the Earth and Planetary Interiors* 83: 101–127.

Ogawa M (1997) A bifurcation in the coupled magmatism-mantle convection system and its implications for the evolution of the Earth's upper mantle. *Physics of the Earth and Planetary Interiors* 102: 259–276.

Ogawa M (2000a) Coupled magmatism-mantle convection system with variable viscosity. *Tectonophysics* 322: 1–18.

Ogawa M (2000b) Numerical models of magmatism in convecting mantle with temperature-dependent viscosity and their implications for Venus and Earth. *Journal of Geophysical Research* 105: 6997–7012.

Ogawa M (2003) Chemical stratification in a two-dimensional convecting mantle with magmatism and moving plates. *Journal of Geophysical Research* 108: 2561. http://dx.doi.org/10.1029/2002JB002205.

Ogawa M (2007) Superplumes, plates, and mantle magmatism in two-dimensional numerical models. *Journal of Geophysical Research* 112: B06404.

Ogawa M (2010) Variety of plumes and the fate of subducted basaltic crusts. *Physics of the Earth and Planetary Interiors* 183: 366–375.

Ogawa M (2013) Two-stage evolution of the Earth's mantle inferred from numerical simulations of coupled magmatism-mantle convection system with tectonic plates. *Journal of Geophysical Research* 119: 2462–2486.
Ogawa M and Nakamura H (1998) Thermochemical regime of the early mantle inferred from numerical models of the coupled magmatism-mantle convection system with the solid-solid phase transitions at depths around 660 km. *Journal of Geophysical Research* 103: 12161–12180.
Ogawa M and Yanagisawa T (2011) Numerical models of Martian mantle evolution induced by magmatism and solid-state convection beneath stagnant lithosphere. *Journal of Geophysical Research* 116: E08008. http://dx.doi.org/10.1029/2010JE003777.
Oldham D and Davies JH (2004) Numerical investigation of layered convection in a three-dimensional shell with application to planetary mantles. *Geochemistry, Geophysics, Geosystems* 5: Q12C04. http://dx.doi.org/10.1029/2003GC000603.
Olson P (1984) An experimental approach to thermal-convection in a 2-layered mantle. *Journal of Geophysical Research* 89: 1293–1301.
Olson P and Kincaid C (1991) Experiments on the interaction of thermal convection and compositional layering at the base of the mantle. *Journal of Geophysical Research* 96: 4347–4354.
Olson P, Yuen DA, and Balsiger D (1984a) Convective mixing and the fine-structure of mantle heterogeneity. *Physics of the Earth and Planetary Interiors* 36: 291–304.
Olson P, Yuen DA, and Balsiger D (1984b) Mixing of passive heterogeneities by mantle convection. *Journal of Geophysical Research* 89: 425–436.
O'Neill HS and Palme H (2008) Collisional erosion and the non-chondritic composition of the terrestrial planets. *Philosophical Transactions. Series A, Mathematical, Physical, and Engineering Sciences* 366: 4205–4238.
O'Nions RK, Evensen NM, and Hamilton PJ (1979) Geochemical modeling of mantle differentiation and crustal growth. *Journal of Geophysical Research* 84: 6091–6101.
O'Nions RK and Oxburgh ER (1983) Heat and helium in the Earth. *Nature* 306: 429.
O'Nions RK and Tolstikhin IN (1996) Limits on the mass flux between lower and upper mantle and stability of layering. *Earth and Planetary Science Letters* 139: 213–222.
Ono S, Ito E, and Katsura T (2001) Mineralogy of subducted basaltic crust (MORB) from 25 to 37 GPa, and chemical heterogeneity of the lower mantle. *Earth and Planetary Science Letters* 190: 57–63.
Ono S, Oganov AR, and Ohishi Y (2005a) In situ observations of phase transition between perovskite and $CaIrO_3$-type phase in $MgSiO_3$ and pyrolitic mantle composition. *Earth and Planetary Science Letters* 236: 914–932.
Ono S, Oshishi Y, Isshiki M, and Watanuki T (2005b) In situ X-ray observations of phase assemblages in peridotite and basalt compositions at lower mantle conditions: Implications for density of subducted oceanic plate. *Journal of Geophysical Research* 110: B02208. http://dx.doi.org/10.1029/2004JB0003196.
O'Reilly TC and Davies GF (1981) Magma transport of heat on Io: A mechanism allowing a thick lithosphere. *Geophysical Research Letters* 8: 313–316.
Otsuka K and Karato S (2012) Deep penetration of molten iron into the mantle caused by a morphological instability. *Nature* 492: 243–246.
Ottino JM (1989) *The Kinematics of Mixing: Stretching, Chaos, and Transport*. Cambridge: Cambridge University Press.
Ozima M and Kudo K (1972) Excess argon in submarine basalts and an Earth-atmosphere evolution model. *Nature* 239: 23–24.
Palme H and O'Neill HSC (2003) Cosmochemical estimates of mantle composition. In: Carlson RW (ed.) *Treatise on Geochemistry*, pp. 1–38. Oxford: Elsevier.
Parkinson IJ, Hawkesworth CJ, and Cohen AS (1998) Ancient mantle in a modern arc: Osmium isotopes in Izu-Bonin-Mariana forearc peridotites. *Science* 281: 2011–2013.
Parman SW, Kurz MD, Hart SR, and Grove TL (2005) Helium solubility in olivine and implications for high $^3He/^4He$ in ocean island basalts. *Nature* 437: 1140–1143.
Pearson DG, Davies GR, and Nixon PH (1993) Geochemical constraints on the petrogenesis of diamond facies pyroxenites from the Beni Bousera peridotite massif, north Morocco. *Journal of Petrology* 34: 125–172.
Peltier WR and Solheim LP (1992) Mantle phase-transitions and layered chaotic convection. *Geophysical Research Letters* 19: 321–324.
Pertermann M (2003) Partial melting experiments on a MORB-like pyroxenite between 2 and 3 GPa: Constraints on the presence of pyroxenite in basalt source regions from solidus location and melting rate. *Journal of Geophysical Research* 108: 2125.
Petford N, Yuen D, Rushmer T, Brodholt J, and Stackhouse S (2005) Shear-induced material transfer across the core-mantle boundary aided by the post-perovskite phase transition. *Earth, Planets and Space* 57: 459–464.
Phipps Morgan J (1998) Thermal and rare gas evolution of the mantle. *Chemical Geology* 145: 431–445.
Phipps Morgan J (1999) Isotope topology of individual hotspot basalt arrays: Mixing curves or melt extraction trajectories? *Geochemistry, Geophysics, Geosystems* 1: 1003. http://dx.doi.org/10.1029/1999GC000004.
Phipps Morgan J (2001) Thermodynamics of pressure release melting of a veined plum pudding mantle. *Geochemistry, Geophysics, Geosystems* 2, Paper number 2000GC000049 [000015,000429 words, 000010 figures, 000041 table, 000042 appendix figures, 000041 appendix table].
Phipps Morgan J and Morgan J (1999) Two-stage melting and the geochemical evolution of the mantle: A recipe for mantle plum-pudding. *Earth and Planetary Science Letters* 170: 215–239.
Poirier JP (1993) Core-infiltrated mantle and the nature of the D″ layer. *Journal of Geomagnetism and Geoelectricity* 45: 1221–1227.
Poirier JP and Le Mouel JL (1992) Does infiltration of core material into the lower mantle affect the observed geomagnetic field? *Physics of the Earth and Planetary Interiors* 73: 29–37.
Poirier JP, Malavergne V, and Le Mouel JL (1998) Is there a thin electrically conducting layer at the base of the mantle? In: Gurnis M, Wysession ME, Knittle E, and Buffett BA (eds.) *The Core-Mantle Boundary Region*, pp. 131–137. Washington, DC: American Geophysical Union.
Polve M and Allegre CJ (1980) Orogenic lherzolite complexes studies by 87Rb-87Sr: A clue to understand the mantle convection processes? Earth Planet. *Science Letters* 51: 71–93.
Porcelli D and Halliday AN (2001) The core as a possible source of mantle helium. *Earth and Planetary Science Letters* 192: 45–56.
Porcelli D and Wasserburg GJ (1995) Mass transfer of helium, neon, argon and xenon through a steady-state upper mantle. *Geochimica et Cosmochimica Acta* 23: 4921–4937.
Pozzo M, Davies C, Gubbins D, and Alfe D (2012) Thermal and electrical conductivity of iron at Earth's core conditions. *Nature* 485: 355–358.
Puster P and Jordan TH (1994) Stochastic-analysis of mantle convection experiments using 2-point correlation-functions. *Geophysical Research Letters* 21: 305–308.
Puster P and Jordan TH (1997) How stratified is mantle convection? *Journal of Geophysical Research* 102: 7625–7646.
Puster P, Jordan TH, and Hager BH (1995) Characterization of mantle convection experiments using 2-point correlation-functions. *Journal of Geophysical Research, Solid Earth* 100: 6351–6365.
Rapp RP, Irifune T, Shimizu N, Nishiyama N, Norman MD, and Inoue T (2008) Subduction recycling of continental sediments and the origin of geochemically enriched reservoirs in the deep mantle. *Earth and Planetary Science Letters* 271: 14–23.
Reisberg I and Zindler A (1986) Extreme isotopic variability in the upper mantle: Evidence from Ronda. *Earth and Planetary Science Letters* 81: 29–45.
Revenaugh J and Meyer R (1997) Seismic evidence of partial melt within a possibly ubiquitous low-velocity layer at the base of the mantle. *Science* 277: 670–673.
Revenaugh J and Sipkin SA (1994) Seismic evidence for silicate melt atop the 410-km mantle discontinuity. *Nature* 369: 474–476.
Ricard Y, Froidevaux C, and Fleitout L (1988) Global plate motion and the geoid – A physical model. *Geophysical Journal International* 93: 477–484.
Ricard Y, Vigny C, and Froidevaux C (1989) Mantle heterogeneities, geoid, and plate motion – A Monte-Carlo inversion. *Journal of Geophysical Research* 94: 13739–13754.
Richard GC and Bercovici D (2009) Water-induced convection in the Earth's mantle transition zone. *Journal of Geophysical Research* 114: B01205. http://dx.doi.org/10.1029/2008JB005734.
Richard G, Bercovici D, and Karato S-I (2006) Slab dehydration in the Earth's mantle transition zone. *Earth and Planetary Science Letters* 251: 156–167.
Richard G, Monnereau M, and Ingrin J (2002) Is the transition zone an empty water reservoir? Inferences from numerical models of mantle dynamics. *Earth and Planetary Science Letters* 205: 37–51.
Richards MA and Davies GF (1989) On the separation of relatively buoyant components from subducted lithosphere. *Geophysical Research Letters* 16: 831–834.
Richards MA and Engebretson DC (1992) Large-scale mantle convection and the history of subduction. *Nature* 355: 437–440.
Richards MA and Griffiths RW (1989) Thermal entrainment by deflected mantle plumes. *Nature* 342: 900–902.
Richardson LF (1926) Atmospheric diffusion shown on a distance-neighbor graph. *Proceedings of the Royal Society of London* 110: 709–737.
Richter FM, Daly SF, and Nataf HC (1982) A parameterized model for the evolution of isotopic heterogeneities in a convecting system. *Earth and Planetary Science Letters* 60: 178–194.
Richter FM and Johnson CE (1974) Stability of a chemically layered mantle. *Journal of Geophysical Research* 79: 1635–1639.
Richter FM and McKenzie D (1981) On some consequences and possible causes of layered mantle convection. *Journal of Geophysical Research* 86: 6133–6142.

Richter FM and Ribe NM (1979) On the importance of advection in determining the local isotopic composition of the mantle. *Earth and Planetary Science Letters* 43: 212–222.

Ricolleau A, Perrillat J-P, Fiquet G, et al. (2010) Phase relations and equation of state of a natural MORB: Implications for the density profile of subducted oceanic crust in the Earth's lower mantle. *Journal of Geophysical Research* 115: B08202. http://dx.doi.org/08210.01029/02009jb006709.

Righter K and Drake MJ (2003) Partition coefficients at high pressure and temperature. In: Carlson CW (ed.) *Treatise on Geochemistry*. *The Mantle and Core*, vol. 2, pp. 425–449. Amsterdam: Elsevier.

Ringwood AE (1990a) Earliest history of the Earth-Moon system. In: Newsom HE and Jones JH (eds.) *Origin of the Earth*, pp. 101–134. New York: Oxford University Press.

Ringwood AE (1990b) Slab-mantle interactions. 3. Petrogenesis of intraplate magmas and structure of the upper mantle. *Chemical Geology* 82: 187–207.

Ringwood AE (1991) Phase-transformations and their bearing on the constitution and dynamics of the mantle. *Geochimica et Cosmochimica Acta* 55: 2083–2110.

Ringwood AE (1994) Role of the transition zone and 660 km discontinuity in mantle dynamics. *Physics of the Earth and Planetary Interiors* 86: 5–24.

Ringwood AE and Irifune T (1988) Nature of the 650-km seismic discontinuity – Implications for mantle dynamics and differentiation. *Nature* 331: 131–136.

Rizo H, Boyet M, Blichert-Toft J, O'Neil J, Rosing MT, and Paquette JL (2012) The elusive Hadean enriched reservoir revealed by ^{142}Nd deficits in Isua Archaean rocks. *Nature* 491: 96–100.

Rohrbach A and Schmidt MW (2011) Redox freezing and melting in the Earth's deep mantle resulting from carbon-iron redox coupling. *Nature* 472: 209–212.

Romanowicz B (2001) Can we resolve 3D density heterogeneity in the lower mantle? *Geophysical Research Letters* 28: 1107–1110.

Rubie DC, Melosh HJ, Reid JE, Liebske C, and Righter K (2003) Mechanisms of metal-silicate equilibration in the terrestrial magma ocean. *Earth and Planetary Science Letters* 205: 239–255.

Rudge JF (2006) Mantle pseudo-isochrons revisited. *Earth and Planetary Science Letters* 249: 494–513.

Rudge JF, Bercovici D, and Spiegelman M (2011) Disequilibrium melting of a two phase multicomponent mantle. *Geophysical Journal International* 184: 699–718.

Rudge JF, McKenzie D, and Haynes PH (2005) A theoretical approach to understanding the isotopic heterogeneity of mid-ocean ridge basalt. *Geochimica et Cosmochimica Acta* 69: 3873–3887.

Rudnick RL (1995) Making continental crust. *Nature (London)* 378: 571–578.

Rudnick RL and Fountain DM (1995) Nature and composition of the continental crust; a lower crustal perspective. *Reviews of Geophysics* 33: 267–309.

Ruepke L, Phipps Morgan J, Hort M, and Connolly JAD (2004) Serpentine and the subduction zone water cycle. *Earth and Planetary Science Letters* 223: 17–34.

Saal AE, Hart SR, Shimizu N, Hauri EH, and Layne GD (1998) Pb isotopic variability in melt inclusions from oceanic island basalts, Polynesia. *Science* 282: 1481–1484.

Saal AE, Hauri EH, Langmuir CH, and Perfit MR (2002) Vapour undersaturation in primitive mid-ocean-ridge basalt and the volatile content of Earth's upper mantle. *Nature* 419: 451–455.

Saltzer RL, Stutzmann E, and van der Hilst RD (2004) Poisson's ratio in the lower mantle beneath Alaska: Evidence for compositional heterogeneity. *Journal of Geophysical Research* 109: B06301, http://dx.doi.org/06310.01029/02003jb002712.

Samuel H and Bercovici D (2006) Oscillating and stagnating plumes in the Earth's lower mantle. *Earth and Planetary Science Letters* 248: 90–105.

Samuel H and Farnetani CG (2003) Thermochemical convection and helium concentrations in mantle plumes. *Earth and Planetary Science Letters* 207: 39–56.

Samuel H and Tackley PJ (2008) Dynamics of core formation and equilibrium by negative diapirism. *Geochemistry, Geophysics, Geosystems* 9. http://dx.doi.org/10.1029/2007GC001896.

Sandu C, Lenardic A, and McGovern P (2011) The effects of deep water cycling on planetary thermal evolution. *Journal of Geophysical Research, Solid Earth* 116: B12404.

Sarda P, Moreira M, and Staudacher T (1999) argon-Lead isotopic correlation in mid-Atlantic ridge basalts. *Science* 283: 666–668.

Schersten A, Elliott T, Hawkesworth C, and Norman M (2004) Tungsten isotope evidence that mantle plumes contain no contribution from the Earth's core. *Nature* 427: 234–237.

Schilling J-G (1973) Iceland mantle plume: Geochemical study of Reykjanes ridge. *Nature* 242: 565–571.

Schmalzl J and Hansen U (1994) Mixing the Earths mantle by thermal-convection – A scale-dependent phenomenon. *Geophysical Research Letters* 21: 987–990.

Schmalzl J, Houseman GA, and Hansen U (1995) Mixing properties of three-dimensional (3-D) stationary convection. *Physics of Fluids* 7: 1027–1033.

Schmalzl J, Houseman GA, and Hansen U (1996) Mixing in vigorous, time-dependent three-dimensional convection and application to Earth's mantle. *Journal of Geophysical Research* 101: 21847–21858.

Schmalzl J and Loddoch A (2003) Using subdivision surfaces and adaptive surface simplification algorithms for modeling chemical heterogeneities in geophysical flows. *Geochemistry, Geophysics, Geosystems* 4: 8303. http://dx.doi.org/10.1029/2003GC000578.

Schmandt B, Dueker K, Humphreys E, and Hansen S (2012) Hot mantle upwelling across the 660 beneath Yellowstone. *Earth and Planetary Science Letters* 331–332: 224–236.

Schott B and Yuen DA (2004) Influences of dissipation and rheology on mantle plumes coming from the D″-layer. *Physics of the Earth and Planetary Interiors* 146: 139–145.

Schott B, Yuen DA, and Braun A (2002) The influences of composition-and temperature- dependent rheology in thermal-chemical convection on entrainment of the D″-layer. *Physics of the Earth and Planetary Interiors* 129: 43–65.

Schubert G, Masters G, Olson P, and Tackley P (2004) Superplumes or plume clusters? *Physics of the Earth and Planetary Interiors* 146: 147–162.

Scrivner C and Anderson DL (1992) The effect of post pangea subduction on global mantle tomography and convection. *Geophysical Research Letters* 19: 1053–1056.

Shaw DM (1970) Trace element fractionation during anatexis. *Geochimica et Cosmochimica Acta* 34: 237–242.

Shaw AM, Hauri EH, Behn MD, Hilton DR, Macpherson CG, and Sinton JM (2012) Long-term preservation of slab signatures in the mantle inferred from hydrogen isotopes. *Nature Geoscience* 5: 224–228.

Shen Y, Solomon SC, Bjarnason IT, and Wolfe CJ (1998) Seismic evidence for a lower-mantle origin of the Iceland Plume. *Nature (London)* 395: 62–65.

Simmons NA, Forte AM, Boschi L, and Grand SP (2010) GyPSuM: A joint tomographic model of mantle density and seismic wave speeds. *Journal of Geophysical Research* 115: B12310.

Sleep NH (1984) Tapping of magmas from ubiquitous mantle heterogeneities – An alternative to mantle plumes. *Journal of Geophysical Research* 89: 10029–10041.

Sleep NH (1988) Gradual entrainment of a chemical layer at the base of the mantle by overlying convection. *Geophysical Journal* 95: 437–447.

Sleep NH (1990) Hotspots and mantle plumes – Some phenomenology. *Journal of Geophysical Research – B: Solid Earth and Planets* 95: 6715–6736.

Sleep NH (2000) Evolution of the mode of convection within terrestrial planets. *Journal of Geophysical Research* 105: 17563–17578.

Sleep NH and Zahnle K (2001) Carbon dioxide cycling and implications for climate on ancient Earth. *Journal of Geophysical Research* 106: 1373–1399.

Smith RB, Jordan M, Steinberger B, et al. (2009) Geodynamics of the Yellowstone hotspot and mantle plume: Seismic and GPS imaging, kinematics, and mantle flow. *Journal of Volcanology and Geothermal Research* 188: 26–56.

Smolarkiewicz PK and Margolin LG (1998) MPDATA: A finite-difference solver for geophysical flows. *Journal of Computational Physics* 140: 459–480.

Sneeringer M, Hart SR, and Shimizu N (1984) Strontium and samarium diffusion in diopside. *Geochimica et Cosmochimica Acta* 48: 1589–1608.

Sobolev AV (1996) Melt inclusions in minerals as a source of principal petrological information. *Petrology* 4: 209–220.

Sobolev AV, Hofmann AW, Kuzmin DV, et al. (2007) The amount of recycled crust in sources of mantle-derived melts. *Science* 316: 412–417.

Sobolev AV, Hofmann AW, and Nikogosian IK (2000) Recycled oceanic crust observed in 'ghost plagioclase' within the source of Mauna Loa lavas. *Nature* 404: 986–990.

Sobolev AV, Hofmann AW, Sobolev SV, and Nikogosian IK (2005) An olivine-free mantle source of Hawaiian shield basalts. *Science* 434: 590–597.

Sobolev AV and Shimizu N (1993) Ultra-depleted primary melt included in an olivine from the Mid-Atlantic Ridge. *Nature* 363: 151–154.

Solomatov VS (2000) Fluid dynamics of a terrestrial magma ocean. In: Canup RM and Righter K (eds.) *Origin of the Earth and Moon*. Tucson, AZ: The University of Arizona Press.

Solomatov VS and Moresi LN (2002) Small-scale convection in the D″ layer. *Journal of Geophysical Research* 107. http://dx.doi.org/10.1029/2000JB000063.

Solomatov VS, Olson P, and Stevenson DJ (1993) Entrainment from a bed of particles by thermal-convection. *Earth and Planetary Science Letters* 120: 387–393.

Solomatov VS and Reese CC (2008) Grain size variations in the Earth's mantle and evolution of primordial chemical heterogeneities. *Journal of Geophysical Research* 113: B07408. http://dx.doi.org/10.1029/2007JB005319.

Solomatov VS and Stevenson DJ (1993a) Nonfractional crystallization of a terrestrial magma ocean. *Journal of Geophysical Research: Planets* 98: 5391–5406.

Solomatov VS and Stevenson DJ (1993b) Suspension in convective layers and style of differentiation of a terrestrial magma ocean. *Journal of Geophysical Research: Planets* 98: 5375–5390.

Song X and Ahrens TJ (1994) Pressure-temperature range of reactions between liquid-iron in the outer core and mantle silicates. *Geophysical Research Letters* 21: 153–156.
Song T-RA, Helmberger DV, and Grand SP (2004) Low-velocity zone atop the 410-km seismic discontinuity in the northwestern United States. *Nature* 427: 530–533.
Spence DA, Ockendon JR, Wilmott P, Turcotte DL, and Kellogg LH (1988) Convective mixing in the mantle: The role of viscosity differences. *Geophysical Journal* 95: 79–86.
Stacey FD (1992) *Physics of the Earth*, 3rd edn. Kenmore, Queensland, Australia: Brookfield Press.
Stackhouse S and Brodholt JP (2008) Elastic properties of the post-perovskite phase of Fe_2O_3 and implications for ultra-low velocity zones. *Physics of the Earth and Planetary Interiors* 170: 260–266.
Stackhouse S, Brodholt J, and Price GD (2006) Elastic anisotropy of $FeSiO_3$ end-members of the perovskite and post-perovskite phases. *Geophysical Research Letters* 33: L01304. http://dx.doi.org/10.1029/2005GL023887.
Stagno V, Ojwang DO, McCammon CA, and Frost DJ (2013) The oxidation state of the mantle and the extraction of carbon from Earth's interior. *Nature* 493: 84–88.
Stegman DR, Richards MA, and Baumgardner JR (2002) Effects of depth-dependent viscosity and plate motions on maintaining a relatively uniform mid-ocean ridge basalt reservoir in whole mantle flow. *Journal of Geophysical Research* 107. http://dx.doi.org/10.1029/2001JB000192.
Stein M and Hofmann AW (1994) Mantle plumes and episodic crustal growth. *Nature* 372: 63–68.
Steinberger B and Torsvik TH (2012) A geodynamic model of plumes from the margins of large low shear velocity provinces. *Geochemistry, Geophysics, Geosystems* 13: Q01W09.
Stern RJ and Scholl DW (2010) Yin and yang of continental crust creation and destruction by plate tectonic processes. *International Geology Review* 52: 1–31.
Stevenson DJ (1988) Infiltration, dissolution, and underplating: Rules for mixing core-mantle cocktails. *EOS (Transactions of the American Geophysical Union)* 69: 1404, Fall Meeting Supplement.
Stevenson DJ (1990) Fluid dynamics of core formation. In: Jones JH and Newman HE (eds.) *Origin of the Earth*, pp. 231–249. Oxford: Oxford University Press.
Stixrude L, de Koker N, Sun N, Mookherjee M, and Karki BB (2009) Thermodynamics of silicate liquids in the deep Earth. *Earth and Planetary Science Letters* 278: 226–232.
Stracke A (2012) Earth's heterogeneous mantle: A product of convection-driven interaction between crust and mantle. *Chemical Geology* 330–331: 274–299.
Stracke A, Hofmann AW, and Hart S (2005) FOZO, HIMU, and the rest of the mantle zoo. *Geochemistry, Geophysics, Geosystems* 6: Q05007. http://dx.doi.org/10.1029/2004GC000824.
Stracke A, Zindler A, Salters VJM, et al. (2003) Theistareykir revisited. *Geochemistry, Geophysics, Geosystems* 4(2): 8507. http://dx.doi.org/10.1029/2001GC000201.
Stuart FM, Lass-Evans S, Fitton JG, and Ellam RM (2003) High 3He/4He ratios in picritic basalts from Baffin Island and the role of a mixed reservoir in mantle plumes. *Nature* 424: 57–59.
Su WJ and Dziewonski AM (1997) Simultaneous inversion for 3-D variations in shear and bulk velocity in the mantle. *Physics of the Earth and Planetary Interiors* 100: 135–156.
Subramanian N, Kellogg LH, and Turcotte DL (2009) Statistics of advective stretching in three-dimensional incompressible flows. *Journal of Statistical Physics* 136: 926–944.
Suen CJ and Frey FA (1987) Origins of mafic and ultramafic rocks in the Ronda peridotite. *Earth and Planetary Science Letters* 85: 183–202.
Tackley PJ (1998) Three-dimensional simulations of mantle convection with a thermochemical CMB boundary layer: D″? In: Wysession ME, Knittle E, Buffett BA, and Gurnis M (eds.) *The Core-Mantle Boundary Region*, pp. 231–253. Washington, DC: American Geophysical Union.
Tackley PJ (2000) Mantle convection and plate tectonics: Towards an integrated physical and chemical theory. *Science* 288: 2002.
Tackley PJ (2002) Strong heterogeneity caused by deep mantle layering. *Geochemistry, Geophysics, Geosystems* 3. http://dx.doi.org/10.1029/2001GC000167.
Tackley PJ (2011) Living dead slabs in 3-D: The dynamics of compositionally-stratified slabs entering a "slab graveyard" above the core-mantle boundary. *Physics of the Earth and Planetary Interiors* 188: 150–162.
Tackley PJ (2012) Dynamics and evolution of the deep mantle resulting from thermal, chemical, phase and melting effects. *Earth Science Reviews* 110: 1–25.
Tackley PJ and King SD (2003) Testing the tracer ratio method for modeling active compositional fields in mantle convection simulations. *Geochemistry, Geophysics, Geosystems* 4: 8302. http://dx.doi.org/10.1029/2001GC000214.
Tackley PJ, Nakagawa T, and Hernlund JW (2007) Influence of the post-perovskite transition on thermal and thermo-chemical mantle convection. In: Hirose K, Brodholt J, Lay T, and Yuen DA (eds.) *Post-perovskite: The Last Mantle Phase Transition*. *AGU Geophysical Monograph Series*, vol. 174, pp. 229–248. Washington, DC: American Geophysical Union.
Tackley PJ, Stevenson DJ, Glatzmaier GA, and Schubert G (1994) Effects of multiple phase transitions in a 3-dimensional spherical model of convection in Earth's mantle. *Journal of Geophysical Research* 99: 15877–15901.
Tackley PJ and Xie S (2002) The thermo-chemical structure and evolution of Earth's mantle: Constraints and numerical models. *Philosophical Transactions of the Royal Society A* 360: 2593–2609.
Tackley PJ, Xie S, Nakagawa T, and Hernlund JW (2005) Numerical and laboratory studies of mantle convection: Philosophy, accomplishments and thermo-chemical structure and evolution. In: van der Hilst RD, Bass J, Matas J, and Trampert J (eds.) *AGU Geophysical Monograph on Earth's Deep Mantle: Structure, Composition and Evolution*, pp. 85–102. Washington, DC: AGU.
Tajika E and Matsui T (1992) Evolution of terrestrial proto-CO_2 atmosphere coupled with thermal history of the Earth. *Earth and Planetary Science Letters* 113: 251–266.
Tajika E and Matsui T (1993) Evolution of sea-floor spreading rate-based on Ar-40 degassing history. *Geophysical Research Letters* 20: 851–854.
Tan E and Gurnis M (2005) Metastable superplumes and mantle compressibility. *Geophysical Research Letters* 32: L20307, http://dx.doi.org/20310.21029/22005GL024190.
Tan E and Gurnis M (2007) Compressible thermochemical convection and application to lower mantle structures. *Journal of Geophysical Research* 112: B06304, http://dx.doi.org/06310.01029/02006jb004505.
Tan E, Gurnis M, and Han L (2002) Slabs in the lower mantle and their modulation of plume formation. *Geochemistry, Geophysics, Geosystems* 3: 1067, http://dx.doi.org/1010.1029/2001GC000238.
Tan E, Leng W, Zhong S, and Gurnis M (2011) On the location of plumes and lateral movement of thermo-chemical structures with high bulk modulus in the 3-D compressible mantle. *Geochemistry, Geophysics, Geosystems* 12: Q07005. http://dx.doi.org/10.1029/2011GC003665.
Tatsumi Y, Suzuki T, Ozawa H, Hirose K, Hanyu T, and Ohishi Y (2013) Accumulation of 'anti-continent' at the base of the mantle and its recycling in mantle plumes. *Geochimica et Cosmochimica Acta*. http://dx.doi.org/10.1016/j.gca.2013.11.019.
Tauzin B, Debayle E, and Wittlinger G (2010) Seismic evidence for a global low-velocity layer within the Earth/'s upper mantle. *Nature Geoscience* 3: 718–721.
Taylor SR and McLennan SM (1995) The geochemical evolution of the continental crust. *Reviews of Geophysics* 33: 241–265.
Ten AA, Podladchikov YY, Yuen DA, Larsen TB, and Malevsky AV (1998) Comparison of mixing properties in convection with the particle-line method. *Geophysical Research Letters* 25: 3205–3208.
Ten A, Yuen DA, Larsen TB, and Malevsky AV (1996) The evolution of material-surfaces in convection with variable viscosity as monitored by a characteristics-based method. *Geophysical Research Letters* 23: 2001–2004.
Ten A, Yuen DA, Podladchikov YY, Larsen TB, Pachepsky E, and Malevsky AV (1997) Fractal features in mixing of non-newtonian and newtonian mantle convection. *Earth and Planetary Science Letters* 146: 401–414.
Thorne MS, Garnero EJ, Jahnke G, Igel H, and McNamara AK (2013) Mega ultra low velocity zone and mantle flow. *Earth and Planetary Science Letters* 364: 59–67.
Thorne MS, Grand SP, and Garnero EJ (2004) Geographic correlation between hot spots and deep mantle lateral shear-wave velocity gradients. *Physics of the Earth and Planetary Interiors* 146: 47–63.
Tolstikhin IN and Hofmann AW (2005) Early crust on top of the Earth's core. *Physics of the Earth and Planetary Interiors* 148: 109–130.
Tolstikhin IN, Kramers JD, and Hofmann AW (2006) A chemical Earth model with whole mantle convection: The importance of a core-mantle boundary layer (D″) and its early formation. *Chemical Geology* 226: 79–99.
Tonks WB and Melosh HJ (1990) The physics of crystal settling and suspension in a turbulent magma ocean. In: Newsom HE and Jones JH (eds.) *Origin of the Earth*, pp. 151–174. New York: Oxford University Press.
Torsvik T, Burke K, Steinberger B, Webb SJ, and Ashwal LD (2010) Diamonds sampled by plumes from the core-mantle boundary. *Nature* 466: 352–355.
Torsvik TH, Smethurst MA, Burke K, and Steinberger B (2006) Large igneous provinces generated from the margins of the large low-velocity provinces in the deep mantle. *Geophysical Journal International* 167: 1447–1460.
Torsvik TH, Smethurst MA, Burke K, and Steinberger B (2008) Long term stability in deep mantle structure: Evidence from the ~300 Ma Skagerrak-Centered Large Igneous Province (the SCLIP). *Earth and Planetary Science Letters* 267: 444–452.
Trail D, Watson EB, and Tailby ND (2011) The oxidation state of Hadean magmas and implications for early Earth/'s atmosphere. *Nature* 480: 79–82.

Trampert J, Deschamps F, Resovsky JS, and Yuen D (2004) Probabilistic tomography maps significant chemical heterogeneities in the lower mantle. *Science* 306: 853–856.

Trieloff M, Kunz J, Clague DA, Harrison D, and Allegre CJ (2000) The nature of pristine noble gases in mantle plumes. *Science* 288: 1036–1038.

Turcotte DL, Paul D, and White WM (2001) Thorium-uranium systematics require layered mantle convection. *Journal of Geophysical Research* 106: 4265–4276.

Turcotte DL and Schubert G (1982) *Geodynamics: Applications of Continuum Physics to Geological Problems*. New York: Wiley.

Turner G (1989) The outgassing history of the Earth's atmosphere. *Journal of the Geological Society of London* 146: 147–154.

Ulvrova M, Coltice N, Ricard Y, et al. (2011) Compositional and thermal equilibration of particles, drops, and diapirs in geophysical flows. *Geochemistry, Geophysics, Geosystems* 12: Q10014.

Ulvrová M, Labrosse S, Coltice N, Råback P, and Tackley PJ (2012) Numerical modelling of convection interacting with a melting and solidification front: Application to the thermal evolution of the basal magma ocean. *Physics of the Earth and Planetary Interiors* 206–207: 51–66.

van den Berg AP, Jacobs MH, and de Jong BH (2002) Numerical models of mantle convection based on thermodynamic data for the MgOSiO2 olivine-pyroxene system. *EOS Transactions, American Geophysical Union* 83, Fall Meeting Supplement. Abstract MR72B-1041.

van der Hilst RD and Karason H (1999) Compositional heterogeneity in the bottom 1000 kilometers of Earth's mantle: Toward a hybrid convection model. *Science* 283: 1885–1888.

Van der Hilst RD, Widlyantoro S, and Engdahl ER (1997) Evidence for deep mantle circulation from global tomography. *Nature* 386: 578–584.

van der Meer DG, Spakman W, van Hinsbergen DJJ, Amaru ML, and Torsvik TH (2009) Towards absolute plate motions constrained by lower-mantle slab remnants. *Nature Geoscience* 3: 36–40.

van Keken PE and Ballentine CJ (1998) Whole-mantle versus layered mantle convection and the role of a high-viscosity lower mantle in terrestrial volatile evolution. *Earth and Planetary Science Letters* 156: 19–32.

van Keken PE and Ballentine CJ (1999) Dynamical models of mantle volatile evolution and the role of phase transitions and temperature-dependent rheology. *Journal of Geophysical Research* 104: 7137–7151.

van Keken PE, Ballentine CJ, and Hauri EH (2003) Convective mixing in the Earth's mantle. In: Carlson RW (ed.) *Treatise on Geochemistry*, pp. 471–491. Oxford: Elsevier.

van Keken PE, Ballentine CJ, and Porcelli D (2001) A dynamical investigation of the heat and helium imbalance. *Earth and Planetary Science Letters* 188: 421–434.

van Keken PE, Hacker BR, Syracuse EM, and Abers GA (2011) Subduction factory: 4. Depth-dependent flux of H_2O from subducting slabs worldwide. *Journal of Geophysical Research* 116: B01401.

van Keken PE, Karato S, and Yuen DA (1996) Rheological control of oceanic crust separation in the transition zone. *Geophysical Research Letters* 23: 1821–1824.

van Keken PE, Kiefer B, and Peacock SM (2002) High-resolution models of subduction zones: Implications for mineral hydration reactions and the transport of water into the deep mantle. *Geochemistry, Geophysics, Geosystems* 3: 1056. http://dx.doi.org/10.1029/2001GC000256.

van Keken PE, King SD, Schmeling H, Christensen UR, Neumeister D, and Doin MP (1997) A comparison of methods for the modeling of thermochemical convection. *Journal of Geophysical Research* 102: 22477–22495.

van Keken PE and Zhong S (1999) Mixing in a 3D spherical model of present-day mantle convection. *Earth and Planetary Science Letters* 171: 533–547.

van Summeren JRG, van den Berg AP, and van der Hilst RD (2009) Upwellings from a deep mantle reservoir filtered at the 660 km phase transition in thermo-chemical convection models and implications for intra-plate volcanism. *Physics of the Earth and Planetary Interiors* 172: 210–224.

van Thienen P, van den Berg AP, and Vlaar NJ (2004) Production and recycling of oceanic crust in the early Earth. *Tectonophysics* 386: 41–65.

van Thienen P, van Summeren J, van der Hilst RD, van den Berg AP, and Vlaar NJ (2005a) Numerical study of the origin and stability of chemically distinct reservoirs deep in Earth's mantle. In: van der Hilst, RD, Bass J, Matas J, and Trampert J (eds.) *The Structure, Evolution and Composition of Earth's Mantle. AGU Geophysical Monograph*, vol. 160, pp. 117–136. Washington, DC: American Geophysical Union.

van Thienen P, Vlaar NJ, and van den Berg AP (2005b) Assessment of the cooling capacity of plate tectonics and flood volcanism in the evolution of Earth, Mars and Venus. *Physics of the Earth and Planetary Interiors* 150: 287–315.

Vidale JE and Hedlin MAH (1998) Evidence for partial melt at the core-mantle boundary north of Tonga from the strong scattering of seismic waves. *Nature* 391: 682–685.

Vidale JE, Schubert G, and Earle PS (2001) Unsuccessful initial search for a midmantle chemical boundary layer with seismic arrays. *Geophysical Research Letters* 28: 859–862.

Vlaar NJ (1985) Precambrian geodynamical constraints. In: Touret JLR and Tobi AC (eds.) *The Deep Proterozoic Crust in the North Atlantic Provinces*, pp. 3–20. Dordrecht: D. Riedel Publishing Company.

Vlaar NJ (1986) Archaean global dynamics. In: *Dutch Contributions to the International Lithosphere Program; Meeting 65,* pp. 91–101.

Walker JCG, Hays PB, and Kasting JF (1981) A negative feedback mechanism for the long-term stabilization of Earth's surface temperature. *Journal of Geophysical Research* 86: 9776–9782.

Walker RJ, Morgan JW, and Horan MF (1995) 187Os enrichment in some mantle plume sources: Evidence for core-mantle interaction? *Science* 269: 819–822.

Walter MJ, Kohn SC, Araujo D, et al. (2011) Deep mantle cycling of oceanic crust: Evidence from diamonds and their mineral inclusions. *Science* 334: 54–57.

Walzer U and Hendel R (1997a) Tectonic episodicity and convective feedback mechanisms. *Physics of the Earth and Planetary Interiors* 100: 167–188.

Walzer U and Hendel R (1997b) Time-dependent thermal convection, mantle differentiation and continental-crust growth. *Geophysical Journal International* 130: 303–325.

Walzer U and Hendel R (1999) A new convection-fractionation model for the evolution of the principal geochemical reservoirs of the Earth's mantle. *Physics of the Earth and Planetary Interiors* 112: 211–256.

Walzer U and Hendel R (2008) Mantle convection and evolution with growing continents. *Journal of Geophysical Research* 113: B09405.

Wang Y and Wen L (2007) Geometry and P and S velocity structure of the "African Anomaly". *Journal of Geophysical Research* 112: B05313. http://dx.doi.org/05310.01029/02006jb004483.

Weinstein SA (1992) Induced compositional layering in a convecting fluid layer by an endothermic phase-transition. *Earth and Planetary Science Letters* 113: 23–39.

Weinstein SA (1993) Catastrophic overturn of the earths mantle driven by multiple phase-changes and internal heat-generation. *Geophysical Research Letters* 20: 101–104.

Wen L (2001) Seismic evidence for a rapidly-varying compositional anomaly at the base of the Earth's mantle beneath the Indian ocean. *Earth and Planetary Science Letters* 194: 83–95.

Wen LX (2002) An SH hybrid method and shear velocity structures in the lowermost mantle beneath the central Pacific and South Atlantic Oceans. *Journal of Geophysical Research: Solid Earth* 107. http://dx.doi.org/10.1029/2001JB000499.

Wen LX and Anderson DL (1997) Layered mantle convection – A model for geoid and topography. *Earth and Planetary Science Letters* 146: 367–377.

Wen L and Helmberger DV (1998) Ultra-low velocity zones near the core-mantle boundary from broadband PKP precursors. *Science* 279: 1701–1703.

White WM (1985) Sources of oceanic basalts: Radiogenic isotope evidence. *Earth and Planetary Science Letters* 115: 211–226.

White WM (2010) Oceanic island basalts and mantle plumes: The geochemical perspective. *Annual Review of Earth and Planetary Sciences* 38: 133–160.

Wicks JK, Jackson JM, and Sturhahn W (2010) Very low sound velocities in iron-rich (Mg, Fe)O: Implications for the core-mantle boundary region. *Geophysical Research Letters* 37: L15304.

Williams Q and Garnero EJ (1996) Seismic evidence for partial melt at the base of earths mantle. *Science* 273: 1528–1530.

Williams Q, Revenaugh J, and Garnero E (1998) A correlation between ultra-low basal velocities in the mantle and hot spots. *Science* 281: 546–549.

Wolf A (1986) Quantifying chaos with Lyapunov exponents. In: Holden AV (ed.) *Chaos*, pp. 273–290. Princeton, NJ: Princeton University Press.

Wolfe CJ, Solomon SC, Laske G, et al. (2011) Mantle P-wave velocity structure beneath the Hawaiian hotspot. *Earth and Planetary Science Letters* 303: 267–280.

Wood BJ and Blundy JD (2003) Trace element partitioning under crustal and uppermost mantle conditions: The influences of ionic radius, cation charge, pressure, and temperature. In: Carlson RW (ed.) *Treatise on Geochemistry. The Mantle and Core*, vol. 2, pp. 395–424. Amsterdam: Elsevier.

Xie S and Tackley PJ (2004a) Evolution of helium and argon isotopes in a convecting mantle. *Physics of the Earth and Planetary Interiors* 146: 417–439.

Xie S and Tackley PJ (2004b) Evolution of U-Pb and Sm-Nd systems in numerical models of mantle convection. *Journal of Geophysical Research* 109: B11204. http://dx.doi.org/10.1029/2004JB003176.

Xu W, Lithgow-Bertelloni C, Stixrude L, and Ritsema J (2008) The effect of bulk composition and temperature on mantle seismic structure. *Earth and Planetary Science Letters* 275: 70–79.

Xu-Dong L and Osher S (1996) Nonoscillatory high order accurate self-similar maximum principle satisfying shock capturing schemes I. *The SIAM Journal on Numerical Analysis* 33: 760–779.

Yabe T, Ogata Y, Takizawa K, Kawai T, Segawa A, and Sakurai K (2002) The next generation CIP as a conservative semi-Lagrangian solver for solid, liquid and gas. *Journal of Computational and Applied Mathematics* 149: 267–277.

Yamazaki D and Karato S (2001) Some mineral physics constraints on the rheology and geothermal structure of Earth's lower mantle. *American Mineralogist* 86: 385–391.

Yokochi R and Marty B (2004) A determination of the neon isotopic composition of the deep mantle. *Earth and Planetary Science Letters* 225: 77–88.

Yoshida M and Ogawa M (2004) The role of hot uprising plumes in the initiation of plate-like regime of three-dimensional mantle convection. *Geophysical Research Letters* 31: 5607.

Youngs BAR and Bercovici D (2009) Stability of a compressible hydrous melt layer above the transition zone. *Earth and Planetary Science Letters* 278: 78–86.

Yuan K and Beghein C (2013) Seismic anisotropy changes across upper mantle phase transitions. *Earth and Planetary Science Letters* 374: 132–144.

Zahnle K, Schaefer L, and Fegley B (2010) Earth's earliest atmospheres. *Cold Spring Harbor Perspectives in Biology* 2: a004895.

Zhong S (2006) Constraints on thermochemical convection of the mantle from plume heat flux, plume excess temperature, and upper mantle temperature. *Journal of Geophysical Research* 111: B04409. http://dx.doi.org/10.1029/2005JB003972.

Zhong SJ and Hager BH (2003) Entrainment of a dense layer by thermal plumes. *Geophysical Journal International* 154: 666–676.

Ziegler LB and Stegman DR (2013) Implications of a long-lived basal magma ocean in generating earth's ancient magnetic field. *Geochemistry, Geophysics, Geosystems* 14: 4735–4742.

Zindler A and Hart S (1986) Geochemical geodynamics. *Earth and Planetary Science Letters* 14: 493–571.